2022-06

ADDITIVE MANUFACTURING HOLLOW METAL PARTS WITH LIQUID METAL

Magnusson, Jacob J.

Monterey, CA; Naval Postgraduate School

NAVAL POSTGRADUATE SCHOOL

MONTEREY, CALIFORNIA

THESIS

ADDITIVE MANUFACTURING HOLLOW METAL PARTS WITH LIQUID METAL

by

Jacob J. Magnusson

June 2022

Thesis Advisor: Walter C. Smith
Co-Advisor: David F. Dausen

THIS PAGE INTENTIONALLY LEFT BLANK

REPORT DOCUMENTATION PAGE			*Form Approved OMB No. 0704-0188*

1. AGENCY USE ONLY *(Leave blank)*	**2. REPORT DATE** June 2022	**3. REPORT TYPE AND DATES COVERED** Master's thesis

4. TITLE AND SUBTITLE ADDITIVE MANUFACTURING HOLLOW METAL PARTS WITH LIQUID METAL	**5. FUNDING NUMBERS**
6. AUTHOR(S) Jacob J. Magnusson	
7. PERFORMING ORGANIZATION NAME(S) AND ADDRESS(ES) Naval Postgraduate School Monterey, CA 93943-5000	**8. PERFORMING ORGANIZATION REPORT NUMBER**
9. SPONSORING / MONITORING AGENCY NAME(S) AND ADDRESS(ES) N/A	**10. SPONSORING / MONITORING AGENCY REPORT NUMBER**

11. SUPPLEMENTARY NOTES The views expressed in this thesis are those of the author and do not reflect the official policy or position of the Department of Defense or the U.S. Government.

12a. DISTRIBUTION / AVAILABILITY STATEMENT Approved for public release. Distribution is unlimited.	**12b. DISTRIBUTION CODE** A

13. ABSTRACT (maximum 200 words)

Liquid-metal additive manufacturing is a new technology whose limits have not been fully tested. Unique molten-metal droplet printing allows for new metal structures to be made that cannot be built with traditional (powder)-based metal additive manufacturing. This research focuses on the potential to build hollow metal parts with no secondary manufacturing. The research provides a brief background in additive manufacturing and the reason for choosing liquid-metal jet printing. Multiple experiments are performed to test the design limitations of the additive manufacturing printer chosen. This leads to the design of the hollow metal part configurations that are ultimately buckling tested to prove they can support substantial sea pressure. As for the applicability of this research, it focuses on the buoyancy potential of the hollow parts and the potential use they could be to the undersea warfare community.

14. SUBJECT TERMS AM, additive manufacturing	**15. NUMBER OF PAGES** 129
	16. PRICE CODE

17. SECURITY CLASSIFICATION OF REPORT	**18. SECURITY CLASSIFICATION OF THIS PAGE**	**19. SECURITY CLASSIFICATION OF ABSTRACT**	**20. LIMITATION OF ABSTRACT**
Unclassified	Unclassified	Unclassified	UU

NSN 7540-01-280-5500

Standard Form 298 (Rev. 2-89)
Prescribed by ANSI Std. 239-18

THIS PAGE INTENTIONALLY LEFT BLANK

Approved for public release. Distribution is unlimited.

ADDITIVE MANUFACTURING HOLLOW METAL PARTS WITH LIQUID METAL

Jacob J. Magnusson
Lieutenant, United States Navy
BS, Michigan State University, 2015

Submitted in partial fulfillment of the
requirements for the degree of

MASTER OF SCIENCE IN MECHANICAL ENGINEERING

from the

NAVAL POSTGRADUATE SCHOOL
June 2022

Approved by: Walter C. Smith
Advisor

David F. Dausen
Co-Advisor

Garth V. Hobson
Chair, Department of Mechanical and Aerospace Engineering

THIS PAGE INTENTIONALLY LEFT BLANK

ABSTRACT

Liquid-metal additive manufacturing is a new technology whose limits have not been fully tested. Unique molten-metal droplet printing allows for new metal structures to be made that cannot be built with traditional (powder)-based metal additive manufacturing. This research focuses on the potential to build hollow metal parts with no secondary manufacturing. The research provides a brief background in additive manufacturing and the reason for choosing liquid-metal jet printing. Multiple experiments are performed to test the design limitations of the additive manufacturing printer chosen. This leads to the design of the hollow metal part configurations that are ultimately buckling tested to prove they can support substantial sea pressure. As for the applicability of this research, it focuses on the buoyancy potential of the hollow parts and the potential use they could be to the undersea warfare community.

THIS PAGE INTENTIONALLY LEFT BLANK

TABLE OF CONTENTS

LIST OF FIGURES

LIST OF TABLES

LIST OF ACRONYMS AND ABBREVIATIONS

AM	additive manufacturing
ASTM	American Society for Testing and Materials
BC	boundary condition
DED	directed energy deposition
DFAM	design for additive manufacturing
DMLS	direct metal laser sintering
EBM	electron beam melting
FDM	fuse deposition modeling
FEA	finite element analysis
FMJP	fusion metal jet printing
LC	long cylinder
LOM	laminated object manufacturing
MAS	mesh analysis setting
PBF	powder bed fusion
SC	short cylinder
SHS	selective heat sintering
SL	stereolithography
SLM	selective laser melting
SLS	selective laser sintering
TPRC	tolerance piece round corners
TPSC	tolerance piece sharp corners
UAM	ultrasonic additive manufacturing
UV	ultraviolet
VFD	variational finite-differential
VLC	very long cylinder

THIS PAGE INTENTIONALLY LEFT BLANK

ACKNOWLEDGMENTS

I was extremely nervous coming back to school after being away from it for over five years while serving on the USS Missouri (SSN 780). Grad school came at me fast. I had no knowledge of how to write a thesis or what to write about. I jumped at the first thing I could, and ultimately learned the importance of considering all options before committing to something. After stepping away from my first thesis plan, I met Dr. Walter Smith, Mr. David Dausen, and the Xerox ElemX printer. I knew instantly that this was the topic I needed to study and write about.

I came into this experience with zero knowledge on additive manufacturing and the Xerox ElemX liquid metal 3D printer. Dr. Smith and Mr. Dausen guided and taught me to be one of the first student operators of the printer. I am now comfortable operating and even troubleshooting the machine as well as training future students. The process has taught me so much, and I cannot thank Dr. Smith and Mr. Dausen enough for their time and knowledge sharing.

Lastly, and most importantly, I want to thank my fiancée, Jessica, for supporting me through this process, working as a full-time teacher and coming home and still cooking and keeping up the house while I typed and spent countless late nights researching. This unwavering and relentless support can't be understated, and it allowed me to conduct meaningful research and fulfill my thesis requirements on time.

THIS PAGE INTENTIONALLY LEFT BLANK

I. INTRODUCTION

A. MOTIVATION

1. Submarine Capabilities

The United States submarine force is a small but vital factor in the United States Navy (USN). From gathering intelligence and searching for enemy submarines, to supporting U.S. Special Forces' missions, the role of submarines is expanding every day. As the capabilities of the U.S. submarine force grows, we must continue to challenge ourselves to learn new abilities and keep the U.S. submarine force as the most elite submarine force in the world. This paper aims to show how new additive manufacturing (AM) techniques can be used to increase the capabilities of our submarine force and give us a leg up on our adversaries.

2. Submarine Onboard Storage

The logistics to support a U.S. submarine are extremely complex [1]. Many shore facilities help the coordination or submarines coming in and out of port because of the limited communication submarines have while underway. Aside from submarines going from point A to B, the logistics onboard submarines are also complex due to limited space. Every inch of a submarine is used to support storage. Often it has been reported of submariners walking on top of canned goods as the hallways were used for even more storage. Much of the storage onboard a submarine is to support extra parts in case a vital valve or switch were to break while the submarine is underway [1]. AM and 3D printers offer a unique solution to this limited storage problem. If a 3D printer can be installed onboard a submarine, although the machine itself will take up space, the printer will save space in removal of extra part storage. Although AM technology may not be ready to support making high quality metal parts immediately off the printer at this moment, as time goes on the technology will improve and the machines will get smaller. This thesis will show the practicality of using metal AM right off the printer and how they could be used to support submarine missions.

3. Sound Speed Profile

When submarines are submerged, they see with their ears [2]. Acoustic sensors are strategically placed on the outside of the boats to receive noise traveling in the water. An important aspect to what noise is received is the sound speed profile. The sound speed profile shows how the speed of sound in water is not a constant value with depth. The speed of sound in seawater is a factor of three things: temperature, salinity and pressure [3].

From the University of Rhode Island, Figure 1 shows how temperature, salinity, and pressure change with seawater depth. Combining these figures into one graph and adding the speed of sound in water, we can see Figure 2. Figure 2 illustrates how the sound speed is largely dependent on temperature for the first 1000 meters and then largely dependent on pressure. Salinity plays a minor role in the sound speed profile as salinity usually only changes ~1 to 2 ppt with depth [3]. There are regions of the world that have much higher-than-normal salinities and those areas require their own unique analysis. Overall, the relationships exist that the speed of sound increases with rising water temperature, rising salinity, and rising pressure [3].

An important part to the sound speed profile graph is the surface layer or surface layer duct (SLD). The surface layer exists because the sun heats the surface of the ocean [4]. This heating action is the reason for the constant straight line in the temperature depth profile. Below the layer the temperature starts to decrease. Sound can refract differently depending on if it is above and below the SLD [4].

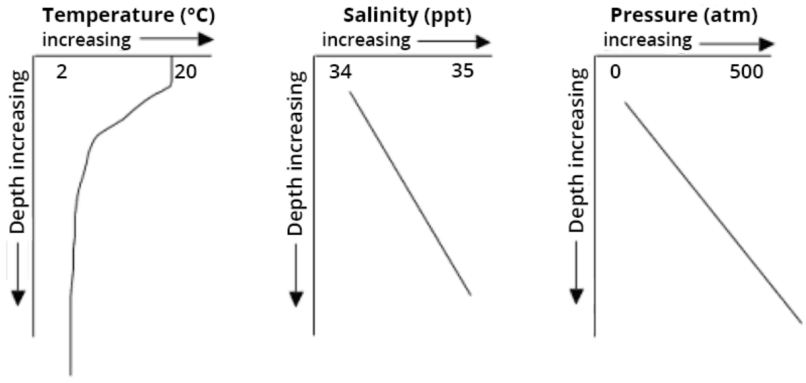

Figure 1. Depth Profiles for Temperature, Salinity, and Pressure. Source: [3].

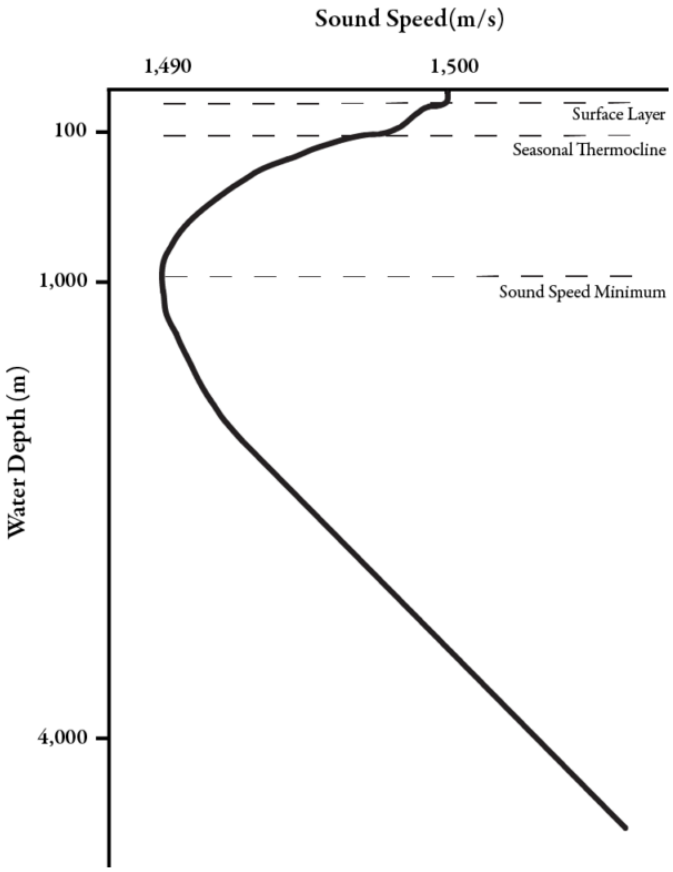

Figure 2. Sound Speed Profile. Source: [3].

Figure 3 represents how sound propagates above and below the SLD. Above the SLD sound can get trapped by the warm water and bend back to the surface. Below the SLD the sound will bend away from the SLD and towards the deeper ocean water. Since sound is such a vital asset to submarines, the location of a submarine in relationship to the SLD is also important. If a submarine is located below the layer, often times it can't hear weak sound signals on the surface, such as a small boat, because those sound signals are trapped in the SLD. This paper will offer a unique solution to this problem by using new AM techniques to build hollow metal parts to hear above the sound layer.

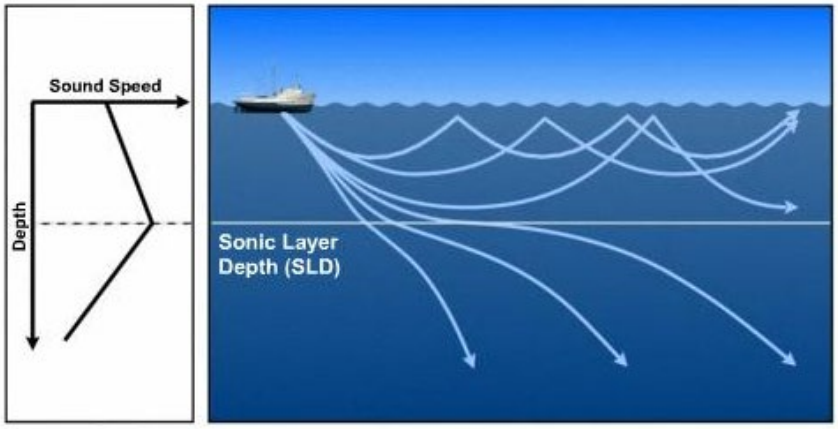

Figure 3. Ship Acoustics Related to Sound Layer. Source: [4].

B. PROBLEM STATEMENT

Liquid metal additive manufacturing is a new technology whose limits have not been fully tested [5]. Unique molten metal-droplet printing allows for new metal structures to be made that cannot be built with traditional (powder) based metal additive manufacturing [6]. This research will focus on the potential to build hollow metal parts with no secondary manufacturing. As for the applicability of this research, it will focus on the buoyancy potential of these hollow parts and the potential use they could be to the Undersea Warfare community. There are three objectives in this research:

1. Build positively buoyant metal structures using liquid metal AM.
2. Have the metal structures be able to support a payload and remain positively buoyant.
3. Prove the metal structures can sustain substantial sea pressure without buckling.

C. DELIMINATIONS

To provide a clear understanding of the content in this thesis, the following list illustrates areas that will not be studied:

- Conclusions from this thesis are based on theoretical data and experimental data, however data will not be collected on board a submarine and can only be applied theoretically.
- The study will focus on the buoyancy potential and payload support of hollow metal parts to support sensors. A sensor will not be attached and studied.
- Products manufactured through AM often require post processing to meet the designed material properties. This study will focus on the practicality of using parts as printed with no secondary post processing.
- Design parts were made and measured to generate correlations. However, these correlations could be due to significant statistical uncertainty and more test pieces would need to be printed to have conclusive results.

THIS PAGE INTENTIONALLY LEFT BLANK

II. CONTEXTUAL REVIEW

A. INTRODUCTION

Additive manufacturing was first introduced by 3D Systems in 1987 with stereolithography (SL) and its ability to solidify thin layers of polymer with a laser. It was not until the late 1990s that additive manufacturing began using metal as its base material [7]. There are currently seven major methods to AM according to ASTM Committee F42 [8]. Liquid metal jet printing (LMJP) is a new type of metal AM, which was developed in 2017 and became commercially available in 2020 [5]. This chapter aims to give a history of AM and show why LMJP was chosen for this study.

B. ADDITIVE MANUFACTURING

Additive manufacturing enables new possibilities in product development and testing [8]. The unique building process allows for complex designs to be developed in typically a shorter amount of time and less waste of material. AM was originally seen as a helpful tool for prototyping but is now seen in large-scale production. Figure 4 shows a summary of the seven major types of additive manufacturing according to the ASTM Committee F42. The next sections will discuss each method and the advantages and limitations of each.

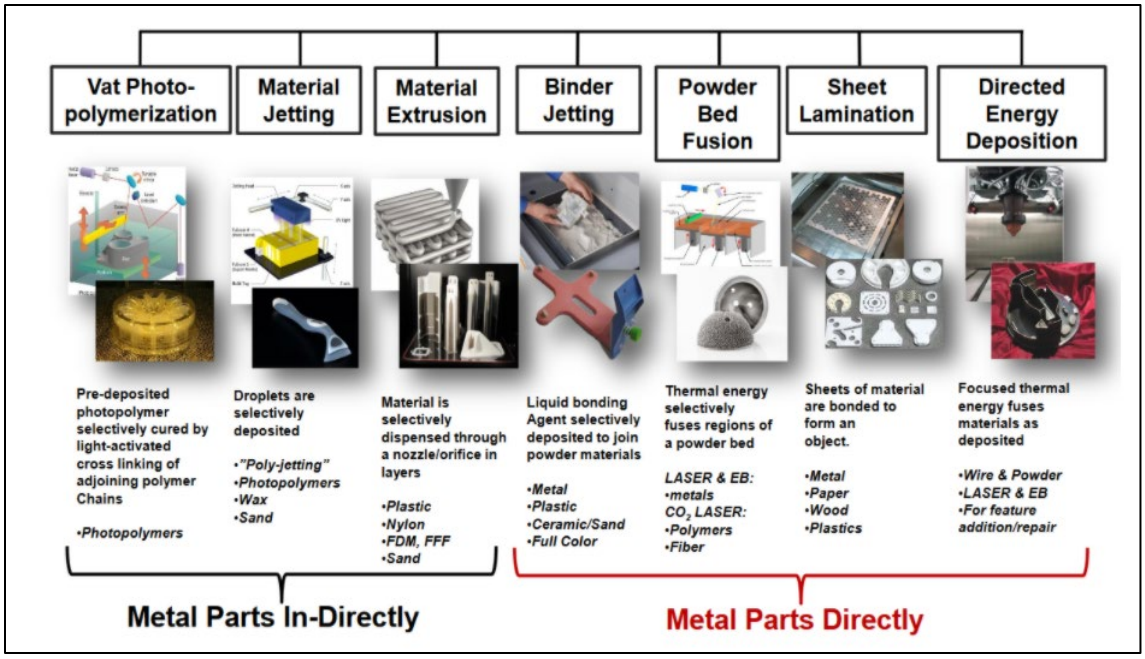

Figure 4. Seven AM Processes According to ASTM Committee F42 on Additive Manufacturing. Source: [9].

1. Vat Photopolymerization

Vat photopolymerization is a process that uses ultraviolet (UV) light to harden photopolymer resin [8]. The resin sits in a vat of liquid on a platform. Depending on the machine type, the platform of UV light moves to build where required. The UV light builds the model on a layer-by-layer process. The advantages of vat photopolymerization are the high level of accuracy, speed of the process, and relatively large build areas. Disadvantages are the relatively high cost, long post processing time to remove resin, user-added support design and support removal process, and the limitations on material as it must be a photopolymer resin [8].

2. Material Jetting

Material Jetting refers to the process in which material is jetted out of a nozzle to build a structure in a drop-by-drop basis. This method is often compared to two-dimensional ink jet printers. As material is jetted from the nozzle it solidifies on the model drop-by-drop and then layer-by-layer to complete a whole structure [8]. Material jetting machines vary in complexity and base material used. For the most part, advantages of

material jetting include high accuracy of deposition, low waste of material, and some machines allow for multiple material parts and colors to be used in one process. Disadvantages include that support material is often required, and limitations in material [8].

3. Material Extrusion

Material extrusion is a process that uses fuse deposition modeling (FDM) to build models. In this process a material spool is used as a supply for the machine [8]. Material can be drawn from the spool and fed into a nozzle where it is heated and then deposited layer by layer. Machine complexity varies but typically the nozzle moves horizontally, and the build platform moves up and down vertically as the layers are built. FDM is similar to the previous mentioned processes however the major difference is the material is continuously fed into the nozzle under constant pressure to ensure accurate results. Material layers are bonded by either temperature or using chemical agents. The biggest advantage of FDM is it is very inexpensive and widely used. FDM is often the AM process of 3D printing hobbyist. Disadvantages of FDM are the quality of results often depend on nozzle size and quality, and accuracy and speed can be low varying on the machine used [8]. LMJP was mentioned in the introduction and will be discussed in 2.2.8 which shares some similarities to material extrusion.

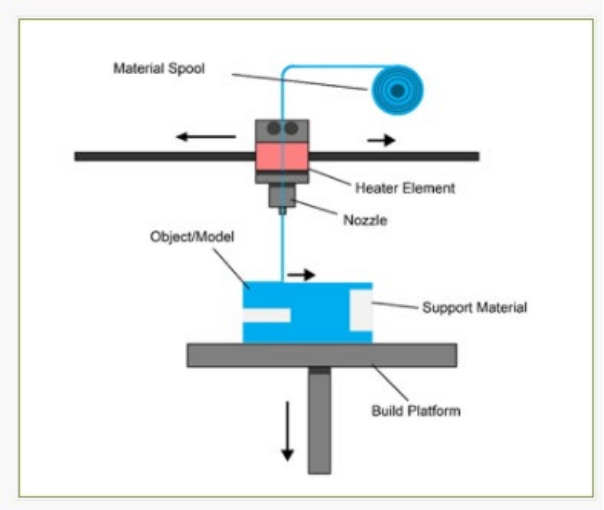

Figure 5. Simple Model for Material Extrusion. Source: [8].

4. Binder Jetting

Binder jetting is a process that uses a build material and a binding material to build models. Typically, the build material is in powder form and the binding material is in powder form. The printer head moves in x and y directions and alternates depositing layers of build material and binding material. Just as described the binding material binds the build material as it is sandwiched between them. The build platform lowers as each layer is completed. Advantages of binder jetting include the range of colors which can be used, wide range of materials including metals, relatively fast process, and a large number of powder-binder combinations. Disadvantages to binder jetting include it is not very suitable for structural parts because of the binding agent, additional post processing can add cost and time to the process, and the waste of extra powder material that cannot be recycled [8].

5. Powder Bed Fusion

Selective heat sintering (SHS), selective laser sintering (SLS), selective laser melting (SLM), electron beam melting (EBM), and direct metal laser sintering (DMLS), are all common additive manufacturing techniques which fall under the category of powder bed fusion (PBF). PBF uses either an electron beam or a laser to melt/fuse a powder based material together. In PBF machines there exists a supply stock of powder base material. This powder-based material is spread or rolled over a thin layer onto the build plate. The laser or electron beam will then fuse the material one layer at a time [8]. The build plate will then move down, a new layer of base material is rolled over the build plate, and the process continues. Advantages of PBF include the wide variety of materials to be used including metals, some machines include auto-generated support structures, and the relative cost is low. Disadvantages of PBF include the size limitations, high power usage, and waste of extra powder that cannot be recycled [8].

6. Sheet Lamination

Laminated object manufacturing (LOM) and ultrasonic additive manufacturing (UAM) and common AM processes included in the process of sheet lamination [8]. Sheet lamination uses thin sheets of material which are bounded together using ultrasonic welding in the UAM case, or the sheets are bonded together by paper layers between them

in the LOM case. Both processes require post processing to remove the unbonded layers of material. Advantages of sheet lamination are the relatively low cost, high speed, and strength depending on the base material used. Disadvantages include post processing must be used for a finished product, limitations of material that can used, and generally high user training is required to use a sheet lamination machine [8].

7. Directed Energy Deposition

Directed energy deposition (DED) is similar to material extrusion except that in DED the nozzle is not fixed and can move in multiple directions. Material is extruded from a source and deposited onto a build plate where it is melted with a laser or electron beam. Advantages of DED include the high quality of DED models and the ability to control grain structure. Disadvantages include the limited materials that can be used and generally high user training required to understand the fusion process [8].

8. Liquid Metal Jet Printing

LMJP is a new process that uses the techniques from metal extrusion and applies them to metal. A metal spool of material is used as a source for the machine. That metal material is then fed into a ceramic nozzle and heated to a point beyond the metals melting point. There is an electromagnetic coil that sits outside of the nozzle [6]. A current is applied that energizes the coil and creates a magnetic field. This magnetic field pushes on the liquid pool of metal and creates a droplet, as seen in Figure 6. Doing this about 500 times a second allows a machine to produce many small molten droplets which are dropped onto a hot build plate. The build plate can move in the x and y direction while the nozzle moves in the z direction. The machine produces droplets and builds models on a layer-by-layer basis [6]. Advantages to LMJP include the low cost, high cycle times, and ability to produce hollow metal parts with no post processing [6]. Disadvantages of the LMJP include the build volume limitations, design limitations due to droplet style of printing, and it is a new technology that has not been fully tested.

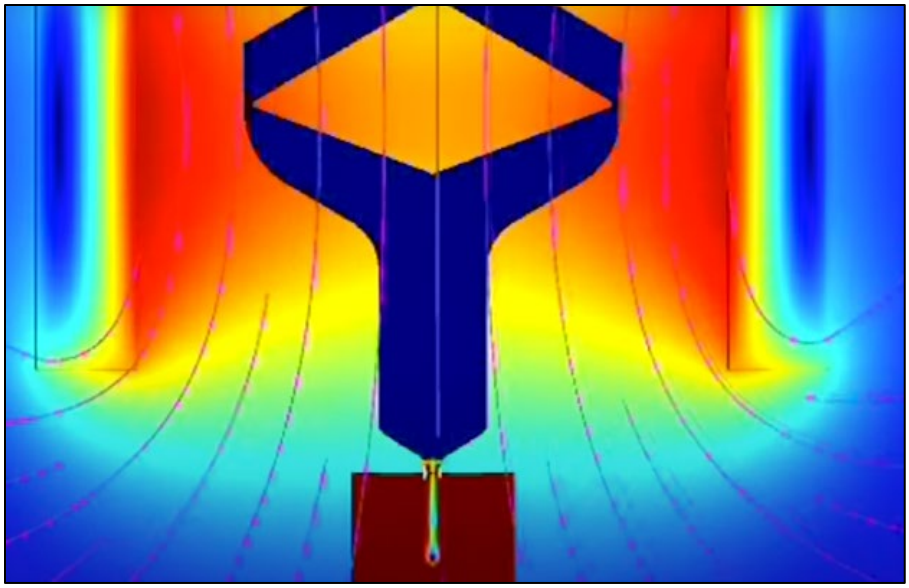

Figure 6. Droplet Production by Electromagnetic Field in LMJP Process. Source: [6].

C. DESIGN FOR ADDITIVE MANUFACTURING

In terms of typical manufacturing in a production line, developing new products can be costly and time consuming. Mistakes in the process can take time to notice which will lead to a large amount of waste [10]. When a mistake is found, the manufacturing process restarts with a new design which will add more lead time and cost. AM has been thought of a way to fix this approach, saving time and money. A study by Alex Staffanson and Philip Ragnartz [10] found that there is a massive potential savings in lead time (up to 85%) if AM is used in the manufacturing and development process. The study also found that AM today, cannot be used to save cost in the manufacturing or development process due to the high cost of metal 3D printers. However, the study done by Staffanson and Ragnartz evaluated four different metal printers, two metal FDM printers, an EBM printer, and a SLS printer [10]. The study did not look at the cost effectiveness of using LMJP technology as this technology had not yet been invented or commercially available. LMJP has a high upfront cost but is much cheaper to run compared to other metal printers due to there not being any high voltage lasers in the machine needed for metal fusion [6].

D. HOLLOW METAL PARTS

With traditional manufacturing, hollow metal parts can be made by casting however it requires secondary processing to bond two halves of the metal part, or to seal off the last portion of an almost completely sealed object. Hollow metal geometries have been made and studied with additive manufacturing in the past including David McCarthy's study from 2012 [11]. However, McCarthy's hollow metal geometries were made by additive manufacturing complex parts with polymers, coating the polymer in metal (in his case copper), and then heating the model to remove the plastic mold [11]. With this process it is impossible to create hollow metal parts. LMJP is the first metal printing technology to be able to build hollow metal parts with no internal structures, and no secondary processing.

E. BUCKLING OF CONE-CYLINDER TRANSITION

The choice of design for the cone-cylinder transition will be discussed more in Chapter III as it relates more to the design limitations of the machine used. Cylinder shells with conical ends exerted to external pressure can be found in applications such as submarine hulls, pipelines, buildings, and energy facilities [12]. The cone-cylinder assembly under external pressure have been shown to buckle in two ways: locally at the cylinder or conical portion, or at both the cylinder and conical portions at the same time [13]. Wenk Jr and Taylor (1953) are considered the first to research the cone-cylinder transition under external pressure. They derived equilibrium equations to solve the buckling of the cone-cylinder transition [14]. Wenk Jr and Taylor studied both non-reinforced and reinforced transitions [14]. Aylward (1973, 1975) continued the study by comparing theoretical written buckling equations to finite-difference program BOSOR 3 [15].

Galletly (1974) compared BOSOR 3 and BOSOR 5 theoretical calculations with experimental data [13]. Galletly machined thin-walled cone-cylinder models using an aluminum alloy (HE-15), and put them under external pressure with a water-based pressure chamber. Galletly's models can be seen in Figures 7 and 8, and his results are in Figure 9.

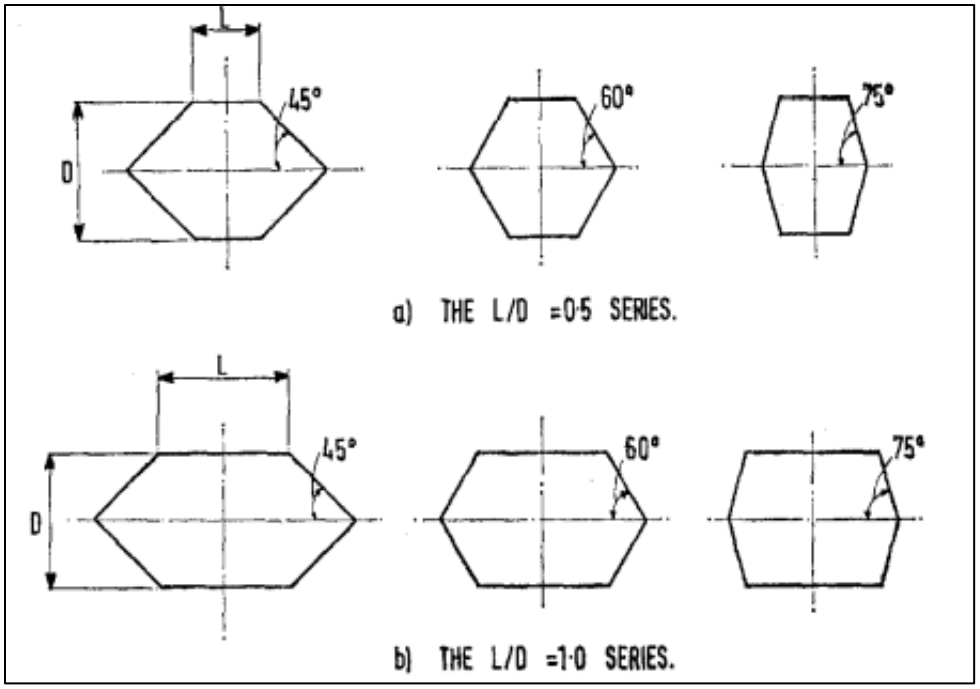

Figure 7. Galletly Model Sections. Source: [13].

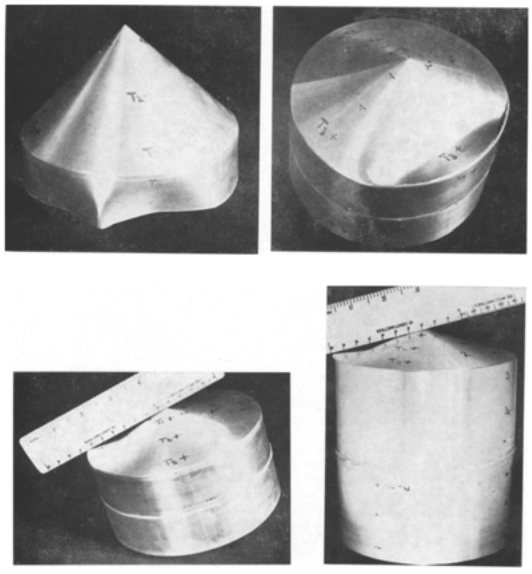

Figure 8. Four of Six Galletly Models Postbuckling. Source: [13].

Model No.	L/D	α	Predicted Buckling Pressure lbf/in²		Experimental Buckling Pressure lbf/in²
			BOSOR 3	BOSOR 5	
1	0.5	45°	598(6)	553(6) 561(6)	559
2	0.5	60°	472(4)	397(3) 408(3)	410
3	0.5	75°	210(2)	184(2) 190(2)	185
4	1.0	45°	287(5)	288(5) —	279
5	1.0	60°	287(5)	287(5) —	274
6	1.0	75°	210(2)	183(2) —	186

Figure 9. Galletly Comparison of Theoretical vs. Experimental Results. Source: [13].

Galletly made the two important conclusions [13]:

1. Theory and experimental data agreed within 5% for elastic asymmetric buckling.
2. Theory and experimental data agreed within 2% for elastic-plastic asymmetric buckling.

F. EIGENVALUE BUCKLING VS. NONLINEAR BUCKLING

Buckling involves a sudden loss of stiffness of a structure and a drastic deformation change. There is also local buckling in which small dents occur on a structure, but the structure can still maintain shape [16]. Buckling is not always a bad thing. In some examples, such as foldable bowls for camping, buckling is used to allow utensils to be folded into convenient storage sizes.

There are few methods in that engineers use to perform buckling analysis of a material. Eigenvalue buckling is one of the most efficient ways to predict buckling loads and understand all possible buckling modes. Eigenvalue buckling is often seen as a critical first step in any study of instability. It is important to note that buckling is a highly nonlinear process [17].

Sometimes buckling even involves a snap-through phenomenon, which means the displacement jumps from one configuration to another, even without an increase of the applied load [16]. A visual representation of the snap-through phenomenon can be seen in Figure 10. Solving the entire buckling behavior of a structure can be challenging and computationally expensive. Eigenvalue buckling analysis avoids the complexity of solving a nonlinear system [17]. Eigenvalue buckling analysis solves a linear set of equations, allowing us to predict the theoretical buckling strength of an ideal elastic structure. This method corresponds to textbook approaches to an elastic buckling analysis. The benefit of eigenvalue buckling is it is computationally efficient and gives us a rough estimate of the buckling loads [17].

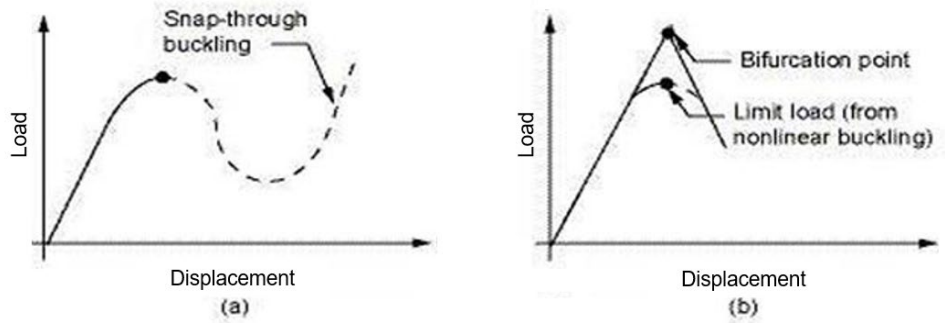

Figure 10. (a) Nonlinear Load-Deflection Curve (b) Linear (Eigenvalue) Buckling. Adapted from [18].

It is important to note that the eigenvalue results are unconservative since they do not include any nonlinearities that the real-world structures experience [17]. Eigenvalue buckling analysis is based on a classic eigenvalue problem and uses linear perturbation method [17]. The linear perturbation method uses a prior linear or nonlinear preloaded status to solve a linear problem [17]. The prior linear or nonlinear analysis is called the

base analysis. The perturbation analysis "freezes" the effects from the base analysis for reuse in the current or future analysis scenarios.

The governing equation of the eigenvalue problem:

$$[K_t] + \lambda_i[S]\{\psi_i\} = 0 \quad (1)$$

Just like classic eigenvalue problems, the eigenvalue analysis solves for eigenvalues λ, and eigenvectors ψ. K_t is a matrix which represents the total tangent stiffness. S is a matrix for the linear perturbed stress stiffening matrix. Stress stiffening is the stiffening of a structure due to its stressed state. The solved λ turns out to be the load factors or buckling load magnitudes. Ψ is the corresponding buckling modes. The subscript "i" indicates there is more than one way in which the structure may buckle under the given loads.

Load factors or buckling load magnitudes can be described with the equation below

$$\{F_{buckling}\} = \lambda_i\{F_{perturbed}\} \quad (2)$$

For linear based eigenvalue buckling analysis the perturbed load $F_{perturbed}$ equals the applied load in the base analysis [17]. However, when the base analysis is nonlinear, for example when contact nonlinearities exists, the buckling load is calculated differently. In an eigenvalue buckling analysis with a nonlinear base state, we can define a different perturbation load in the buckling analysis compared with the applied loads in the nonlinear base analysis [17]. Therefore, the load multiplier 'λ' scales only the loads applied in the buckling analysis. The total buckling load is the sum of the load applied in the nonlinear base analysis and the scaled perturbation load.

$$\{F_{buckling}\} = \{F_{base}\} + \lambda_i\{F_{perturbed}\} \quad (3)$$

The key takeaway is that for eigenvalue buckling analysis, the applied load in the linear base analysis does not affect the buckling results. However, for nonlinear-based eigenvalue buckling analysis, the applied load does affect the buckling results because the applied load is added to the nonlinear base analysis with the scaled perturbed load in the eigenvalue buckling analysis. The proportional relationship is lost due to the summation of the two parts [17].

In summary, eigenvalue buckling analysis is an efficient way to predict the buckling loads and associated buckling modes of a structure. It's an important first step in any study of instabilities of buckling [17]. It is a linear analysis that calculates the unconservative, theoretical buckling strength. Eigenvalue buckling analysis proVFDes us with information on whether there may be more than one way a structure can buckle. Also allows us to be able to identify and review possible global and local buckling modes. Such information is not possible to obtain from a nonlinear buckling analysis as it only generates one buckling solution. Linear buckling analysis can be beneficial in approximating the applied load for the nonlinear buckling analysis.

G. SUMMARY

The purpose of this chapter is to provide a contextual review for the research presented in this paper. Technologies are advancing and changing every day and with those advancements, companies and militaries must adapt. Metal AM technology specifically is still rapidly growing as seen with the invention of liquid metal jet printing. LMJP has opened the possibility to produce hollow metal parts with no secondary processing or internal supports. Hollow metal parts have a unique application to the commercial and military industry. The hollow cone-cylinder design under external pressure has been theoretically and experimentally tested but not in conjunction with additive manufacturing. Eigenvalue buckling analysis is an engineering tool to help quickly determine an unconservative critical buckling load for a structure. Eigenvalue buckling analysis avoids the complexity of solving a nonlinear buckling analysis and enables the ability to find multiple modes of buckling which is not possible with nonlinear buckling analysis.

Additive manufacturing is an essential tool for the U.S. Armed Forces to adapt to help with the design and lead time of new products. Hollow metal parts produced with no secondary processing is a cutting-edge technology which can provide many uses to the U.S. Navy, submarines, and special forces. This paper will explore the benefits and usefulness of hollow metal cylinders with conical ends made with LMJP.

III. EXPERIMENTAL METHODS

A. PRINTER DESIGN GUIDELINES

Chapter 2 established LMJP will be used for this study because of its high accuracy, low cost, and most importantly its ability to print hollow metal parts with no internal supports and no secondary processing. With the type of printing is being established, the full potential of AM can be reached by designing the part with careful consideration of the printing machines' design guidelines. For this study specifically, we will use the **Xerox ElemX liquid metal 3D printer** as it is one of the first machines developed which uses the LMJP technology.

Prior to discussing the design guidelines, it is important to discuss the machine's orientation definitions. The Xerox ElemX Design Manual [19] defines the orientations as:

- X is moving left and right.
- Y is moving closer and farther away.
- Z is the normal line to the build plate.
- Up-facing surfaces have a normal pointing away from the build plate.
- Down-facing surfaces have a normal pointing toward the build plate. [19].

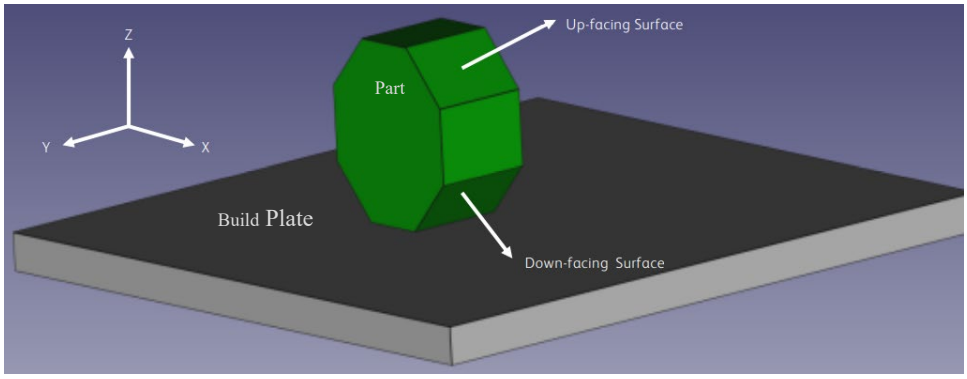

Figure 11. Orientation Definition. Adapted from [19].

1. Xerox Design Criteria

Table 1. Xerox Design Criteria. Adapted from [19].

Criteria	Specification
Build Volume	300 mm (Length) x 300 mm (Width) x 120 mm (Height) or (12 in x 12 in x 4.7 in)
Maximum Build Rate	84 ccc/hour average or (0.5 lbs./hour)
Maximum Build Weight	0.91 kg. or (2 lbs.)
Dimensional Accuracy	XY Plane: +/- 0.6 mm Z Plane: +/- 0.5 mm
Minimum Layer Thickness	0.24 mm
Input Material	Aluminum Alloy 256 (4008)
Input Material Size	1.6 mm diameter, 9.07 kg (20 lb.) spool

2. Minimum Feature Dimensions

Minimum pin size and hole size is 3 mm in diameter. Source: [19].

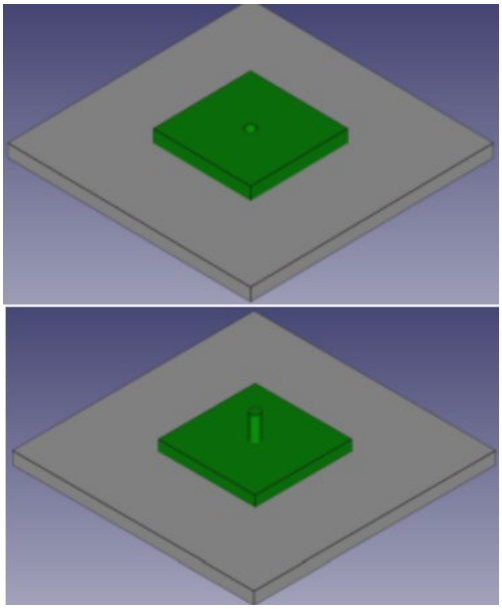

Figure 12. Hole and Pin Design Consideration. Source: [19].

3. Minimum Wall Thickness

The minimum wall thickness for this printer is 3 mm [19].

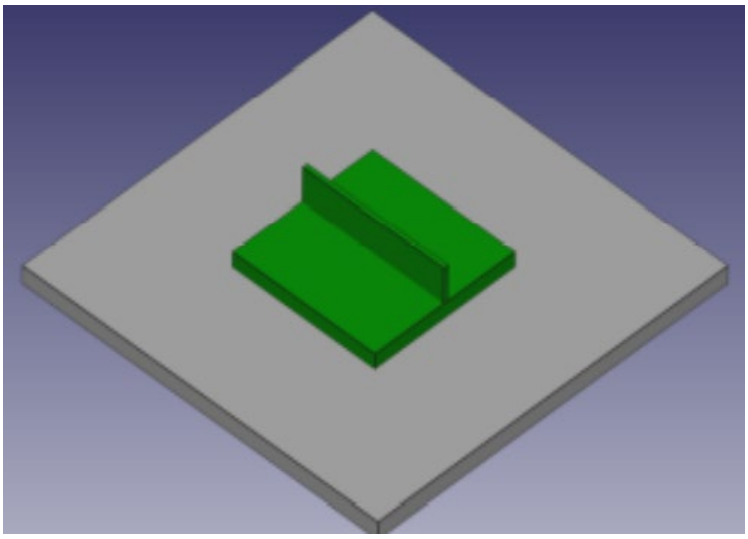

Figure 13. Wall Thickness Design Requirement. Source: [19].

4. Support Structure Requirements

Overhang angles less than 50° will require support structures [19].

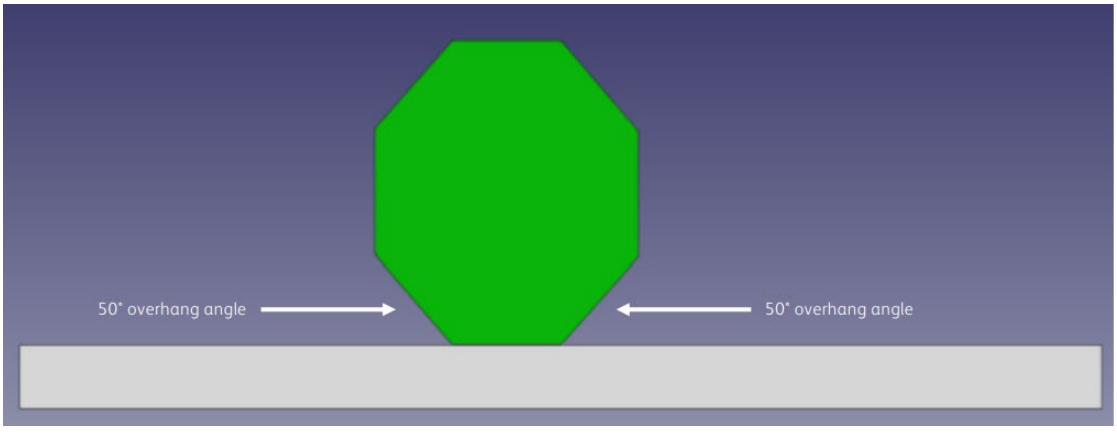

Figure 14. Support Structure Design Requirement. Source: [19].

5. Sharp Corners

Positive and negative sharp angles must be greater than 10° [19].

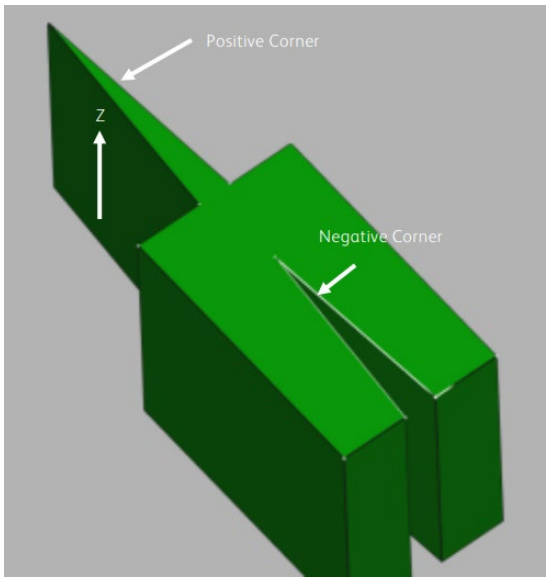

Figure 15. Sharp Corner Design Requirement. Source: [19].

6. Overhangs

In relationship to Figure 16 and overhang design requirements, L1 and/or L2 must be less than 2 mm. If greater than 2 mm, support structures are required [19].

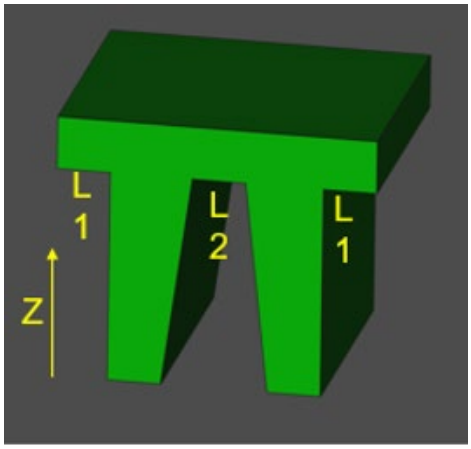

Figure 16. Overhang Design Requirement. Source: [19].

7. Considerations to Improve Productivity

Round corners in the XY plane can greatly improve speed and productivity of the Xerox ElemX as illustrated in Figure 17.

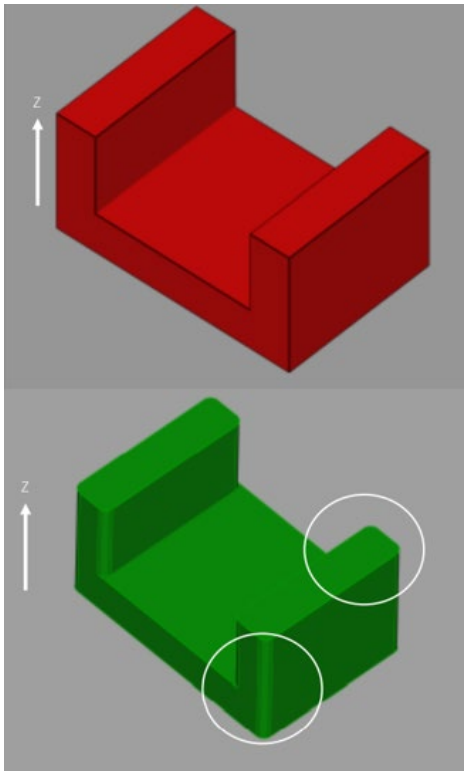

Figure 17. Rounding Corners in XY Plane to Improve Productivity. Source: [19].

B. EXPERIMENTAL DESIGN GUIDELINES

Last section reviewed the design guidelines as they are written in the design manual. Often design manuals from companies are more conservative than what may be achievable for a machine. To verify this theory tolerance pieces were designed and printed. After printing, specifications were measured and compared to theoretical design specifications to verify machines accuracy and limitations. SolidWorks designs of the tolerance pieces can be seen in Figures 18–19.

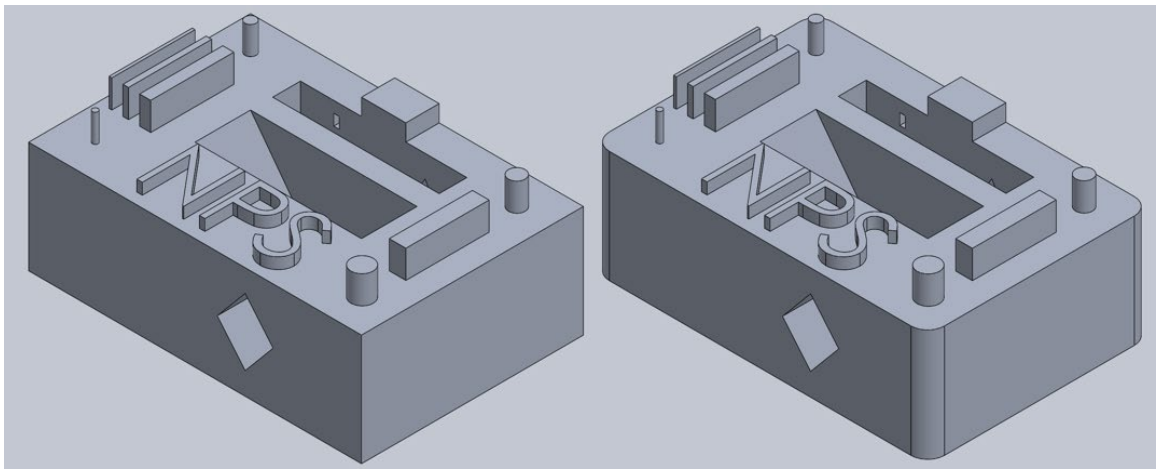

(Sharp corners left, rounded corners right)

Figure 18. Tolerance Pieces – Front View

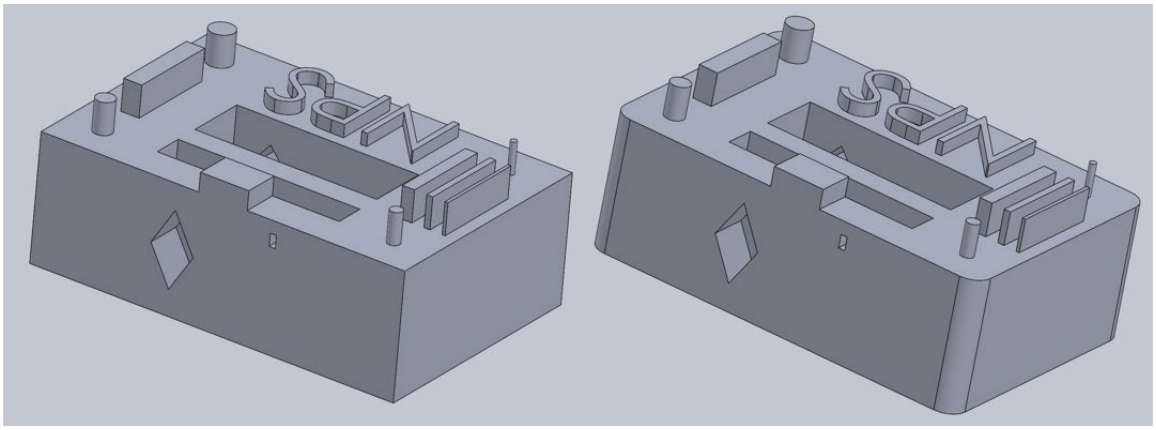

(Sharp corners left, rounded corners right)

Figure 19. Tolerance Piece – Back View

The theory behind the tolerance piece is to test the limitations of the Xerox ElemX to verify what is, and what is not possible for the future designs of the hollow metal parts. Some important features mentioned in the Xerox ElemX Design Guidelines V1.0 [19] that were tested in the tolerance piece include minimum feature dimensions, minimum wall thickness, support structure requirements, overhangs, and considerations to improve productivity. Specifically, for the "considerations to improve productivity," two tolerance pieces were designed. Tolerance Piece Sharp Corners (TPSC) and Tolerance Piece Round Corners (TPRC) were made and a comparison in total print time was computed.

The following three figures, Figures 20–23, show the top, front, and back view of the tolerance piece with labels (A-AH). Measurements were taken of each labeled point and compared to the designed specifications and compared in Tables 13–21 of Appendix A.

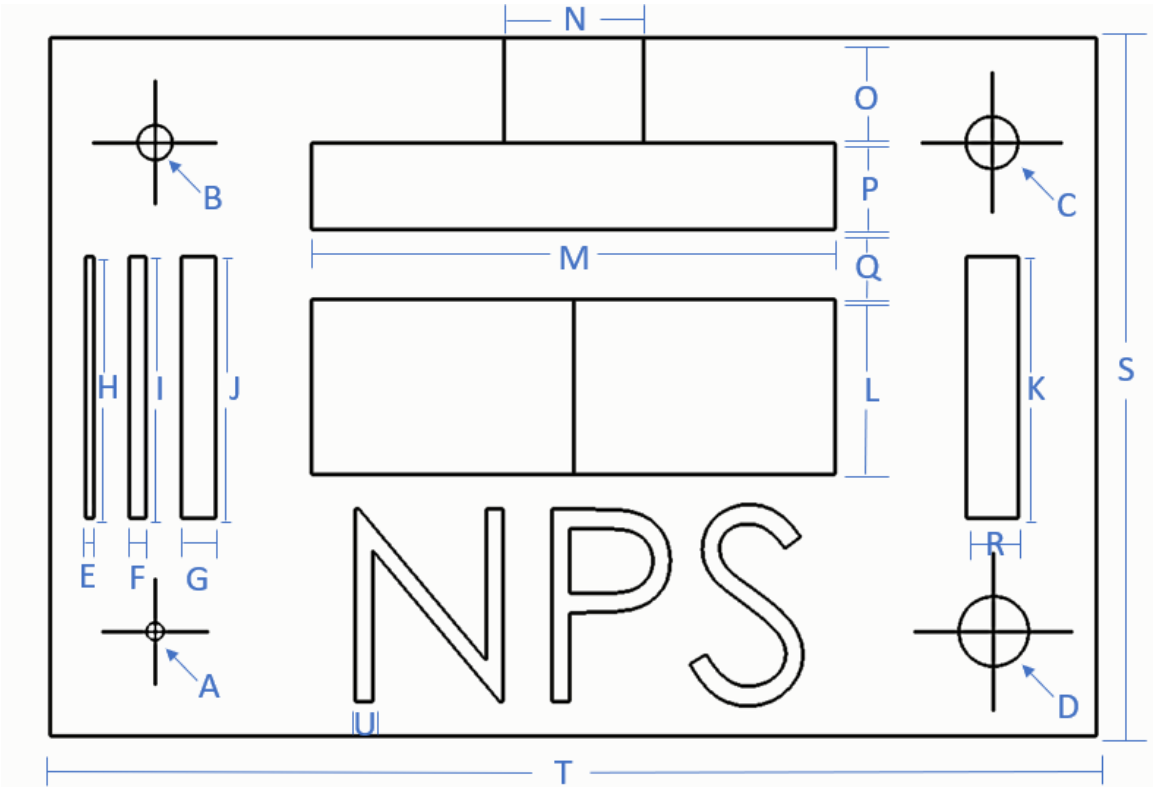

(Sharp corner piece pictured, round corner piece has same labels)

Figure 20. Tolerance Piece Top View Labels

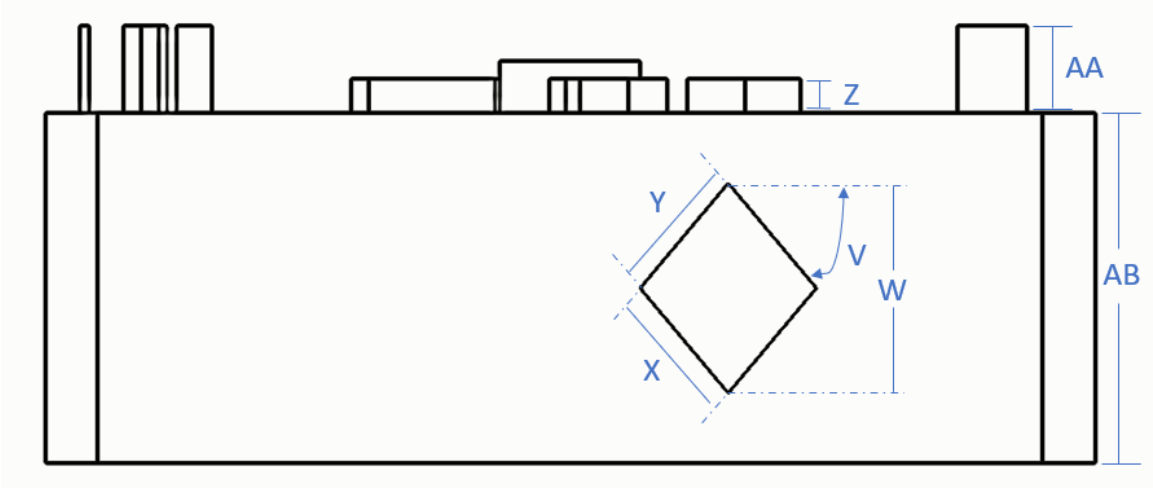

Sharp corner piece pictured, round corner piece has same labels

Figure 21. Tolerance Piece Front View Labels

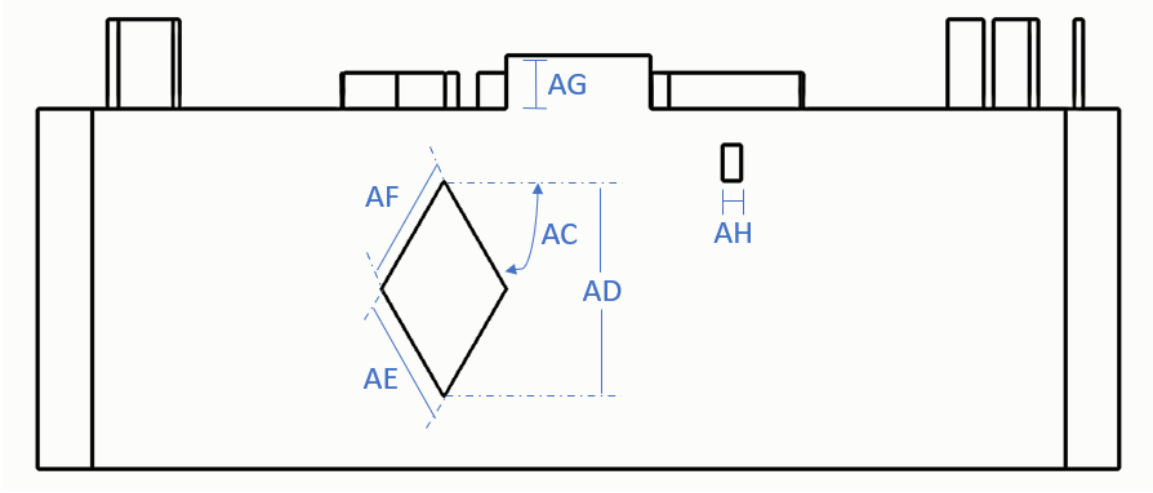

Sharp corner piece pictured, round corner piece has same labels

Figure 22. Tolerance Piece Back View Labels

1. Discussion of Results

A total of eight test pieces were printed. Four TPRC and four TPSC pieces. Four pieces (two TPRC, two TPSC) were printed with 60% frequency, and four pieces (two TPRC, two TPSC) were printed with 100% frequency. The frequency which was adjusted

is that of the current applied to the electromagnetic coil wrapped around the printer's nozzle. Adjusting this frequency will adjust the rate the magnetic field is produced, in turn affect the molten droplet production rate, and melt pool stability.

Appendix A has nine tables showing the specification, measurement, and percent difference for each labeled part on each printed piece. The labeled measurements were also characterized by type of feature. The type of features include exclusion or cut features, if the feature was a detail feature (under 3 mm), the print direction of the features (r,x,y,z), and if the feature is an overhang feature. This chapter will break down the data collected and show the correlations found between type of feature and the accuracy of the print (% difference).

Included under each table is the total time to print each piece. The first noticeable comparison is that the TPRC pieces were printed on average about 2.8% quicker than the TPSC pieces. The theory behind the rounded corners vs. sharp corner pieces is to prove the rounded corners can improve productivity, as the design guide mentions. Although the 2.8% improvement on print time is a noticeable difference, it is also an expected difference. The improved print time is expected because the rounded corner pieces have physically less material to print. The SolidWorks mass properties for the TPRC and TPSC estimate the pieces to weigh 107.43g and 107.84g respectively (0.38% difference). The design guide is correct that rounding corners may improve the machines productivity; however, this improved print time is also expected and is, at least in part, due to less physical material being printed.

There were four orientations measured in this test, r (radial), x, y, and z. Radial is specifically for circular features. Radial was given its own orientation because in this experiment, radial features account for both the x and y direction and the average of those measurements were recorded as one radial measurement. Figure 23 analyzes the relationship between percent difference and the print orientation. The most important correlation seen with radial features is on average they had a positive percent difference. In other words, radial features were mostly over-printed. However, most of the radial features were small features (less than 3 mm) which could account for this error.

The following figures were generated by Kitten Decision Science LLC [20].

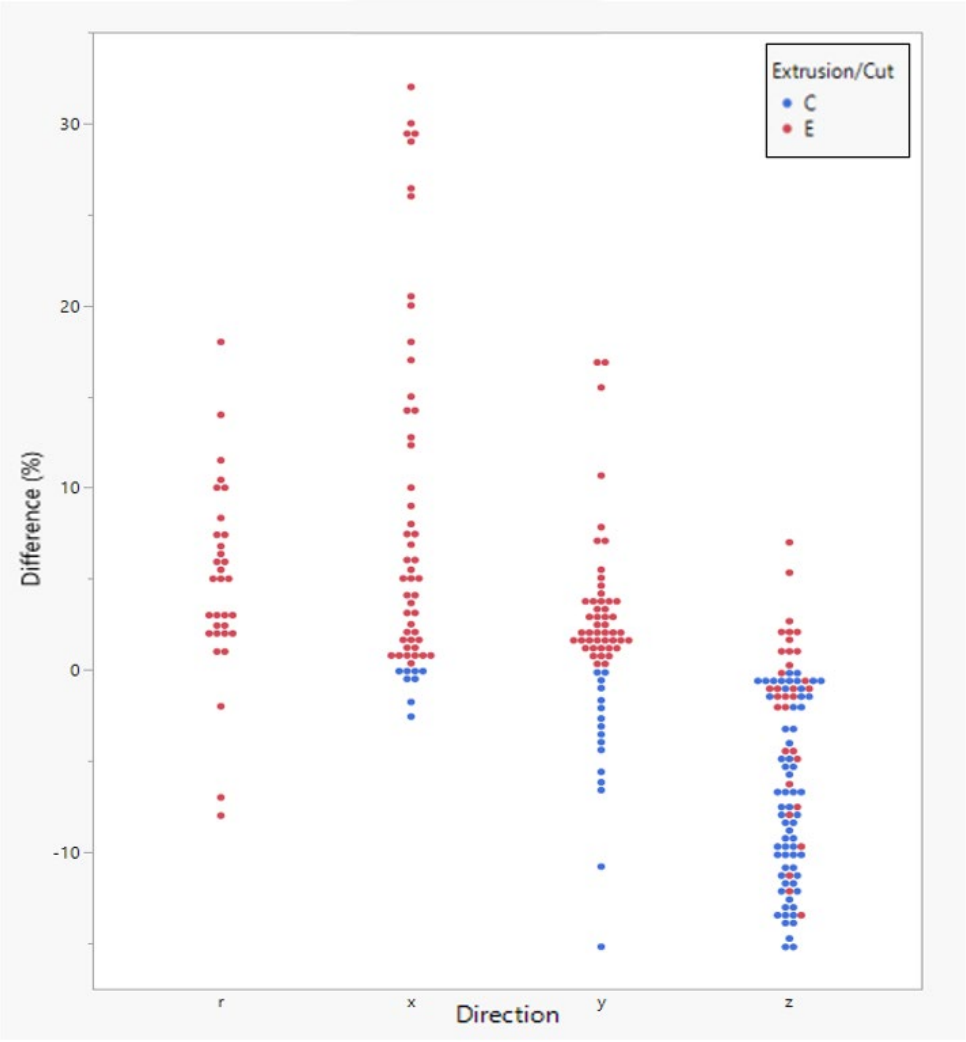

Figure 23. Directionality Based Errors. Extrusion/Cut is also Shown. Source: [20].

Another stand-out correlation in Figure 23 is the x direction had the worst error. This is interesting to note because with the printer, the x and y directions are controlled by similar mechanisms, so one would expect the x and y orientations to have similar error. The z direction error had a negative mean indicating parts usually are undersized in terms of "height." There is a correlation between extrusion features being over printed (positive precent difference) and cut features being under printed (negative percent difference).

These correlations could be random and/or part related, more test pieces with different designs would be needed to be made to confirm this correlation with certainty.

There is an indicated correlation between percent difference and the size of the feature as seen in Figures 24 and 25. Figure 25 helps correlate the specification to the labels as shown in Figures 20–22. The smaller the feature, the worse the error, and vice versa. However, it is important to note the design manual for the printer states the smallest features should be 3 mm. It is clear from Figure 24 that less than 3 mm the print error becomes much worse. This indicates the printer has a lower resolution specification just as the design manual suggests. Figures 24 and 25's appearances are also explained when considering the size of the individual metal droplets. The average size of a single liquid aluminum droplet is 50 µm [6]. 50 µm has a much greater impact on percent difference when compared to smaller features than compared to larger features. Overall, there is a relatively small sample size for each measurement. The previous suggested correlations could be due to chance and more sample data would help determine this.

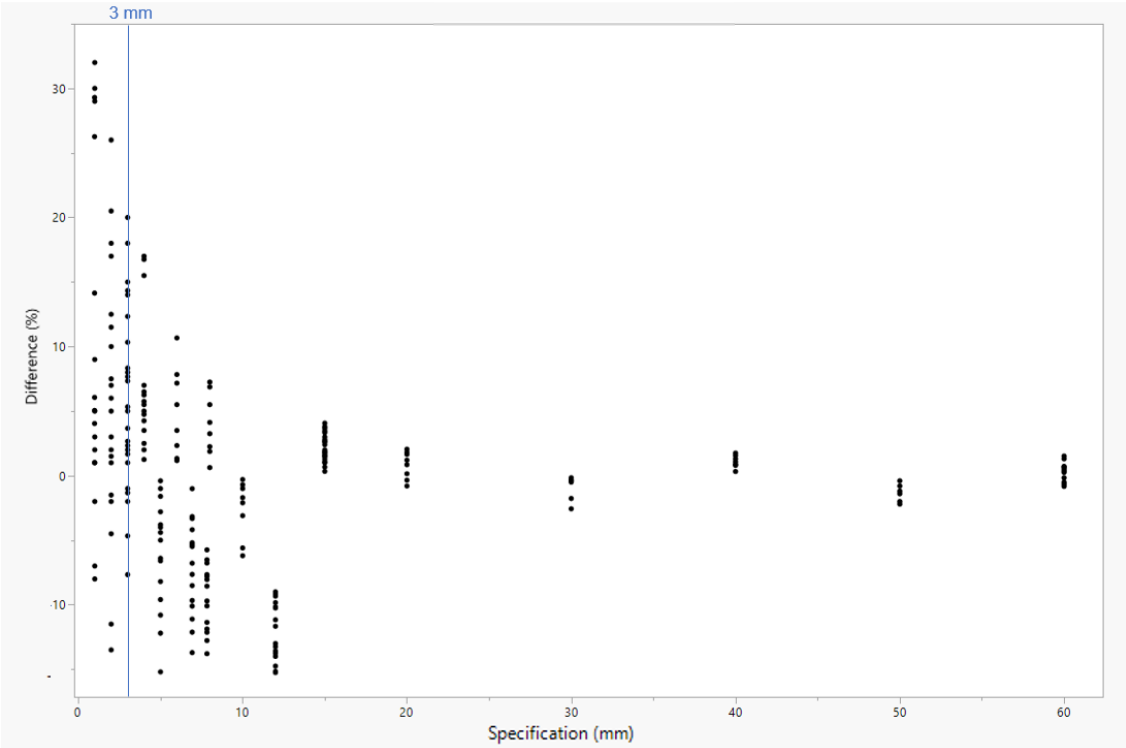

Figure 24. Percent Difference vs. Size of Feature. Source: [20].

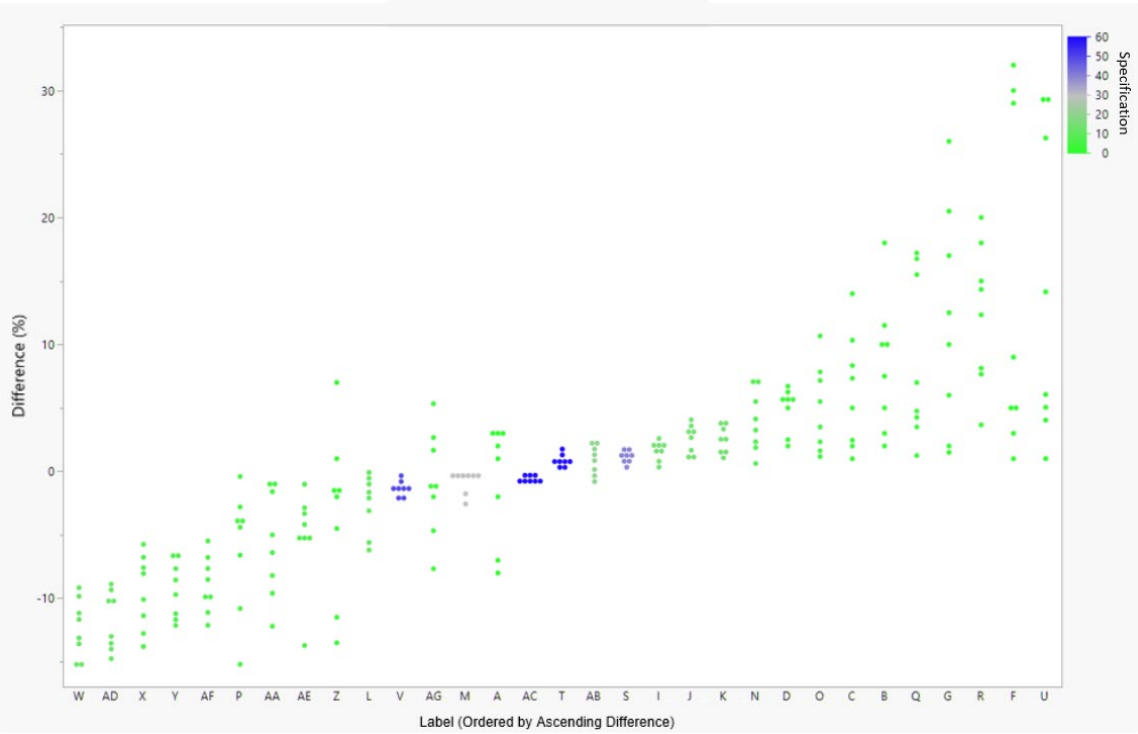

Figure 25. Absolute Difference vs. Label and Specification. Source: [20].

The experiment to determine if the printing frequency improved printer performance returned inconclusive results. The data from the experiment is shown in Figure 26. Although the 100% frequency parts had a wider range of specification error, the average print error between 60% and 100% parts were 0.47 and 0.85 respectively. Almost identical averages considering the relatively small number of parts that were tested. The 60% parts had the largest error at 32% difference however this is only slightly greater than the 100% parts' largest error at 30% difference. The experiment was performed to determine if the lower frequency would improve printer error; however, Figure 26 shows there is a minimal difference between print quality and frequency setting used for the print. The XEROX ElemX manual instructs using 100% frequency for printing and due to the small difference in error, 100% frequency will be used going forward for design purposes.

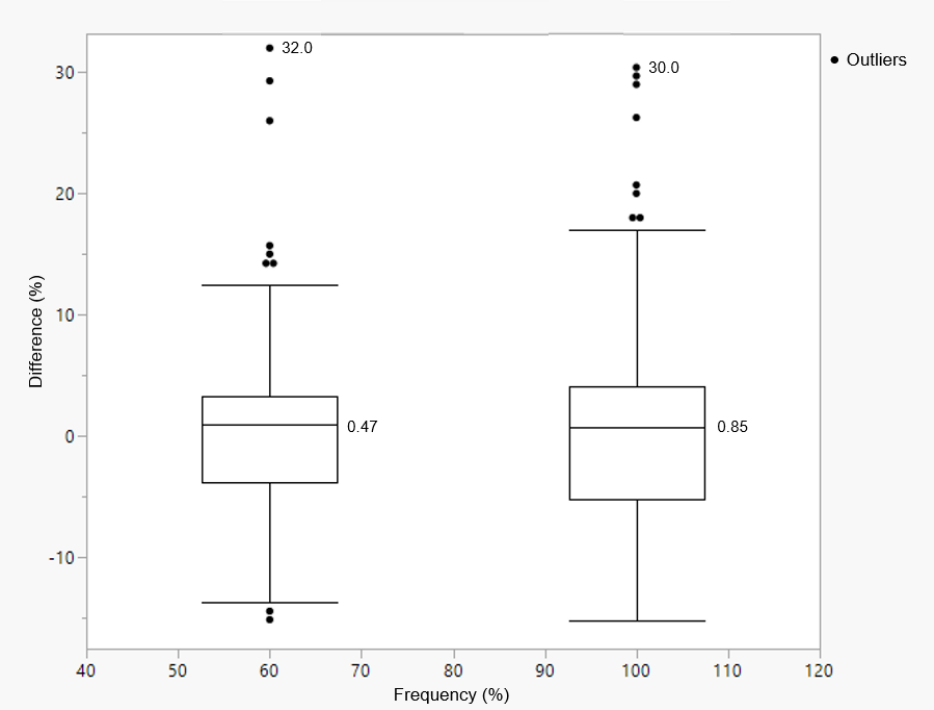

100% frequency = 500 Hz, 60% frequency = 300 Hz

Figure 26. Percent Difference vs. Frequency. Source: [20].

The overhang feature comparison plays a critical role to the design of the hollow metal parts. As the hollow parts will need a way to be closed off at the top, most likely in a conical design (this conical design is discussed more in the next chapter). Figure 27 presents important information on the relationship of overhang features, their accuracy, and the difference in accuracy between the 50° and 60° overhang features in the TPRC and TPSC. The Xerox Design Manual discusses that any overhang feature less than 50° would require support structure [19]. The printer successfully printed both diamond shaped overhang features in the TPRC and TPSC. However, the 60° diamond overhang feature had better results in all areas. The diamond overhang features were measured with respect to diamond angle (V and AC), height (W and AD) bottom arch length (X and AE), and top arch length (Y and AF). In all cases, the 60° features had less error than their respective 50° feature. With only 8 samples printed, this cannot be determined to be conclusive evidence. However, for conservative purposes, and the critical roll overhang features play

in the design of hollow parts, Figure 27 will be considered in the ultimate design of the parts that will be tested.

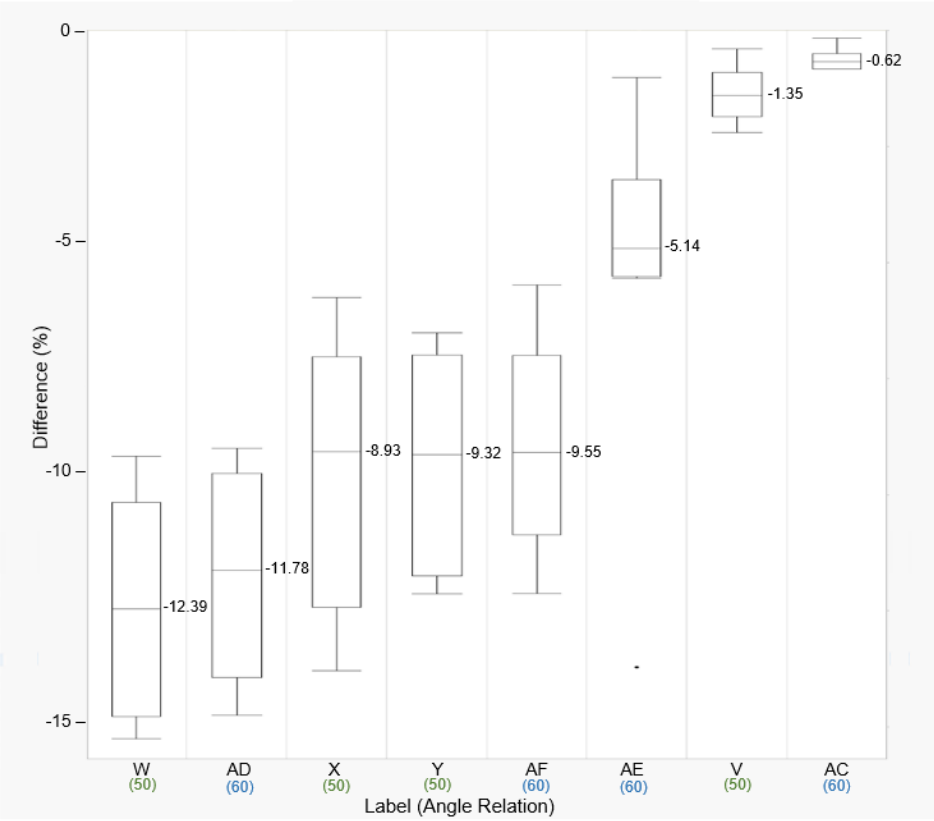

Figure 27. Comparison of Overhang Features. Source: [20].

a. Important design features to discuss that were not captured in graphs

Three features on the tolerance pieces failed to print. Features measured by labels E, H, and AH. Labels E and H are related to the same feature, a thin extruded wall on the top of the tolerance piece. This thin wall had the design dimensions of 0.5 mm x 15 mm. The wall was designed in SolidWorks, however when the file was "sliced," the 0.5mm wall was lost. This observation can be seen in Figure 28.

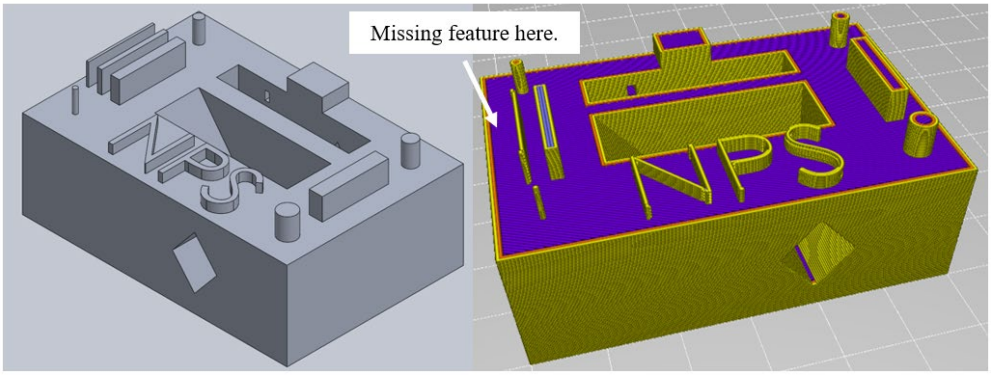

TPSC pictured, TPRC had same results.

Figure 28. SolidWorks Design of TPSC (left) Compared to Xerox Slicer Design of TPSC (right).

Since the feature could not be sliced this indicates the 0.5 mm wall is smaller than the printer's lowest resolution. The design manual suggests the smallest feature has a minimum specification of 3 mm; however, the tolerance pieces show features as small as 1 mm can be printed with relatively good accuracy. Features as small as 0.5 mm cannot be printed as indicated by the 0.5 mm thin wall.

The design criteria as mentioned in Chapter III.1.6 discusses overhang features. The criteria suggest small overhang features are possible if they are less than 2 mm. The AH labeled feature is a small 1 mm overhang that failed to print on all pieces. The best AH feature that was printed was on TPRC (2) 60% as seen in Figure 29.

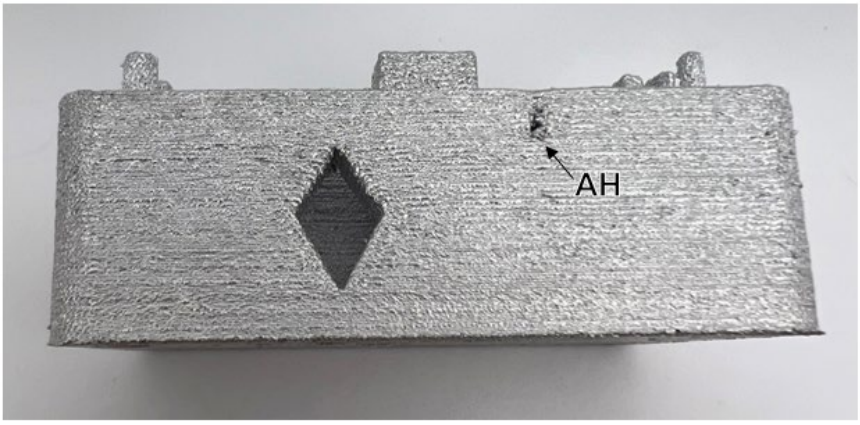

Figure 29. TPRC (2) 60% Back View. AH Feature Labeled

Some test pieces completely closed in the AH overhang feature, and some test pieces attempted to print it but failed in all cases. The most successful AH feature is seen in Figure 29; however, still far below standards and documented as a failed printed feature.

2. Results Summary

The data found suggests there exists a difference in machine error based on the printer output orientation, the size of the feature, if the feature is an extrusion or cut, and if the feature is an overhang feature. Significant data points to notice:

- The worst error occurred in the x direction.
- The z direction error had a negative mean indicating parts usually are undersized in terms of "height."
- There is a correlation between extrusion features being over printed (positive precent difference) and cut features being under printed (negative percent difference).
- There is a correlation between the size of the feature and the percent error. However, is it important to note the printer design manual's minimum feature requirement and the size of the molten metal-droplet and that impact on this correlation.
- There is no significant difference in the printer's error and the print frequency.
- The 60° overhang features met design specifications better than the 50° overhang features.
- The design feature of 2 mm overhangs failed to print on all pieces despite the feature being more conservative than the design manual suggests.

C. PART DESIGN

Now that the experimental guidelines are known, the design can be made in relation to the goals to be achieved. To meet the goals of the research, the designed part must be positively buoyant, be able to support a payload, and be able to sustain substantial sea pressure.

1. Design of Positive Buoyancy

To be positively buoyant, the amount of water displaced by an object weighs more than the object itself [21]. The average density of an object ultimately determines whether the object will sink or float. If an object's average density is less than that of the surrounding fluid, it will float. If the average density is more than the surrounding fluid, it will sink [22]. To build a positively buoyant metal part, the part must have a sufficient volume of air to keep the density less than that of the surrounding seawater.

As shown in Figure 30, the sphere offers the best volume to surface area ratio for a given radius. For a given radius, and assuming the radius is equal to the height in the cylinder and cone designs, a sphere offers 33% more volume than a cylinder and 300% more volume than a cone. Ideally a sphere would be used in the design for this research to maximize the volume while simultaneously using less material as compared to other designs. However, as seen in the last chapter, a perfect sphere is not possible due to the overhang limitations and support restrictions of the printer.

Cylinders offer the second-best volume to surface area ratios when compared to spheres and cones. However, the top, flat portion of the cylinder is not possible to be printed without including supports due to the overhang constraints. The solution to these design constraints is to combine the cylinder and cone designs. As seen in Figure 30, a design with a cone base and a cylinder top will have a large volume equal to that of a sphere, with only a 10.35% greater surface area, and most importantly, this design is feasibly able to be printed. This design offers the best volume to surface area ratio which is possible to be printed. The maximized volume ensures the largest possible air volume which will result in a less dense and positively buoyant object. The small surface area also ensures limited

waste of material. This cone and cylinder design is the same design Galletly (1974) focused on in his work [13].

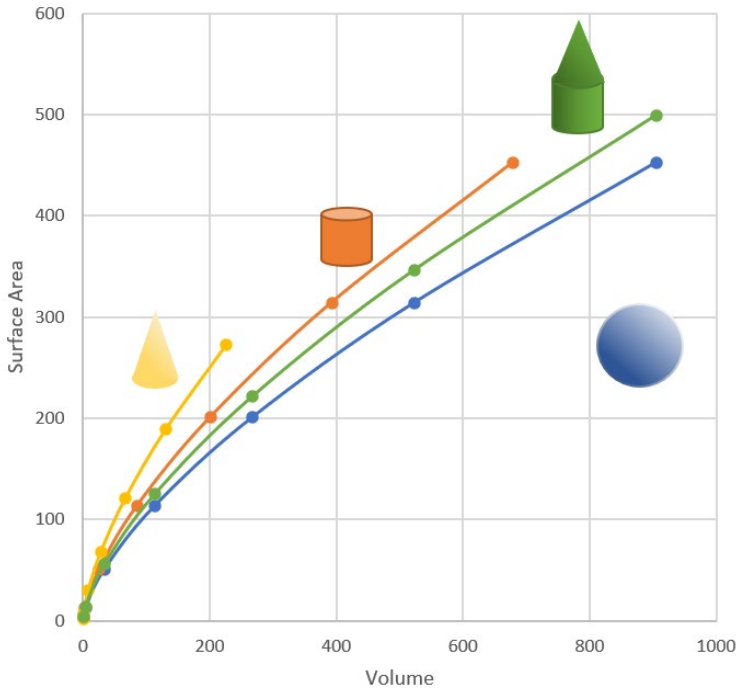

Figure 30. Surface Area vs. Volume for a Cone, Sphere, Cylinder, and Cylinder & Cone

The six designs studied by Galletly are seen above in Figure 7. Three different alpha angles were modeled with angles of 45º, 60º, and 75º. Also, two different L/D designs were made, one with a ratio of 0.5 and one with a ratio of 1.0. Figure 9 shows the results of the buckling testing performed on the test pieces. The model with the best results was model 1 with an alpha of 45º and a L/D of 0.5. The model with the second-best results was model 2 with an alpha of 60º and a L/D of 0.5. Keeping these results in mind and considering the experimental design guidelines found in the last section, the design for the hollow metal part, which this thesis will focus on, can be made.

The SolidWorks image for Configuration 1 is shown in Figure 31. Technical drawings can be found in Appendix B. Ideally the design would exactly replicate the best modeled design from Galletly's work, model 1. However, as seen from the experimental

design guidelines, the diamond overhang feature with a 50º overhang had worse results than the 60º overhang. Also, the 60º overhang did not meet expected standards. Because of this, Configuration 1 was made with a 65º overhang. In relation to Galletly's study, Configuration 1 has an alpha angle of about 25º. Although 25º is much less than Galletly's models smallest angle of 45º, the 25º alpha angle is much better in relation to the design limitations of the printer.

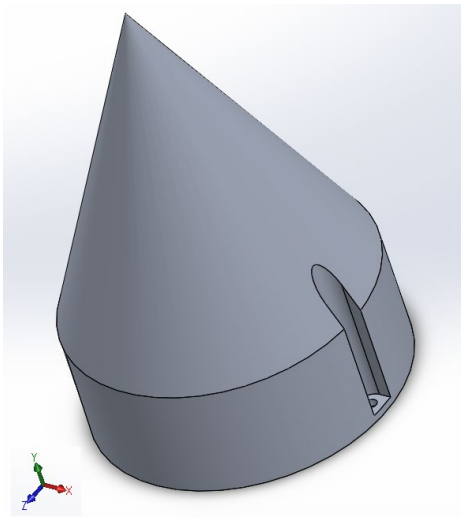

Figure 31. Configuration 1 SolidWorks Image

The wall thickness of Configuration 1 is 1 mm. This was chosen as it was the minimum wall thickness that the printer can support. With a wall thickness of 1 mm, the following expected part density can be calculated.

$$Density_{C1} = \frac{m_{hollow\ part_{C1}}}{V_{solid\ part_{C1}}} = \frac{60.92\ g}{289673.22\ mm^3} = 210.31\frac{kg}{m^3} \quad 4$$

With a 1 mm walled thick part, Configuration 1 has a density of 210.31 kg/m^3, well below the density of seawater at 1026 kg/m^3. The low density of Configuration 1 ensures it will be positively buoyant.

Two more configurations were made with different wall thicknesses than Configuration 1. 1.5 mm wall thickness and 2.0 mm wall thickness for Configuration 2 and Configuration 3 respectively. The increased wall thicknesses should increase the buckling

strength of the hollow metal parts. The buckling of each configuration will be further analyzed in Chapter IV.C Objective 3.

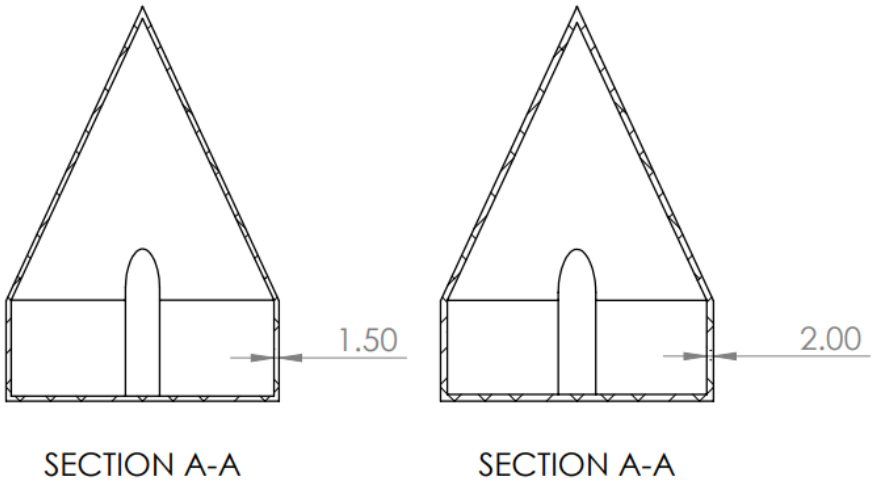

Figure 32. Configuration 2 (left) and Configuration 3 (right) Cross Sections

$$Density_{C2} = \frac{m_{hollow\ part_{C2}}}{V_{solid\ part_{C2}}} = \frac{92.15\ g}{289673.22\ mm^3} = 318.12\frac{kg}{m^3} \quad 5$$

$$Density_{C3} = \frac{m_{hollow\ part_{C3}}}{V_{solid\ part_{C3}}} = \frac{122.44\ g}{289673.22\ mm^3} = 422.68\frac{kg}{m^3} \quad 6$$

With the increased wall thicknesses, Configurations 2 and 3 are still positively buoyant as their densities are far less than seawater. The increased wall thickness may add buckling strength, however the configurations become denser as the wall thickness is increased, as expected. The denser pieces are less positively buoyant and therefore can support less of a payload. The payload support design will be analyzed in the next section.

2. Design to Support a Payload

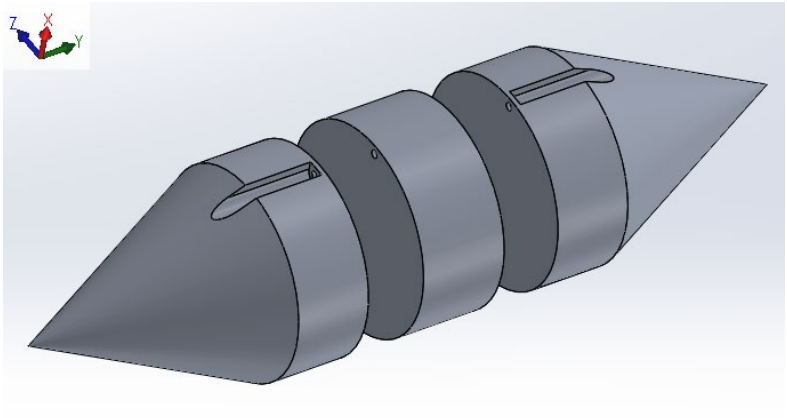

Figure 33. Assembly 1 Exploded View

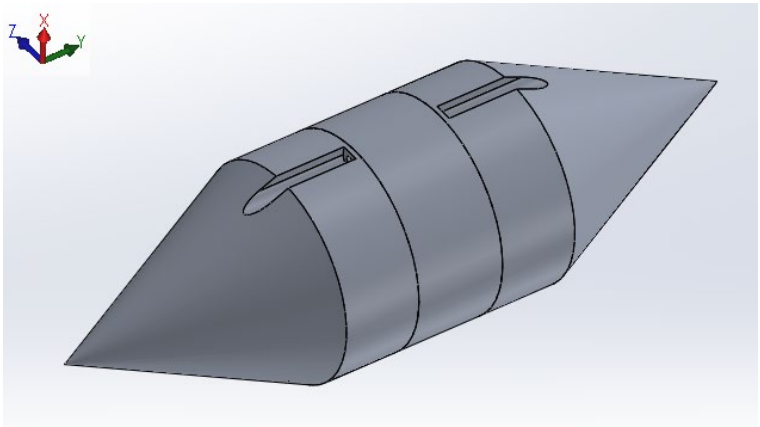

Figure 34. Assembly 1 Attached View

Dissimilar from Galletly's models, the configuration designs include two cut extruded notches 180º apart. These notches allow for the configurations to be fastened together with a "payload" between them. Future work will discuss the applicability of the payload. This research will focus on if the ability of an additive manufactured hollow metal part to support a payload and remain positively buoyant. For this study a 453 g (~1 lb.) payload was designed. The actual designed mass is 456.73 g. The following density calculations were made for each assembly 1 through 3. The assemblies correlate to Configurations 1 through 3.

$$Density_{A1} = \frac{m_{Assembly1}}{V_{Assembly1}} = \frac{578.57\ g}{749768.42\ mm^3} = 771.67 \frac{kg}{m^3} \quad (7)$$

$$Density_{A2} = \frac{m_{Assembly2}}{V_{Assembly2}} = \frac{641.03\ g}{749768.42\ mm^3} = 854.97 \frac{kg}{m^3} \quad (8)$$

$$Density_{A3} = \frac{m_{Assembly3}}{V_{Assembly3}} = \frac{701.61\ g}{749768.42\ mm^3} = 935.77 \frac{kg}{\mathrm{m}^3} \quad (9)$$

As seen in the above equations, all configurations in an assembly with the 1 lb. payload have a density less than that of seawater (1026 kg/m^3), and therefore will be positively buoyant. In the last section it was mentioned that the increased wall thickness would add buckling strength, however it would also increase the parts density and therefore limit the ability to support a payload. All three configuration designs can support a 453 g (~1 lb.). payload and remain positively buoyant; however, the density calculations show Configuration 1, the design with the thinnest walls, could possibly support much more than a 1 lb. payload as its density is the lowest at 771.67 kg/m^3. Depending on the results of the buckling testing, this inverse correlation between wall thickness and ability to support a payload will be considered in the ultimate design of the configuration.

3. Design to Sustain Substantial Sea Pressure

In this section, the Stress Analysis Manual [23], MATLAB, and Ansys were used to help prove the thin-walled configurations can support substantial sea pressure. To prove the thin-walled configurations can support substantial sea pressure, the following steps were taken:

1. Analyze the buckling stress of multiple thin-walled cylinders under external pressure using MATLAB and the Stress Analysis Manual [23].
2. Prove Ansys analysis simulation works for a simple long cylinder under a compressive axial load.
3. Compare the Ansys Eigenvalue buckling analysis for thin-walled cylinders to MATLAB values.

a. Analysis of thin-walled cylinders under external pressure with MATLAB.

As discussed in III.E, the buckling determination for the cone-cylinder design is very complex. The Stress Analysis Manual discusses the cone to cylinder transition but only in context to pressure vessels with internal pressure [23]. This study focuses on the cone to cylinder transition in reference to external pressure or sea pressure. In a first step to prove the configurations can support substantial sea pressure, an analysis was done using MATLAB to analyze multiple models of the thin-walled simple cylinders under external pressure.

Section 8.3.1.3.1 of the Stress Analysis Manual breaks down the cylinders critical buckling equations into three different types, based on the length of the cylinders evaluated. It is important to mention the qualification of a thin-walled vessel per the Stress Analysis Manual requires a radius to wall thickness ratio greater than 10 [23]. The critical buckling equations and criteria for use are summarized in Table 2.

Table 2. Critical Stress of Cylinders under External Pressure. Adapted from [23].

Type	Criteria	Formula	Eq #
Short Cylinders	$\frac{L^2}{rt} < 100$	$F_{cr} = \frac{k_y \pi^2 E}{12(1-\mu_e^2)}\left(\frac{t}{L}\right)^2$	10
Long Cylinders	$100 * \frac{t}{r} < \left(\frac{L}{r}\right)^2 < 5 * \frac{r}{t}$	$F_{cr} = 0.93E\left(\frac{t}{r}\right)^{\frac{3}{2}}(\frac{r}{L})$	11
Very Long Cylinders	$5 * \frac{r}{t} < \left(\frac{L}{r}\right)^2$	$F_{cr} = \eta\frac{0.25E}{(1-\mu_e^2)}\left(\frac{t}{r}\right)^2$	12

F_{cr} – critical stress

L - length of cylinder

r – radius of cylinder

t – wall thickness

E – modulus of elasticity

μ_e – elastic Poisson's ratio

η – plasticity-reduction factor given by:

$$\eta = \frac{E_s}{E} = \frac{(1-\mu_e^2)}{(1-\mu)}\left(\frac{1}{4}+\frac{3}{4}*\frac{E_t}{E_s}\right) \qquad 13$$

k_y – obtained from Figure 35

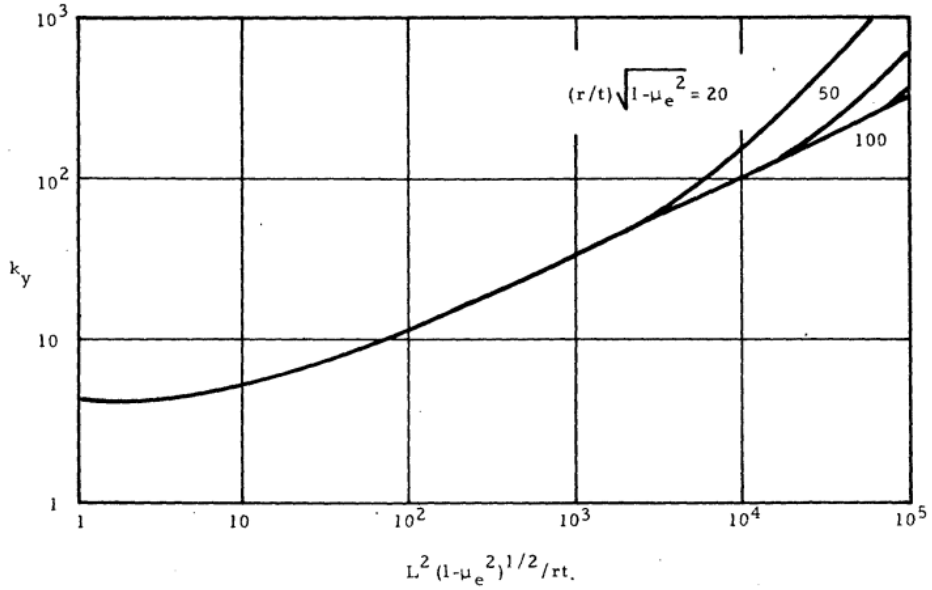

Figure 35. Chart To Obtain k_y. Source: [23].

MATLAB was used to generate three plots in relation to the three critical stress scenarios outlined in the Stress Analysis Manual. The scripts used can be found in APPENDIX B.

The following three figures, Figures 36–38, help visualize the relationship between the thin-walled cylinders design and the design's relationship to a cylinder's respective critical buckling load from an external pressure source. The length of the cylinders is on

the y axis and varied from 30 mm to 600 mm. The thickness of the thin-walls is on the x-axis and varies from 1 mm to 3.5 mm. The radius was kept constant at 30 mm. In Figure 37 the depths greater than 10,000 m were dismissed and graphed as white to help visualize the shallower depths. The following key takeaways can be noted from the graphs:

- For analysis type 3, very long cylinders (VLC), with the previously mentioned length, radius, and thicknesses, the crush depth is between 40m and 1200 m.
- There is a very small difference between analysis type 1, short cylinders (SC), and analysis type 2, long cylinders (LC).
- Analysis type 1 and analysis type 2 have expected crush depths varying from 50m to 4600m depending mostly on wall-thickness.
- In relationship to Configuration 1, with a wall thickness of 1 mm, the crush depth is around 50m to 350m varying minimally with length.

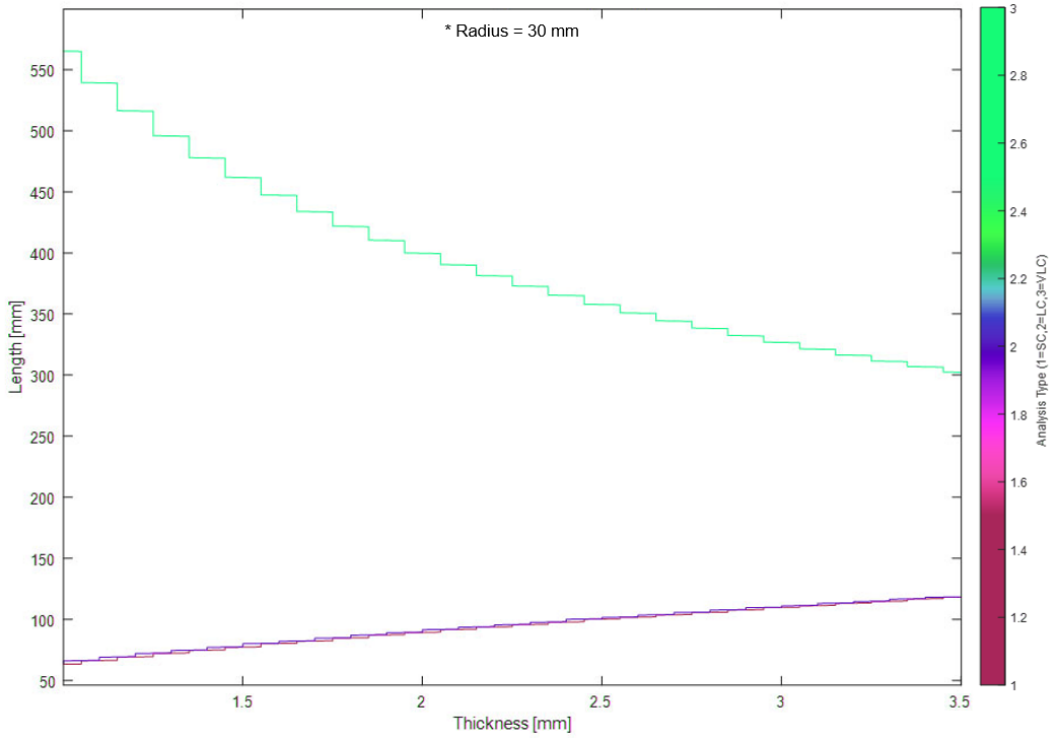

Figure 36. Length vs. Thickness and Analysis Type

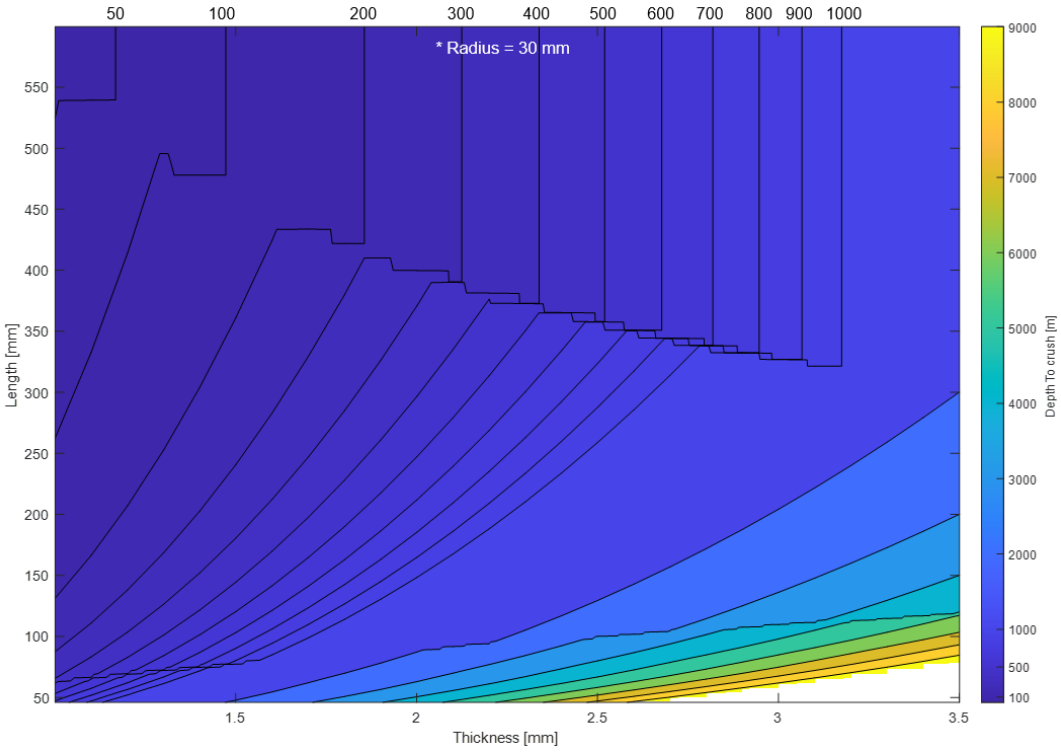

Figure 37. Length vs. Thickness and Depth to Crush

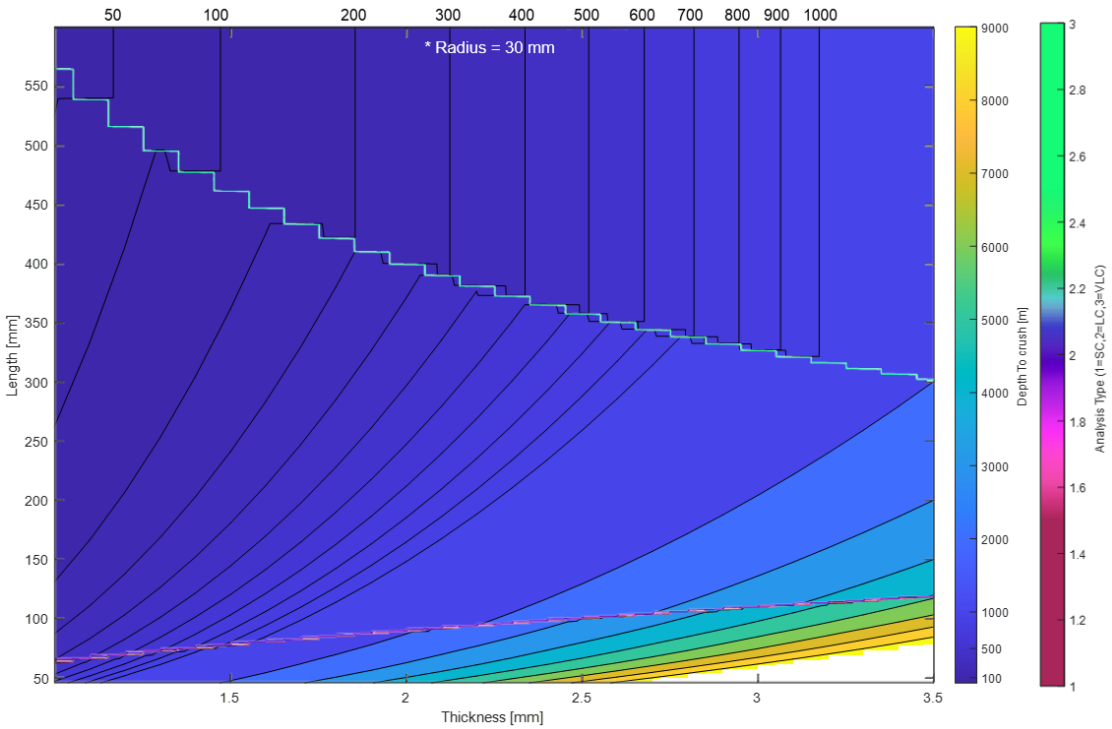

Figure 38. Overlay of Figure 36 and Figure 37

b. Comparison of Ansys and MATLAB results

The next step to prove the configurations can support substantial sea pressure, was to use Ansys Eigenvalue buckling analysis and compare the results to the MATLAB results. Before diving straight into Eigenvalue buckling analysis of thin-walled cylinders under external pressure, the first goal was to prove Ansys could replicate a simpler buckling analysis found in the Stress Analysis Manual [23]. Chapter 2 (Column Analysis) of the Stress Analysis Manual introduces critical buckling loads for columns under different conditions. For a fixed-free column the critical buckling can be calculated using Euler's solution [23]:

$$P_{cr} = \frac{\pi^2 EI}{4L^2} \qquad 14$$

In this case P_{cr} is the critical buckling load, E is the modulus of elasticity, I is the minimum moment of inertia, L is the length. For comparison's sake, an example problem

was made. Goal is to find the buckling load of a fixed-free column that is 5.5m long, outer diameter of 130 mm, thickness of 13 mm, with a modulus of elasticity of 70 GPa.

$$P_{cr} = \frac{\pi^2 EI}{4L^2} = \frac{\pi^2 * 70 * 10^9\, Pa * 8.2773 * 10^{-6}\, m^4}{4 * (5.5m)^2} = 47260.8\, N \qquad 15$$

Eigenvalue buckling is a linear analysis tool inside of Ansys to find critical buckling loads. The problem was entered into Ansys and simulated using the criteria described above. Figure 39 displays the results as well as the simulated total deformation from mode 1 failure. The table in the bottom right of Figure 39 displays the different modes of failure as well as their respective load multipliers. The load multiplier is a scalar value which represents how much greater or less than the applied load will cause the buckling. From the calculated results using equations from the Stress Analysis Manual, a critical load of 47260.8 N was found. When this load was applied to a fixed-free column in Ansys, the mode 1 failure has a load multiplier of 1.0147. In other words, Ansys simulated the same buckling analysis as the Euler's solution to within 1.47% accuracy.

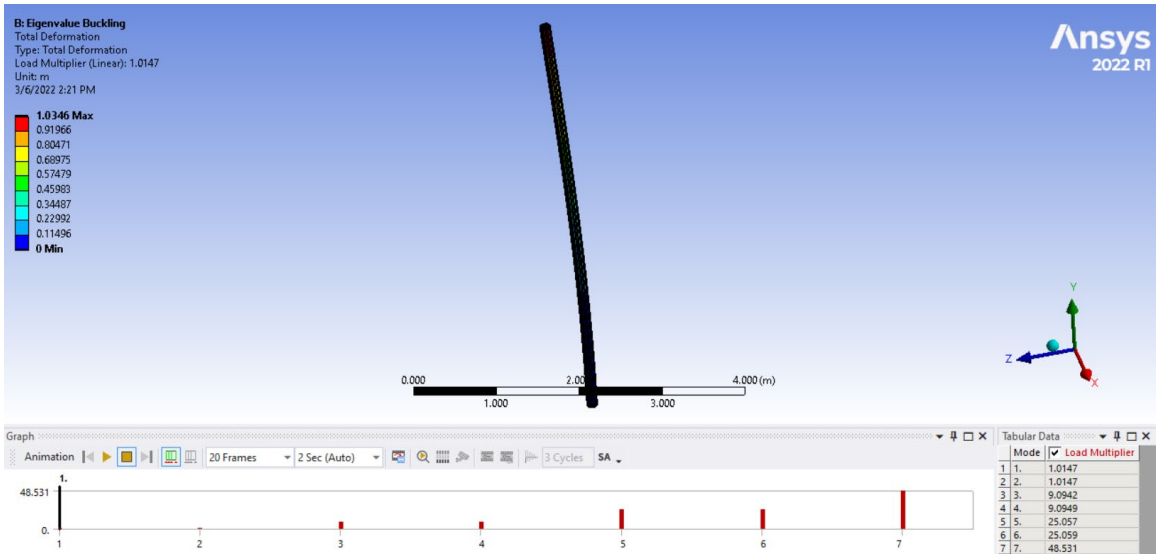

Figure 39. Ansys Analysis for Theoretical Long Cylinder

SolidWorks was used to design twelve thin-walled cylinders (r/t >10) that match the criteria in Table 2, and can be used to compare the results found from MATLAB. Summary of the twelve designs is in Table 3.

Table 3. Summary of SolidWorks Cylinder Designs

Type	**Name**	**Radius (r) (mm)**	**Length (L) (mm)**	**Wall Thickness (t) (mm)**
Short Cylinder 1	SC1	40	30	1
Short Cylinder 1.5	SC15	40	30	1.5
Short Cylinder 2	SC2	40	30	2
Short Cylinder 5	SC35	40	30	3.5
Long Cylinder 1	LC1	40	200	1
Long Cylinder 1.5	LC15	40	200	1.5
Long Cylinder 2	LC2	40	200	2
Long Cylinder 5	LC35	40	600	3.5
Very Long Cylinder 1	VLC1	40	600	1
Very Long Cylinder 1.5	VLC15	40	600	1.5
Very Long Cylinder 2	VLC2	40	600	2
Very Long Cylinder 5	VLC35	40	600	3.5

The buckling analysis performed in Figure 39 had clear and easy to control boundary conditions (BCs). The cylinder was fixed at the base, and free at the top. However, for thin-walled cylinders that are being simulated being exposed to deep sea pressure, it is not as simple to control the boundary conditions. The cylinders being exposed to deep sea pressure are not fixed to anything; they are experiencing an external pressure from all sides of the cylinder. Symmetry and displacement BCs were used to overcome this obstacle.

Figures 40 and 41 display the usage of symmetry and displacement BCs to perform the buckling analysis on the thin-walled cylinders. Figure 40 shows a symmetry region with respect to the z axis. Two more symmetry regions were also made with respect to the x and y axis (not pictured). Figure 41 shows the displacement BC which allows zero displacement in the z direction and free to move conditions in both x and y axis. Two more displacement conditions were made in the same manor with respect to the other two symmetry regions (not pictured). This combined usage of symmetry and displacement BCs allows Ansys to simulate a model being exposed to an external pressure from all sides. Figure 69 in Appendix C shows the MATLAB script which was used to find the critical buckling pressure for each model using the equations from Table 2. MATLAB analysis and Ansys buckling analysis was performed for the twelve cylinder designs and the results are seen in Table 4.

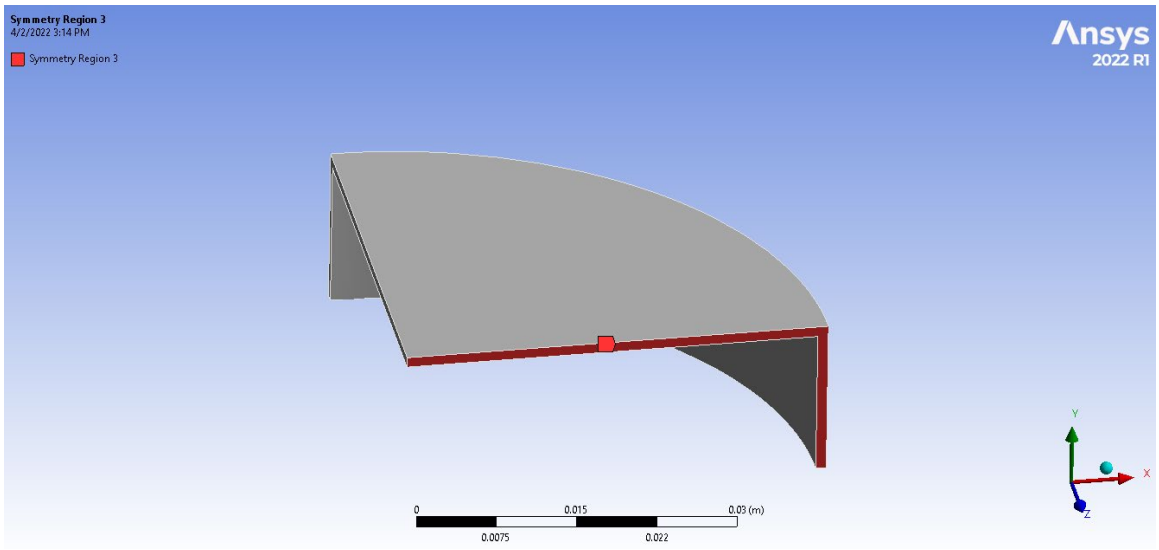

Figure 40. Symmetry Region 3 on SC1, Symmetric to Z Axis

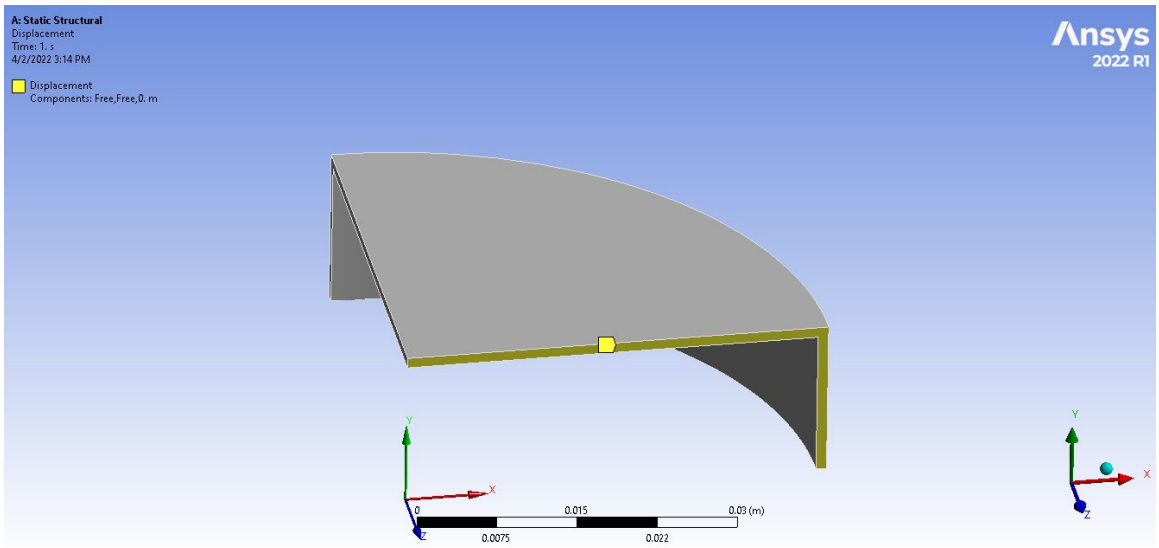

Figure 41. Displacement BC on SC1 (Free, Free, 0m)

Table 4. MATLAB Buckling vs. ANSYS Buckling of Thin-Walled Cylinders Under External Pressure

Name	MATLAB P_{CR} (Pa)	ANSYS P_{CR} Mode 1 (Pa)	Percent Difference
SC1	$2.680*10^8$	$4.813*10^6$	-98.20
SC15	$5.168*10^8$	$6.474*10^6$	-98.75
SC2	$8.377*10^8$	$1.664*10^7$	-98.01
SC35	$2.224*10^9$	$1.067*108^8$	-95.20
LC1	$5.220*10^7$	$1.895*10^6$	-96.37
LC15	$9.590*10^7$	$6.330*10^6$	-93.40
LC2	$1.477*10^8$	$1.242*10^7$	-91.59
LC35	$3.418*10^8$	$3.400*10^7$	-90.05
VLC1	$1.245*10^7$	$2.120*10^6$	-82.97
VLC15	$2.801*10^7$	$3.364*10^6$	-87.99
VLC2	$4.980*10^7$	$4.970*10^6$	-90.02
VLC35	$1.525*10^8$	$1.721*10^7$	-88.71

The results found in Table 4 were highly unexpected. When Ansys was used in comparison to the Euler's formula for buckling of a fixed-free cylinder, they matched to within 1.47% accuracy. However, the percent difference between Ansys and MATLAB for the thin-walled cylinders was over 80% in all cases with an average percent difference of -92.61%. The SC models had the worst error with an average of -97.54%, followed by LC models with an average error of -92.85%, and the "best" models were the VLC models with an average error of -87.43%. Ansys significantly undervalued the critical pressure in comparison to MATLAB. The percent error did tend to become less, in other words Ansys analysis matched MATLAB analysis more closely, as the cylinders became longer. It is

interesting as the Euler example had success for a long cylinder, and the thin-walled cylinders' analysis became more accurate as the models became longer (or more closely matching the Euler problem).

It is important to note that the Ansys analysis was performed under default mesh analysis settings (MAS). The critical pressures found in Table 4 were all from mode 1 of the analysis. The next section will look to improve the Ansys analysis by performing a finite mesh analysis (FEA) and investigate more modes of failure to determine the large error that was found in Table 4.

D. ANSYS FINITE ELEMENT ANALYSIS (FEA)

In a first attempt to investigate the difference between the Ansys results and the MATLAB results, an investigation into the mesh settings was performed. The SC1 model was chosen to perform the mesh analysis on as it is the smallest model in terms of volume and surface area. The small volume and surface area helps with computational complexity and time. By default, Ansys uses a mesh resolution of 2. Changing the mesh resolution changes the number of nodes and elements on the model being analyzed, which in term changes the results found from different analyses. Table 5 shows the nine different Mesh Analysis Settings (MAS), the resolution, number of nodes, and number of elements.

Table 5. Summary of Mesh Analysis Settings on SC1

MAS	Resolution	Nodes	Elements
1	2 (default)	1824	811
2	4	5372	2528
3	6	17719	8612
4	7 (Highest Setting)	49797	27096
5	Body Spacing 0.0008	69508	40773
6	Body Spacing 0.0005	240957	152193
7	Body Spacing 0.0005 Hex Dominant	106098	21597
8	Body Spacing 0.0004 Hex Dominant	217452	47330
9	Body Spacing 0.0003 Hex Dominant	442979	97735

The settings ranges from a lowest of resolution 2 (default settings) to a highest of a resolution with body spacing 0.0003 hex dominant mesh. To help visualize these meshes, Figures 42 and 43 on the next page show how the mesh look on the model.

The increased resolution and changing of mesh settings can be seen in Figures 42 and 43. The default mesh settings uses triangles to shape the elements. Body spacing allows the user to control the size of the element and the hex dominant setting changes the shape of the elements from triangles to four sided polygons. Multiple eigenvalue buckling experiments were run on SC1 with the nine different MAS and eight modes of failure.

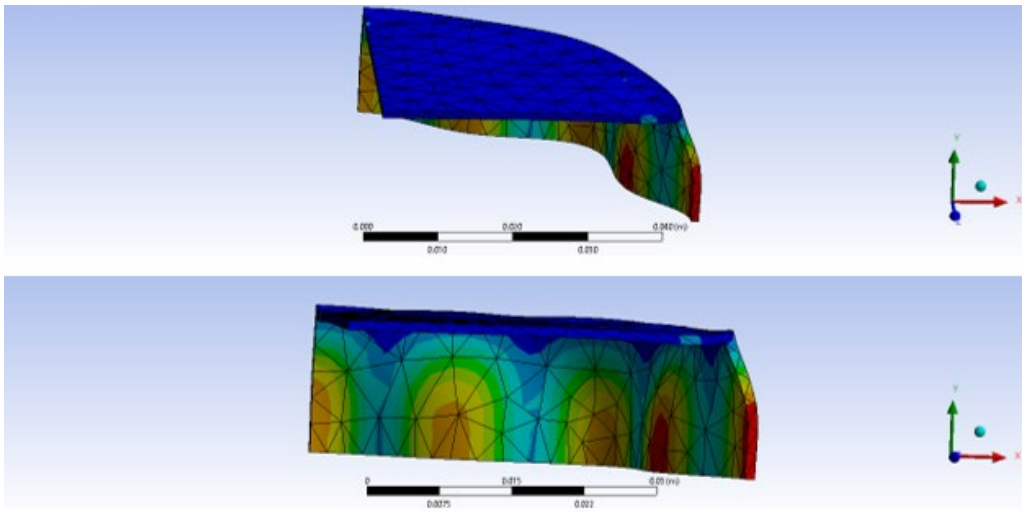

Figure 42. MAS 1 Visualization

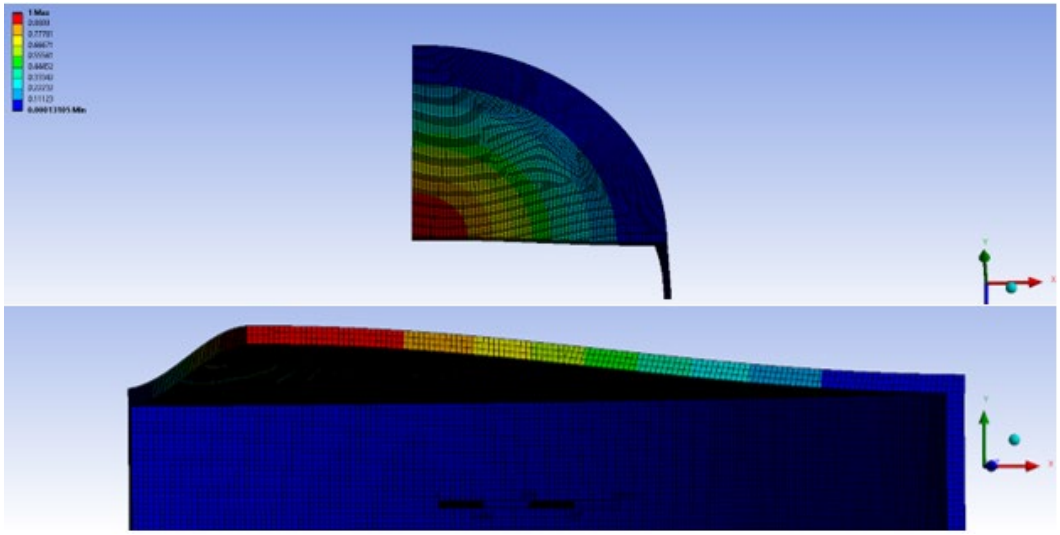

Figure 43. MAS 9 Visualization

Figure 44 breaks down the finite mesh analysis comparison for the SC1 model. The buckling pressure is on the y axis and the eight different buckling modes on the x axis. It is clearly visible that aside from MAS 1 (the default MAS in Ansys), the results trended very well. In fact, MAS 3–9 have almost indistinguishable results and appear to be graphed as one line on Figure 44. An investigation into the different MAS and the effect on results will be discussed with Figure 45.

The last takeaway from Figure 44 is the trend with all nine MAS of the increase in buckling pressure as the mode type increased. The lowest mode result reflects the most conservative form of buckling found by the linear analysis and is usually the mode of interest [24]. The Ansys User Manual discusses how the eigenvalue buckling analysis is a linear perturbation tool used to find multiple modes of a buckling analysis [24]. As the number of modes increases, the frequency of the perturbation is increased. Although these higher modes are typically unlikely, analyzing multiple modes of failure can be useful as not all real-world examples are perfectly built as they are modeled. Figure 44 shows the buckling pressure increase as the mode number increases. This trend is expected as the software is designed to show the most conservative result first, followed by less conservative results.

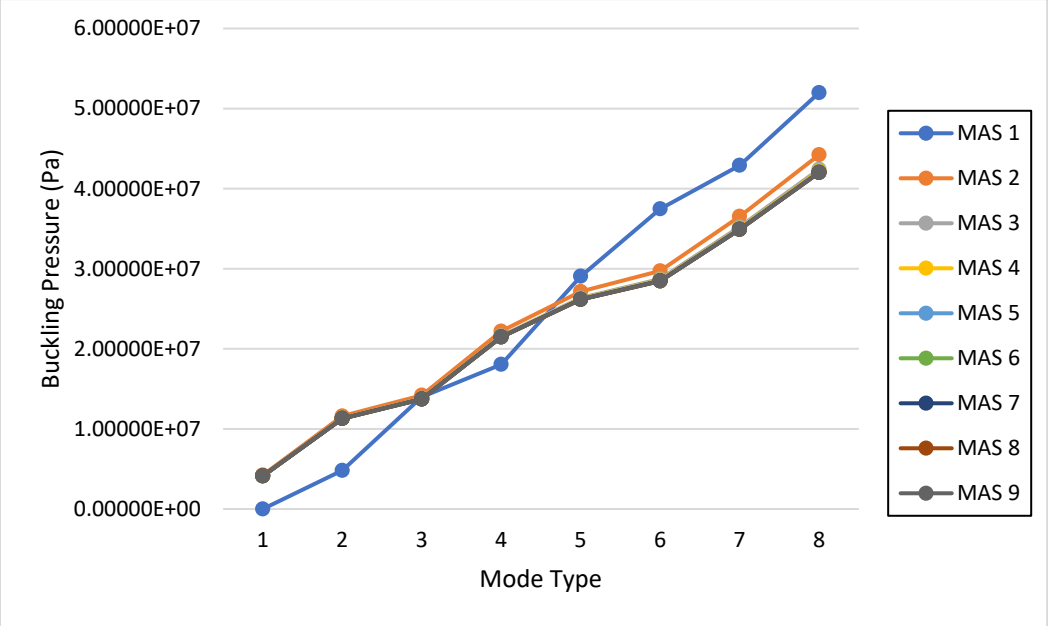

Figure 44. Finite Mesh Analysis Comparison

To help further investigate if the MAS was improving the buckling results of Ansys, Figure 45 was generated. On the left y axis is the percent error between the Ansys result and the MALAB buckling results. The x axis is each MAS, and the right y axis is to show the number of elements and nodes in each MAS. As shown in Figure 45, mode 1 is the

most conservative mode of failure and mode 8 is the least conservative. Therefore, the trend of Mode 1 analysis having the worst error as compared to mode 8 is expected.

What is important to take away from Figure 45 is the percent error is almost unchanged from MAS 4 and greater. It was hypothesized from Figure 44 that MAS 3–9 were identical however there is a slight change in error from MAS 3 to 4. These results indicate any attempt to refine the mesh greater than MAS 4 did not improve any results. MAS 9 has almost ten times the number of nodes MAS 4 has, however the error in the analysis does not change. From these results, MAS 4 (Ansys resolution 7) was chosen for future buckling analysis. MAS 4 was chosen because its results are indistinguishable from MAS 5 though MAS 9, and most importantly, the fewer nodes and elements in MAS 4 allows the buckling analysis to be computationally efficient.

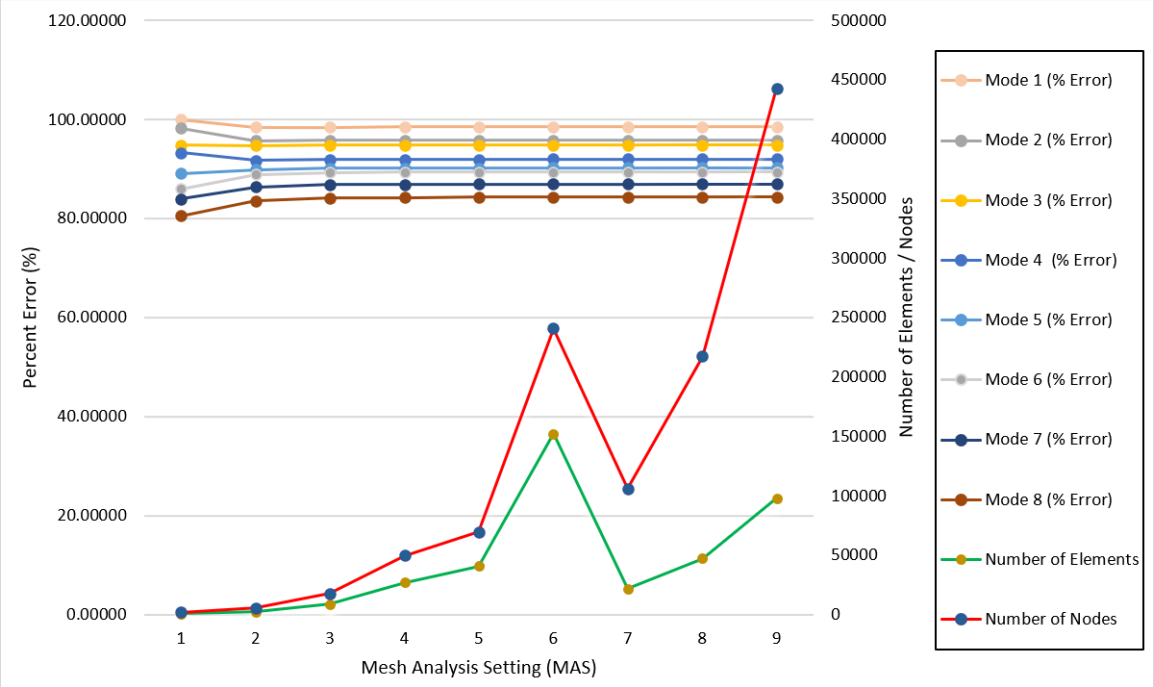

Figure 45. Percent Error vs. MAS vs. Number of Elements / Nodes

E. EXPLORATION TO MATCH ANSYS MODES WITH MATLAB RESULTS

Once the MAS was established, there was an investigation to see if Ansys could match the buckling pressure determined by MATLAB. All models from Table 4 were used in this analysis. The results are summarized in Table 6.

Table 6. Identifying Ansys Modes with MATLAB Buckling Results

Name	MATLAB P_{CR} (Pa)	ANSYS P_{CR} (Pa)	ANSYS Mode Number	Percent Difference
SC1	$2.680*10^8$	$2.679*10^8$	610	0.003
SC15	$5.168*10^8$	-	> 1000	-
SC2	$8.377*10^8$	-	> 1000	-
SC35	$2.224*10^9$	-	> 1000	-
LC1	$5.221*10^7$	$5.220*10^7$	118	0.170
LC15	$9.590*10^7$	$9.651*10^7$	58	-0.630
LC2	$1.477*10^8$	$1.485*10^8$	33	-0.541
LC35	$3.418*10^8$	$3.510*10^8$	13	-2.622
VLC1	$1.245*10^7$	$1.241*10^7$	33	0.321
VLC15	$2.801*10^7$	$2.853*10^7$	27	-1.820
VLC2	$4.980*10^7$	$5.016*10^7$	19	-0.724
VLC35	$1.525*10^8$	$1.660*10^8$	4	-8.131

When analyzing the data presented in Table 6 it is important to remember previous guidance from the Ansys User Manual. The Manual mentions mode 1 is the most conservative, and most likely mode of failure [24]. The higher modes are linear perturbations of the eigenvalue buckling that can produce helpful results in some cases

[24]. The Ansys User Manual suggests using six modes of failure in the analysis [24]. This suggestion is experiment dependent and not suitable for all cases.

In this experiment, the SC model struggled to match the MATLAB numerical results. For the SC1 model, it took 610 modes to find a result which closely resembled the numerical results from MATLAB. For SC15, SC2, and SC35, Ansys failed to reach a numerically matching result in over 1000 modes analyzed. As the Ansys User Manual suggests analyzing 6 modes, the analysis was stopped after modes greater than 1000 and marked as failed.

The LC and VLC models produced better but not ideal results. Aside from LC1, LC15 though VLC35 produced numerically matching results in under 60 modes. The best results came from LC35 and VLC35, which produced results similar to the MATLAB analysis by mode 13 and mode 4 respectively. Using the guidance of the Ansys User Manual, the only valid buckling result for the thin-walled cylinders is the VLC35 model. Even though the VLC35 result had a -8.131 percent error as compared to the MATLAB analysis, the result came from a mode four analysis. The SC and LC models had results that occurred at too high of modes which do not replicate real life expectations.

It is important to note that the most viable result came from VLC35, which more coincidently resembles a long cylinder than when compared to SC and VL. To recall, the most accurate results between Ansys and MATLAB, in this paper, came from the long cylinder under axial compression as discussed in III.C.3.b. This correlation leads to a hypothesis that the Ansys eigenvalue buckling analysis works best for long columns under axial compression.

The following key takeaways can be made from the previous analysis that will be carried into future experiments:

- SC and VL did not produce viable results.
- VLC35 produced the most viable result as it came from a mode four experiment.

- The most viable result came from a very long thin-walled cylinder which closely resembles a long solid cylinder.

F. COMPARING ANSYS TO GALLETLY (1974)

In 1974, G.D. Galletly performed experiments to analyze the buckling of thin-walled cone and cylinder models [13]. The testing and results were summarized in section II.E. Galletly had success in matching theoretical buckling to experimental buckling [13]. Galletly used BOSOR 3 and BOSOR 5 for his computational analysis [13]. BOSOR is a variational finite-difference (VFD) computer program used to find lateral bending in elastic plates [13]. When used to determine the buckling of thin-walled cone and cylinder models, BOSOR had results which were within 5% accurate of experimental results [13]. Galletly's models closely resemble the configuration models designed in this paper.

SolidWorks was used to make the same models Galletly used in his experiments. The models were imported into Ansys and eigenvalue buckling analysis was performed and compared to Galletly's BOSOR results. Six modes of buckling were analyzed as recommended by the Ansys User Manual [24]. Appendix D has a table of the full results from the analysis comparison.

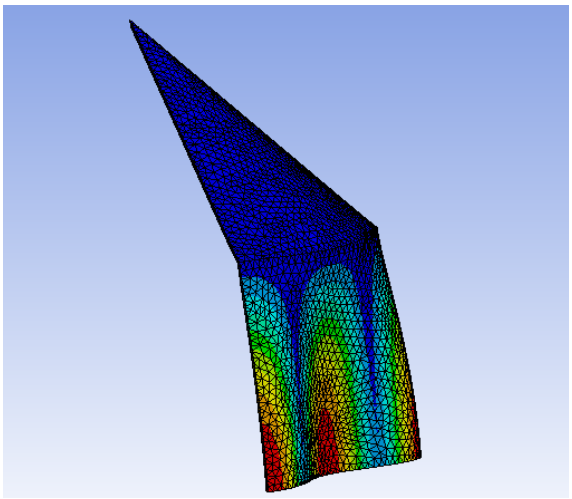

Symmetry and Displacement BCs were used for the Analysis

Figure 46. Galletly's Model 1 in Ansys. Deformation for Mode 1 is Shown.

Table 7. Shortened Summary of Ansys Buckling Results Compared to Galletly Buckling Results

Galletly Model No.	L/D	Alpha Angle	Ansys Mode	Ansys Buckling (Pa)	Galletly BOSOR (Pa)	Galletly Experimental (Pa)	%Diff Ansys to BOSOR	%Diff Ansys to Exp
1	0.5	45°	1	4541400	4123210	3854305	10.14	17.83
2	0.5	60°	1	4174300	3254440	2826950	28.26	47.66
3	0.5	75°	1	2587700	1447950	1275575	78.71	102.87
4	1	45°	1	2288800	1978865	1923705	15.66	18.98
5	1	60°	1	2301600	1978865	1889230	16.31	21.83
6	1	75°	1	2314000	1447950	1282470	59.81	80.43

Although Galletly's BOSOR computation was able to produce theoretical results that closely resembled the experimental results for his models, the Ansys eigenvalue buckling results did not have as much success for the same models. The best results came from model 1, with a 10.14% percent difference between the Ansys results to the Galletly BOSOR results, and a 17.83% percent difference between the Ansys results and the Galletly experimental results.

A review of Figures 7 and 9 from II.E would be helpful for the following discussion. Models 1 through 3 had an L/D ratio of 0.5, and models 4 through 6 had an L/D ratio of 1. L/D is a ratio of length to depth. Galletly also varied his model's alpha ratios. In terms of the models' designs, the alpha ratio changed the slope of the cone portion of the models. There is a trend between Ansys eigenvalue accuracy and the alpha ratio. Models 1 and 4 have alpha angles of 45° and these models also had the best accuracy in the eigenvalue analysis. Models 3 and 6 have alpha angles of 75° and these models had the worst accuracy in the eigenvalue analysis.

Two trends that were found in previous eigenvalue analysis and discussed earlier in this research have been noticed again:

1. Models 1 and 4, that have alpha angles of 45°, had the best results in the eigenvalue analysis.
2. Models 3 and 6, that have alpha angles of 75° and more closely resemble short cylinders, had the worst results in the eigenvalue analysis.

THIS PAGE INTENTIONALLY LEFT BLANK

IV. RESULTS AND DISCUSSION

A. OBJECTIVE 1 – POSITIVE BUOYANCY

Objective 1 was to build positively buoyant hollow metal parts using liquid metal AM. From the printing process, the positive buoyancy of Configurations 1 through 3 was easily observed in the part removal process. To remove parts from the XEROX ElemX build plate, the build plate is removed from the printer and submerged in a tank of water. For Configurations 1 through 3, when the build plate was submerged, the parts would detach themselves from the build plate and float on the surface of the water.

Although positive buoyancy was the objective, this research went a step further to prove these parts had potential use in the undersea warfare community. On the XEROX ElemX, parts are printed by individual droplets combining over time to form one final structure. Although appearing uniform to the naked eye, there may be small lines or cracks between the droplet boundaries. A part may be able to float immediately, but over time have leakage through these droplet boundaries and cause the structure to eventually sink. To test this theory, the following test was performed on Configurations 1 through 3.

Leakage Test

A leakage test was performed on Configurations 1 through 3. The test consisted of tethering each configuration to a 6.8 kg (15 lb.) kettlebell weight which was then submerged in a bucket of water. The tethered configurations remained submerged for 24 hours and then were taken out to determine if leakage had occurred between the metal droplets. Four configurations could be tested as once. Three rounds of tests were performed, a round for each configuration model. A graphic of the test is seen in Figure 47 and a photo taken during test 1 is seen in Figure 48.

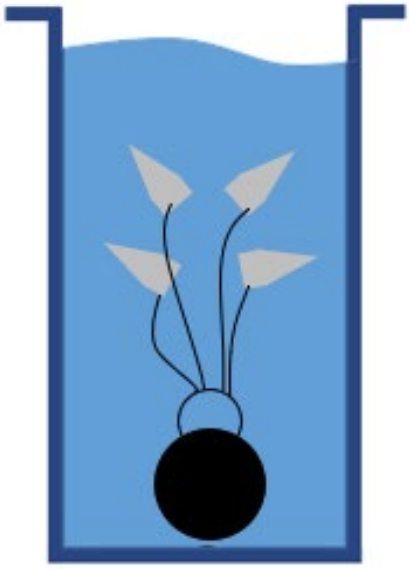

Figure 47. Leakage Test Model

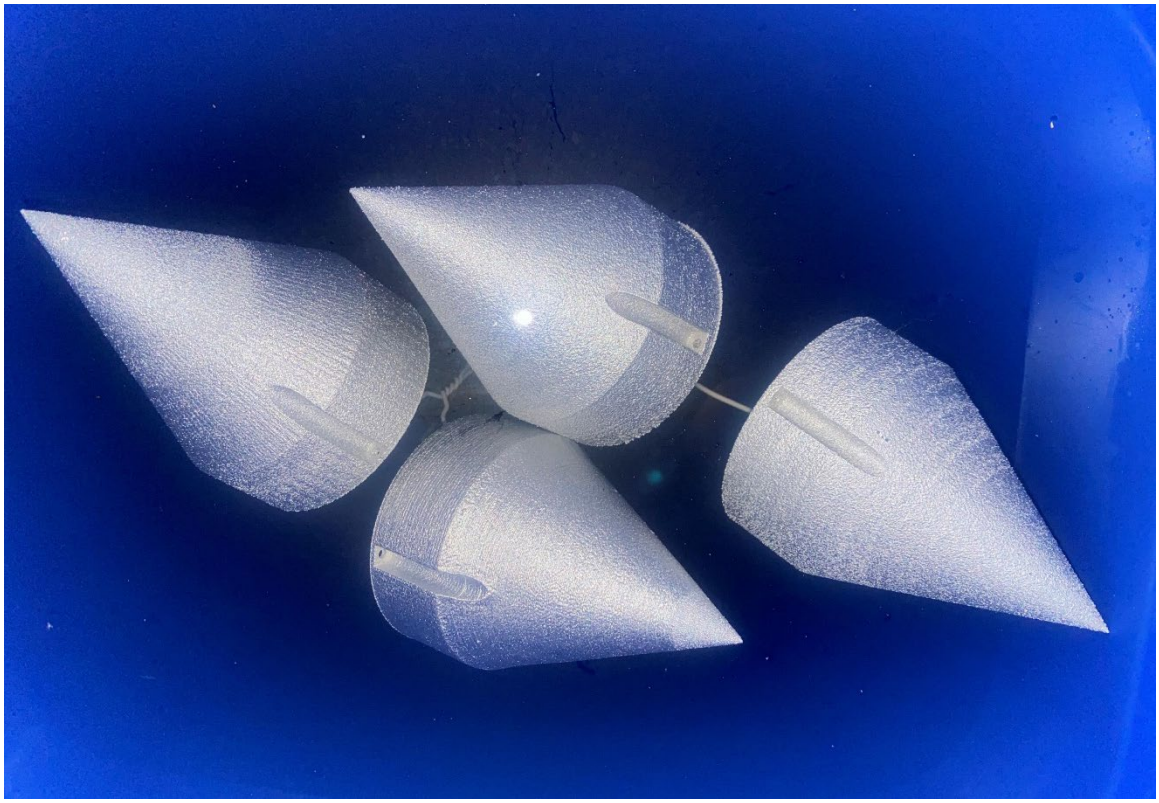

Figure 48. Leakage Test 1 Taken from Top Down View

The results as shown in Table 8 may be initially misleading. Configuration 1 had a 50% success rate, Configuration 2 had a 75% success rate, and Configuration 3 had a 100% success rate. Although it appears wall thickness correlates with ability to prevent water leakage, this is not definitive and could be random based on the printer's accuracy. More test pieces would need to be printed and tested to verify this. In all cases in which leakage occurred, there were no visible cracks or holes on the test pieces. Leakage was identified as water could be heard inside of the model after they were removed from the water. Concluding that there was small microstructural leakage occurring. Enough leakage to make an accumulation of water inside the models, but not enough leakage to make the test pieces sink in 24 hours of testing.

Table 8. Leakage Test Results

Configuration Number	**Wall Thickness (mm)**	**Number of Layers in Slicer**	**Pass/Fail**
1	1	1	Pass
1	1	1	Pass
1	1	1	Fail
1	1	1	Fail
2	1.5	2	Pass
2	1.5	2	Pass
2	1.5	2	Pass
2	1.5	2	Fail
3	2	4	Pass
3	2	4	Pass
3	2	4	Pass
3	2	4	Pass

Overall, the test proved to be successful as leakage was found to be occurring at a microstructural level that was not expected to occur from visual observation of the models. As noted, the correlation between wall thickness and leakage prevention could be random as only twelve test pieces were tested. However, the results will be noted and considered in the final design.

B. OBJECTIVE 2 – PAYLOAD SUPPORT

Objective 2 was to prove the configurations could support a payload and remain positively buoyant. Two different payloads were designed and for the test. Figure 49 shows the two payload types and the payload inserts. Table 9 has a breakdown of the different payload design parameters. Payload v1 is a solid 453 g (~1 lb.) payload. Payload v2 is a ring-shaped cylinder 453 g (~1 lb.), that was made to have adjustable weight inserts added to it to help control buoyancy. Drawings for the payloads and inserts can be found in Appendix B – Design Drawings, Figures 64–66.

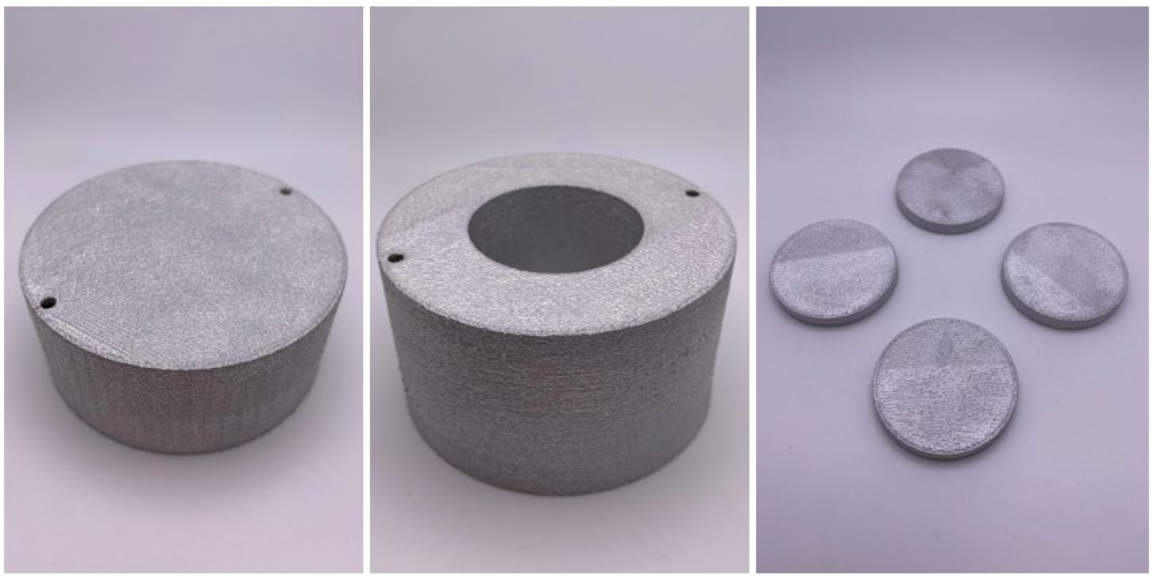

Figure 49. Payload v1 (left), Payload v2 (middle), and Payload Inserts (right)

Table 9. Summary of Payload Parts and Inserts

Name	Weight (g)	Outer Radius (mm)	Inner Radius (mm)	Height (mm)
Payload v1	456.73	40	N/A	34
Payload v2	452.95	20	20	45
Payload Inserts (x8)	16.01	19.5	N/A	5

Note: 1 lb. = 453.59 g

From Chapter III.C.2, the densities of the configuration and Payload v1 assemblies were calculated and shown to be theoretically buoyant. The calculations are shown below:

$$Density_{A1} = \frac{m_{Assembly1}}{V_{Assembly1}} = \frac{578.57\ g}{749768.42\ mm^3} = 771.67\frac{kg}{m^3} \quad 16$$

$$Density_{A2} = \frac{m_{Assembly2}}{V_{Assembly2}} = \frac{641.03\ g}{749768.42\ mm^3} = 854.97\frac{kg}{m^3} \quad 17$$

$$Density_{A3} = \frac{m_{Assembly3}}{V_{Assembly3}} = \frac{701.61\ g}{749768.42\ mm^3} = 935.77\frac{kg}{\mathrm{m}^3} \quad 18$$

There are some minor differences between designed mass and printed mass. Both SolidWorks and the XEROX Slicer have mass calculations, however the actual mass is always slightly different than both the SolidWorks and Slicer mass calculations. Table 20 in Appendix E has a summary of the printed parts and the mass comparison of each part. In general, the mass differences is negligible in comparison to the overall mass of the parts.

Payload Test

The payload test set up to prove the goal of objective 2. For this test, a clear tank was used for the buoyancy of the assemblies could be observed. Parts that passed the leakage test were used for the payload test. There are two subsections of the payload test. The first was to attach the Payload v1 and observe the buoyancy. All assemblies were

expected to pass with Payload v1. The second test involved using Payload v2. If an assembly passed supporting Payload v1, Payload v2 was attached and payload inserts were added to see how this affected buoyancy. Figures 50–52 show Configurations 1 through 3 during the Payload v1 test, all passed.

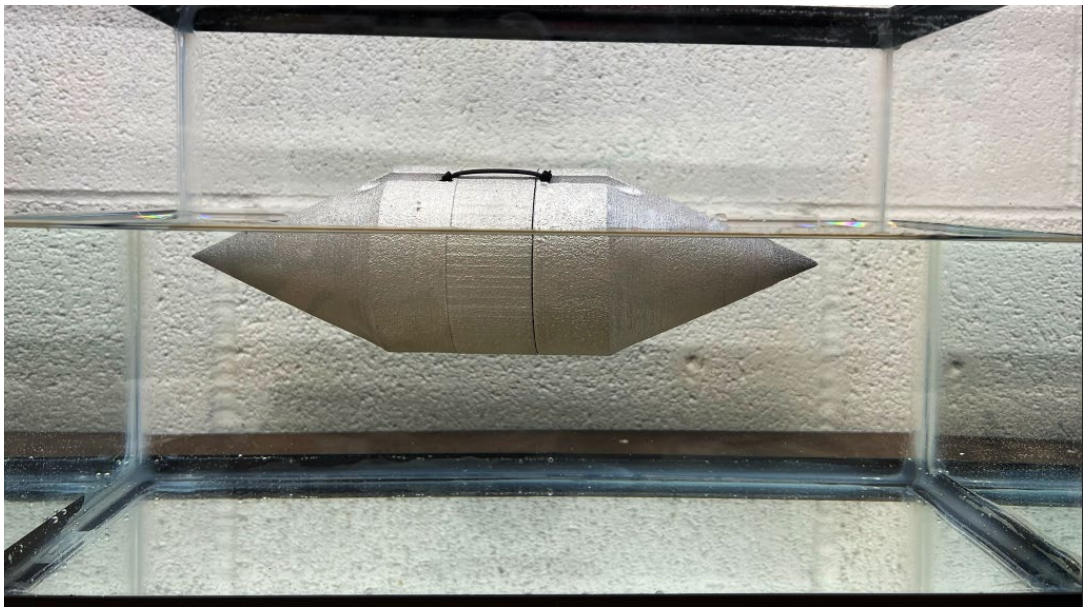

Figure 50. Assembly 1 During Payload v1 Test (Using Configuration 1 – 1 mm Walls)

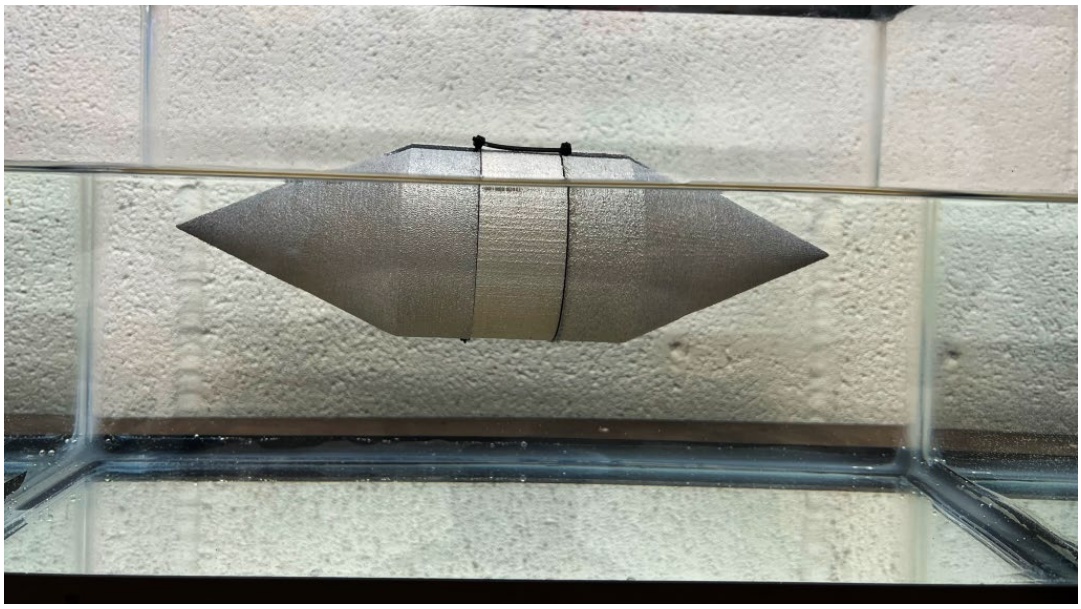

Figure 51. Assembly 2 During Payload v1 Test (Using Configuration 2 – 1.5 mm Walls)

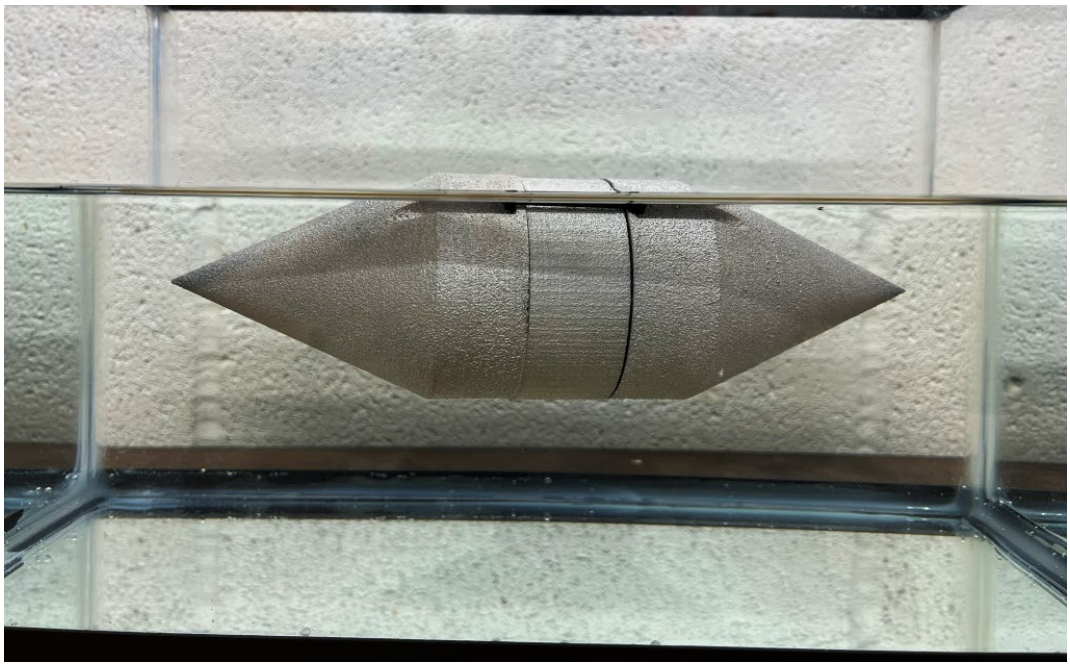

Figure 52. Assembly 3 During Payload v1 Test (Using Configuration 3 – 2 mm Walls)

All assemblies passed using the Payload v1 test. These results were expected from the previous density calculations showing the densities were less than seawater and

therefore should be positively buoyant and float. Payload v2 was used for the next payload test. Payload v2 is roughly 453 g (~1 lb.) and has nine insertable weights available to add to the payload (each weight weighs roughly 15 g).

A summary of the results can be found in Table 10. Table 10 shows the Assembly name, which Configuration model was used, the number of weight inserts (if applicable), the calculated density, and the expected and actual results.

Table 10. Results from the Payload Tests

Name	Configurations Used	Number of 15g Inserts	Calculated Density (kg/m^3)	Expected Float or Sink	Results
Assembly 1	1	-	771.67	Float	Float
Assembly 2	2	-	854.97	Float	Float
Assembly 3	3	-	953.77	Float	Float
Assembly 4	1	0	761.99	Float	Float
Assembly 5	1	1	781.87	Float	Float
Assembly 6	1	2	801.76	Float	Float
Assembly 7	1	3	821.64	Float	Float
Assembly 8	1	4	841.53	Float	Float
Assembly 9	1	5	861.41	Float	Float
Assembly 10	1	6	881.30	Float	Float
Assembly 11	1	7	901.18	Float	Float
Assembly 12	1	8	921.07	Float	Float
Assembly 13	1	9	940.96	Float	Float
Assembly 14	2	0	844.79	Float	Float

Name	Configurations Used	Number of 15g Inserts	Calculated Density (kg/m^3)	Expected Float or Sink	Results
Assembly 15	2	1	864.68	Float	Float
Assembly 16	2	2	884.56	Float	Float
Assembly 17	2	3	904.45	Float	Float
Assembly 18	2	4	924.33	Float	Float
Assembly 19	2	5	944.22	Float	Float
Assembly 20	2	6	964.10	Float	Float
Assembly 21	2	7	983.99	Float	Float
Assembly 22	2	8	1003.87	Float	Float
Assembly 23	2	9	1023.76	Float	Float
Assembly 24	3	0	925.10	Float	Float
Assembly 25	3	1	944.99	Float	Float
Assembly 26	3	2	964.87	Float	Float
Assembly 27	3	3	984.76	Float	Float
Assembly 28	3	4	1004.64	Float	Float
Assembly 29	3	5	1024.53	Float	Float
Assembly 30	3	6	1044.41	Sink	Sink
Assembly 31	3	7	1064.30	Sink	Sink
Assembly 32	3	8	1084.18	Sink	Sink
Assembly 33	3	9	1104.07	Sink	Sink

The results from the payload test matched the expected results exactly. As soon as the calculated density passed the density of seawater (1026 kg/m^3), the assembly sank. Figures 53–56 show some important points of the test.

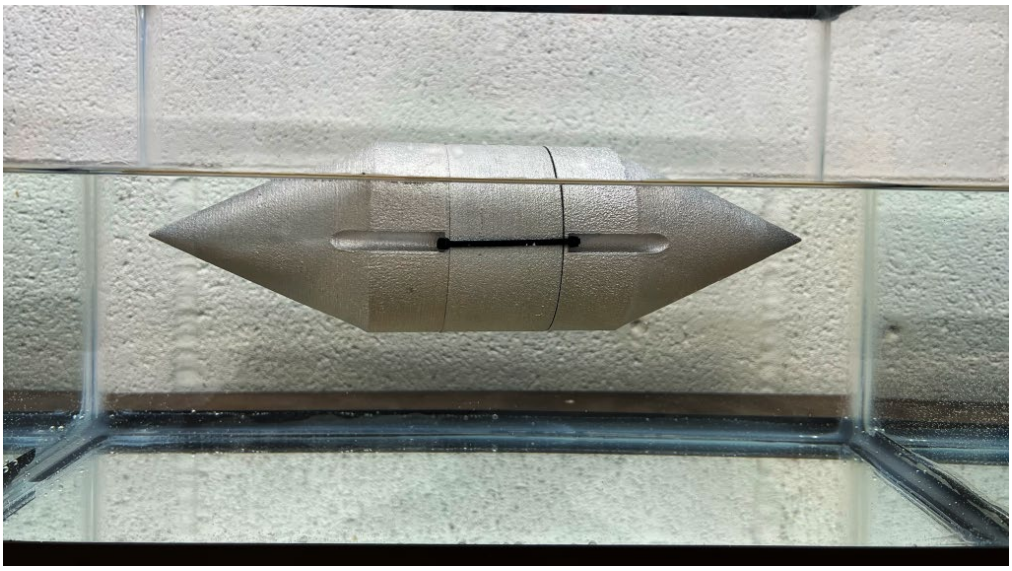

Figure 53. Assembly 13 During Payload v2 Test (Using Configuration 1 – 1 mm Walls)

Figure 54. Assembly 23 During Payload v2 Test (Using Configuration 2 – 1.5 mm Walls)

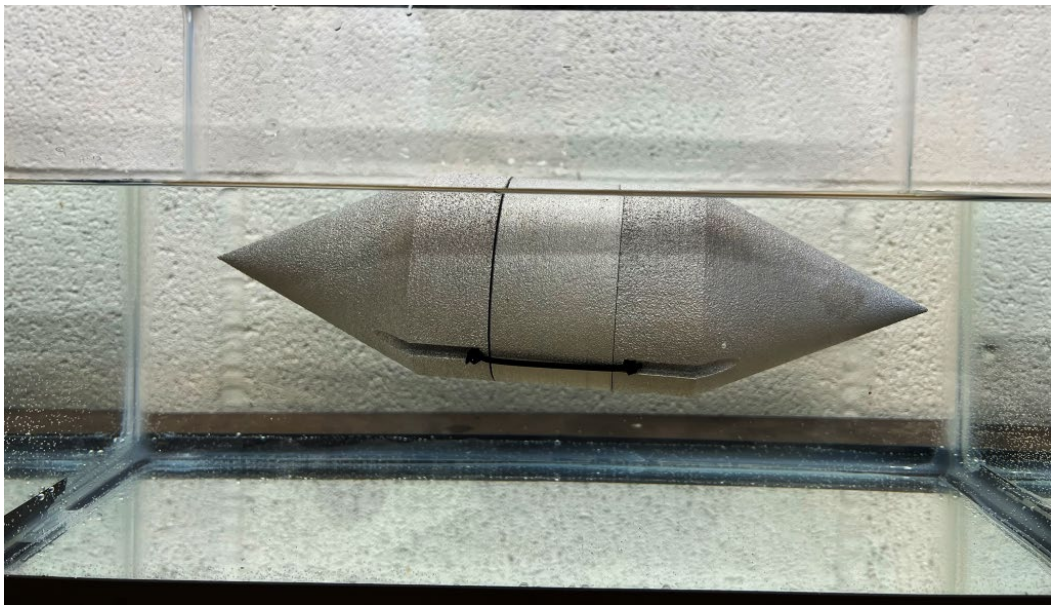

Figure 55. Assembly 29 During Payload v2 Test (Using Configuration 3 – 2 mm Walls)

Figure 56. Assembly 30 During Payload v2 Test (Using Configuration 3 – 2 mm Walls)

C. OBJECTIVE 3 – SUSTAIN SUBSTANTIAL SEA PRESSURE

To prove objective 3 complete, Ansys eigenvalue analysis was performed on the three configuration models. It is important to remember the following observations and trends found from previous Ansys analysis in this paper:

1. Eigenvalue buckling analysis is a linear buckling analysis. Linear buckling analysis is a non-conservative buckling analysis as compared to nonlinear buckling analysis.
2. Ansys eigenvalue analysis produced excellent results (less than 2% difference) in comparison to buckling of a column using Euler's solution.
3. For thin-walled cylinders under external pressure, twelve different models were analyzed with Ansys eigenvalue analysis. Mode 1 results had an average error of -92.6% difference compared to buckling equations in the Stress Analysis Manual. When analyzing modes greater than 1, VLC35 had a viable result; with a mode 4 result and ~8% difference to the Stress Analysis Manual.
4. Ansys eigenvalue analysis was used in comparison to Galletly's thin-walled cone-to-cylinder models under external pressure. Models 1 & 4 had the closest results to Galletly's results with ~10% and ~15% difference respectively.

In previous experiments for determining buckling of thin-walled models under external pressure, symmetry and displacement BCs were used. However, the configuration models are not symmetric about all three axes. The configurations have two notch holes 180º apart that are used to assemble the models to the payloads. These notch holes were used for fixed support BCs.

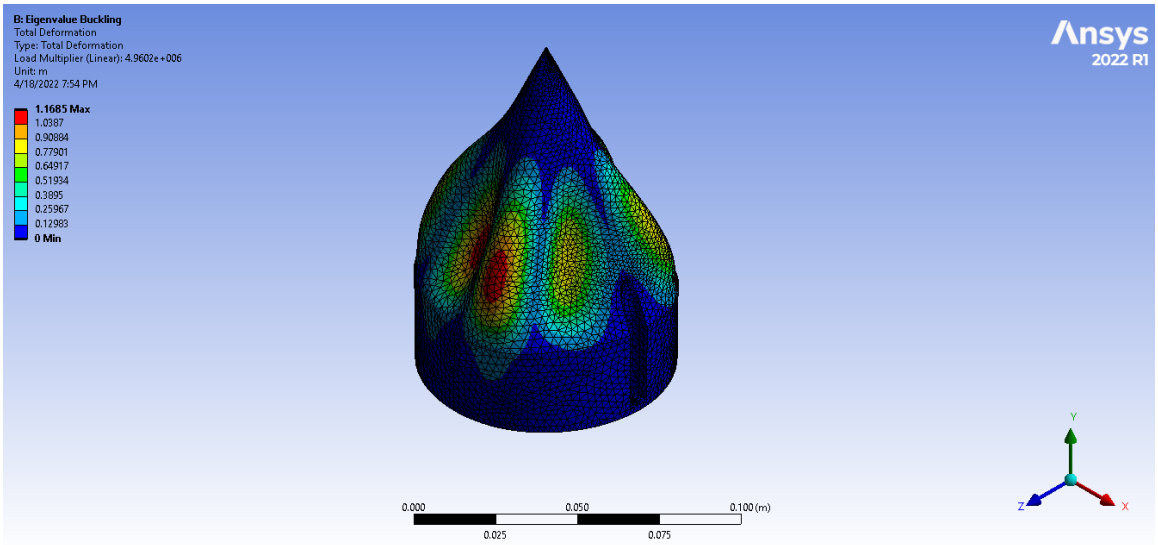

Figure 57. Eigenvalue Buckling Analysis of Configuration 1 (Mode 1 shown)

By placing fixed support BCs on the small notch holes, the configuration models could be simulated being submerged underwater and exposed to pressure on all sides. Mesh sizing 7 was used as this was found to be the most accurate mesh analysis setting. A 1 Pa pressure was placed on the outside of the cylinders. Since a 1 Pa pressure was used, the eigenvalue mode multipliers represent the critical buckling pressure of the model. Six modes were analyzed however, mode 1 produced the most conservative results for all models and will be used for comparison purposes. Using the thumb rule of a 1 atm increase in pressure for each 10 m of water depth, the critical buckling pressures could be converted into depths of water.

Two tables of results were generated, Table 10 is the results from Ansys with no corrections made to the values. However, it is important to remember the previous Ansys results discussed at the beginning of this section. In all cases of using eigenvalue buckling analysis for determining the critical buckling pressure of a model, the Ansys analysis had some degree of error. The models analyzed that most closely resembled the configurations 1 through 3 were models 1 and 4 from the Galletly research. Models 1 and 4 also produced the most accurate results In Ansys in comparison to Galletly's BOSOR analysis. Ansys produced results that were 10% and 15% off from Galletly's results. It is also important to note that eigenvalue analysis is a linear analysis which is non-conservative. Because of

these two facts, Table 11 was generated. Table 11 took the results from Table 10 and assumed a 20% error.

Table 11. Eigenvalue Buckling Results for Configuration Models, with Water Depth Comparison

Configuration Number	Ansys Mode 1 Buckling (kPa)	Equivalent Depth (m)	Equivalent Depth (ft)
1	4960	490	1606
2	15910	1570	5150
3	96706	9544	31305

Table 12. Eigenvalue Buckling Results for Configuration Models, with Water Depth Comparison (20% Overestimation Correction)

Configuration Number	Ansys Mode 1 Buckling (kPa)	Equivalent Depth (m)	Equivalent Depth (ft)
1	3968	392	1285
2	12728	1256	4120
3	77365	7635	25044

With a 20% error included, Configurations 1 through 3 all produced results that could withstand substantial sea pressure. Configuration 1, the thinnest walled model, had the least shallow depth support of 392 m. Configuration 3, the thickest walled model, had the deepest depth support of 7,635 m. All models proved to support substantial sea pressure even with a 20% error assumption.

V. CONCLUSIONS AND FUTURE WORK

This thesis set out to accomplish three objectives to prove additive manufacturing hollow metal parts with liquid metal can produce results suitable for use in the undersea warfare community; (1) Build a positively buoyant hollow metal part using liquid, (2) Prove configurations can support a payload and stay positively buoyant, and (3) Prove the configurations can support substantial sea pressure without buckling.

Objective 1 was observed immediately upon the part removal process of the configurations. However, this research went a step further to see if microscopic leakage was occurring which would affect the configurations buoyancy if submerged for long periods of time. A correlation was found between the wall thickness and leakage occurring. Leakage occurred in Configurations 1 and 2 (1 mm and 1.5 mm thin-walled cylinders), and no leakage occurred in Configuration 3 (2 mm thin-walled cylinders).

All configurations passed objective 2 in being able to support a payload and remain positively buoyant. An attempt was made to add weight to sink the assemblies however only assemblies using Configuration 3 were able to be sank. A larger payload with more weight would be needed to be built to sink assemblies using Configurations 1 and 2. The theoretical densities aligned perfectly with expected sink or float results. As soon as the assembly density was greater then seawater density, the assembly would sink.

Objective 3 was achieved in the combination with some assumptions about the Ansys Eigenvalue analysis. This research set out to prove the eigenvalue analysis was viable for common buckling examples, and then moved to prove its validity to buckling of thin-walled models. Perfect results were not achieved; however, assuming a small degree of error and conservativeness in the analysis, the configurations proved to support sea pressures from substantial depths.

As research was done, many thoughts and ideas presented themselves related to this study. The goal of these next paragraphs is to illustrate the vast majority of work that still needs to be done for liquid metal additive manufacturing.

There was a small correlation found in the study of printing rounded-corner tolerance pieces compared to sharp-corner tolerance pieces. The Xerox User Manual suggests rounding parts edges to improve print time and productivity. Print time was improved with this suggestion; however, it was minimal. The small correlation could be related to the part printed. Future work could analyze this improved productivity suggestion by analyzing multiple parts with many different shapes and sizes.

There were many trends observed in Chapter III.B Experimental Design Guidelines. Some notable trends include print error being worse in the x direction than the y direction, the correlation between print error and size of feature, and the accuracy correlation of the overhang features. Eight test pieces were used for these trends. It would be beneficial to print numerous more parts with a wide variety of shapes and sizes to have conclusive results. If conclusive results are found in the relationships of printer orientation and accuracy, this can be used as important design tool. Design guidelines can be made with the expectation of certain overprinting and/or under printing to meet exact requirements.

This research showed hollow metal parts can be printed, be buoyant with a payload, and sustain substantial sea pressure. The application of the payload was not explored. The payload may need to be remodeled to have a sensor attached to improve its application.

Lastly, this research proved the hollow metal parts can sustain substantial sea pressure theoretically. It is highly recommended future research use a water pressure vessel to find experimental buckling pressures. This is the same experiment Galletly performed in his 1974 research. The comparison of Ansys eigenvalue buckling results to experimental buckling data would be extremely beneficial.

APPENDIX A. TOLERANCE PIECE MEASUREMENTS

Table 13. Labels and Types of Features for TPRC/TPSC

	Type of Feature			
Label	**Extrusion/Cut**	**Detail Feature?**	**Direction**	**Overhang?**
A	E	y	r*	n
B	E	y	r*	n
C	E	y	r*	n
D	E	n	r*	n
E	E	y	x	n
F	E	y	x	n
G	E	y	x	n
H	E	n	y	n
I	E	n	y	n
J	E	n	y	n
K	E	n	y	n
L	C	n	y	n
M	C	n	x	n
N	E	n	x	n
O	E	n	y	n
P	C	n	y	n
Q	E	n	y	n
R	E	y	x	n
S	E	n	y	n
T	E	n	x	n
U	E	n	x	n
V	C	n	z	y
W	C	n	z	y
X	C	n	z	y
Y	C	n	z	y
Z	E	y	z	n
AA	E	n	z	n
AB	E	n	z	n
AC	C	n	z	y
AD	C	n	z	y
AE	C	n	z	y
AF	C	n	z	y
AG	E	n	z	n
AH	C	y	x	y

r* - radial: radial features were measured in both x and y direction and the average was documented.

Table 14. TPRC 60% Frequency Specification Comparison (1)

Label	Specification	Measurement	% Difference
A	1.0 mm Diameter	0.91 mm Diameter	-9.00
B	2.0 mm Diameter	2.04 mm Diameter	2.00
C	3.0 mm Diameter	3.06 mm Diameter	2.00
D	4.0 mm Diameter	4.08 mm Diameter	2.00
E	0.5 mm	Failed to Print	-
F	1.0 mm	1.03 mm	3.00
G	2.0 mm	2.12 mm	6.00
H	15.0 mm	Failed to Print	-
I	15.0 mm	15.23 mm	1.53
J	15.0 mm	15.19 mm	1.27
K	15.0 mm	15.16 mm	1.07
L	10.0 mm	9.83 mm	-1.70
M	30.0 mm	29.85 mm	-0.50
N	8.0 mm	8.15 mm	1.88
O	6.0 mm	6.14 mm	2.33
P	5.0 mm	4.78 mm	-4.40
Q	4.0 mm	4.17 mm	4.25
R	3.0 mm	3.23 mm	7.67
S	40.0 mm	40.32 mm	0.80
T	60.0 mm	60.15 mm	0.25
U	0.99 mm	1.00 mm	1.01
V	50.00 º	49.30 º	-1.40
W	12.00 mm	10.66 mm	-11.17
X	7.83 mm	7.30 mm	-6.77
Y	7.83 mm	7.23 mm	-7.66
Z	2.00 mm	2.14 mm	7.00
AA	5.00 mm	4.95 mm	-1.00
AB	20.00 mm	20.03 mm	0.15
AC	60.00 º	59.70 º	-0.50
AD	12.00 mm	10.44 mm	-13.00
AE	6.93 mm	6.64 mm	-4.18
AF	6.93 mm	6.55 mm	-5.48
AG	3.00 mm	3.08 mm	2.67
AH	1.00 mm	Failed to Print	-

Total print time: 1 hour 12 minutes

Table 15. TPSC 60% Frequency Specification Comparison (1)

Label	Specification	Measurement	% Difference
A	1.0 mm Diameter	1.01 mm Diameter	1.00
B	2.0 mm Diameter	2.20 mm Diameter	10.00
C	3.0 mm Diameter	3.25 mm Diameter	8.33
D	4.0 mm Diameter	4.20 mm Diameter	5.00
E	0.5 mm	Failed to Print	-
F	1.0 mm	1.32 mm	32.00
G	2.0 mm	2.52 mm	26.00
H	15.0 mm	Failed to Print	-
I	15.0 mm	15.30 mm	2.00
J	15.0 mm	15.52 mm	3.47
K	15.0 mm	15.50 mm	3.33
L	10.0 mm	9.44 mm	-5.60
M	30.0 mm	29.23 mm	-2.57
N	8.0 mm	8.58 mm	7.25
O	6.0 mm	6.47 mm	7.83
P	5.0 mm	4.46 mm	-10.80
Q	4.0 mm	4.62 mm	15.50
R	3.0 mm	3.45 mm	15.00
S	40.0 mm	40.62 mm	1.55
T	60.0 mm	60.91 mm	1.52
U	0.99 mm	1.28 mm	29.29
V	50.00 º	49.30 º	-1.40
W	12.00 mm	10.18 mm	-15.17
X	7.83 mm	6.83 mm	-12.77
Y	7.83 mm	6.88 mm	-12.13
Z	2.00 mm	1.96 mm	-2.00
AA	5.00 mm	4.39 mm	-12.20
AB	20.00 mm	19.93 mm	-0.35
AC	60.00 º	59.50 º	-0.83
AD	12.00 mm	10.23 mm	-14.75
AE	6.93 mm	5.98 mm	-13.71
AF	6.93 mm	6.09 mm	-12.12
AG	3.00 mm	3.16 mm	5.33
AH	1.00 mm	Failed to Print	-

Total print time: 1 hour 14 minutes

Table 16. TPRC 100% Frequency Specification Comparison (1)

Label	Specification	Measurement	% Difference
A	1.0 mm Diameter	1.03 mm Diameter	3.00
B	2.0 mm Diameter	2.15 mm Diameter	7.50
C	3.0 mm Diameter	3.22 mm Diameter	7.33
D	4.0 mm Diameter	4.25 mm Diameter	6.25
E	0.5 mm	Failed to Print	-
F	1.0 mm	1.30 mm	30.00
G	2.0 mm	2.34 mm	17.00
H	15.0 mm	Failed to Print	-
I	15.0 mm	15.27 mm	1.80
J	15.0 mm	15.42 mm	2.80
K	15.0 mm	15.55 mm	3.67
L	10.0 mm	9.69 mm	-3.10
M	30.0 mm	29.85 mm	-0.50
N	8.0 mm	8.55 mm	6.88
O	6.0 mm	6.43 mm	7.17
P	5.0 mm	4.67 mm	-6.60
Q	4.0 mm	4.68 mm	17.00
R	3.0 mm	3.54 mm	18.00
S	40.0 mm	40.52 mm	1.30
T	60.0 mm	60.45 mm	0.75
U	0.99 mm	1.25 mm	26.26
V	50.00 º	49.60 º	-0.80
W	12.00 mm	10.37 mm	-13.58
X	7.83 mm	7.20 mm	-8.05
Y	7.83 mm	6.94 mm	-11.37
Z	2.00 mm	1.97 mm	-1.50
AA	5.00 mm	4.68 mm	-6.40
AB	20.00 mm	20.17 mm	0.85
AC	60.00 º	59.60 º	-0.67
AD	12.00 mm	10.32 mm	-14.00
AE	6.93 mm	6.57 mm	-5.19
AF	6.93 mm	6.26 mm	-9.67
AG	3.00 mm	3.05 mm	1.67
AH	1.00 mm	Failed to Print	-

Total print time: 1 hour 5 minutes

Table 17. TPSC 100% Frequency Specification Comparison (1)

Label	Specification	Measurement	% Difference
A	1.0 mm Diameter	0.98 mm Diameter	-2.00
B	2.0 mm Diameter	2.36 mm Diameter	18.00
C	3.0 mm Diameter	3.42 mm Diameter	14.00
D	4.0 mm Diameter	4.22 mm Diameter	5.50
E	0.5 mm	Failed to Print	-
F	1.0 mm	1.29 mm	29.00
G	2.0 mm	2.41 mm	20.50
H	15.0 mm	Failed to Print	-
I	15.0 mm	15.39 mm	2.60
J	15.0 mm	15.45 mm	3.00
K	15.0 mm	15.57 mm	3.80
L	10.0 mm	9.38 mm	-6.20
M	30.0 mm	29.47 mm	-1.77
N	8.0 mm	8.44 mm	5.50
O	6.0 mm	6.64 mm	10.67
P	5.0 mm	4.24 mm	-15.20
Q	4.0 mm	4.67 mm	16.75
R	3.0 mm	3.60 mm	20.00
S	40.0 mm	40.70 mm	1.75
T	60.0 mm	60.78 mm	1.30
U	0.99 mm	1.28 mm	29.29
V	50.00 º	49.80 º	-0.40
W	12.00 mm	10.17 mm	-15.25
X	7.83 mm	6.75 mm	-13.79
Y	7.83 mm	6.90 mm	-11.88
Z	2.00 mm	1.77 mm	-11.50
AA	5.00 mm	4.52 mm	-9.60
AB	20.00 mm	20.41 mm	2.05
AC	60.00 º	59.90 º	-0.17
AD	12.00 mm	10.35 mm	-13.75
AE	6.93 mm	6.56 mm	-5.34
AF	6.93 mm	6.16 mm	-11.11
AG	3.00 mm	2.94 mm	-2.00
AH	1.00 mm	Failed to Print	-

Total print time: 1 hour 8 minutes

Table 18. TPRC 60% Frequency Specification Comparison (2)

Label	Specification	Measurement	% Difference
A	1.0 mm Diameter	0.93 mm Diameter	-7.00
B	2.0 mm Diameter	2.23 mm Diameter	11.50
C	3.0 mm Diameter	3.07 mm Diameter	2.33
D	4.0 mm Diameter	4.23 mm Diameter	5.75
E	0.5 mm	Failed to Print	-
F	1.0 mm	1.01 mm	1.00
G	2.0 mm	2.03 mm	1.50
H	15.0 mm	Failed to Print	-
I	15.0 mm	15.10 mm	0.67
J	15.0 mm	15.40 mm	2.67
K	15.0 mm	15.22 mm	1.47
L	10.0 mm	9.90 mm	-1.00
M	30.0 mm	29.88 mm	-0.40
N	8.0 mm	8.18 mm	2.25
O	6.0 mm	6.33 mm	5.50
P	5.0 mm	4.86 mm	-2.80
Q	4.0 mm	4.14 mm	3.50
R	3.0 mm	3.37 mm	12.33
S	40.0 mm	40.43 mm	1.08
T	60.0 mm	60.40 mm	0.67
U	0.99 mm	1.04 mm	5.05
V	50.00 º	49.00 º	-2.00
W	12.00 mm	10.82 mm	-9.83
X	7.83 mm	7.38 mm	-5.75
Y	7.83 mm	7.32 mm	-6.51
Z	2.00 mm	2.02 mm	1.00
AA	5.00 mm	4.95 mm	-1.00
AB	20.00 mm	20.24 mm	1.20
AC	60.00 º	59.60 º	-0.67
AD	12.00 mm	10.88 mm	-9.33
AE	6.93 mm	6.71 mm	-3.17
AF	6.93 mm	6.34 mm	-8.51
AG	3.00 mm	2.86 mm	-4.67
AH	1.00 mm	Failed to Print	-

Total print time: 1 hour 13 minutes

Table 19. TPSC 60% Frequency Specification Comparison (2)

Label	Specification	Measurement	% Difference
A	1.0 mm Diameter	1.02 mm Diameter	2.00
B	2.0 mm Diameter	2.06 mm Diameter	3.00
C	3.0 mm Diameter	3.31 mm Diameter	10.33
D	4.0 mm Diameter	4.26 mm Diameter	6.50
E	0.5 mm	Failed to Print	-
F	1.0 mm	1.09 mm	9.00
G	2.0 mm	2.25 mm	12.50
H	15.0 mm	Failed to Print	-
I	15.0 mm	15.28 mm	1.87
J	15.0 mm	15.25 mm	1.67
K	15.0 mm	15.36 mm	2.40
L	10.0 mm	9.93 mm	-0.70
M	30.0 mm	29.96 mm	-0.13
N	8.0 mm	8.33 mm	4.13
O	6.0 mm	6.08 mm	1.33
P	5.0 mm	4.80 mm	-4.00
Q	4.0 mm	4.19 mm	4.75
R	3.0 mm	3.43 mm	14.33
S	40.0 mm	40.35 mm	0.88
T	60.0 mm	60.32 mm	0.53
U	0.99 mm	1.13 mm	14.14
V	50.00 º	48.90	-2.20
W	12.00 mm	10.41 mm	-13.25
X	7.83 mm	7.22 mm	-7.79
Y	7.83 mm	7.16 mm	-8.56
Z	2.00 mm	1.73 mm	-13.50
AA	5.00 mm	4.75 mm	-5.00
AB	20.00 mm	19.84 mm	-0.80
AC	60.00 º	59.50	-0.83
AD	12.00 mm	10.77 mm	-10.25
AE	6.93 mm	6.70 mm	-3.32
AF	6.93 mm	6.46 mm	-6.78
AG	3.00 mm	2.97 mm	-1.00
AH	1.00 mm	Failed to Print	-

Total print time: 1 hour 15 minutes

Table 20. TPRC 100% Frequency Specification Comparison (2)

Label	Specification	Measurement	% Difference
A	1.0 mm Diameter	0.98 mm Diameter	-2.00
B	2.0 mm Diameter	2.20 mm Diameter	10.00
C	3.0 mm Diameter	3.15 mm Diameter	5.00
D	4.0 mm Diameter	4.23 mm Diameter	5.75
E	0.5 mm	Failed to Print	-
F	1.0 mm	1.05 mm	5.00
G	2.0 mm	2.20 mm	10.00
H	15.0 mm	Failed to Print	-
I	15.0 mm	15.05 mm	0.33
J	15.0 mm	15.61 mm	4.07
K	15.0 mm	15.40 mm	2.67
L	10.0 mm	9.79 mm	-2.10
M	30.0 mm	29.90 mm	-0.33
N	8.0 mm	8.26 mm	3.25
O	6.0 mm	6.21 mm	3.50
P	5.0 mm	4.81 mm	-3.80
Q	4.0 mm	4.28 mm	7.00
R	3.0 mm	3.24 mm	8.00
S	40.0 mm	40.32 mm	0.80
T	60.0 mm	60.43 mm	0.72
U	0.99 mm	1.05 mm	6.06
V	50.00 º	49.40 º	-1.20
W	12.00 mm	10.90 mm	-9.17
X	7.83 mm	7.04 mm	-10.09
Y	7.83 mm	7.30 mm	-6.77
Z	2.00 mm	1.91 mm	-4.50
AA	5.00 mm	4.59 mm	-8.20
AB	20.00 mm	20.33 mm	1.65
AC	60.00 º	59.70 º	-0.50
AD	12.00 mm	10.78 mm	-10.17
AE	6.93 mm	6.57 mm	-5.19
AF	6.93 mm	6.23 mm	-10.10
AG	3.00 mm	2.77 mm	-7.67
AH	1.00 mm	Failed to Print	-

Total print time: 1 hour 10 minutes

Table 21. TPSC 100% Frequency Specification Comparison (2)

Label	Specification	Measurement	% Difference
A	1.0 mm Diameter	0.92 mm Diameter	-8.00
B	2.0 mm Diameter	2.10 mm Diameter	5.00
C	3.0 mm Diameter	3.03 mm Diameter	1.00
D	4.0 mm Diameter	4.10 mm Diameter	2.50
E	0.5 mm	Failed to Print	-
F	1.0 mm	1.05 mm	5.00
G	2.0 mm	2.04 mm	2.00
H	15.0 mm	Failed to Print	-
I	15.0 mm	15.25 mm	1.67
J	15.0 mm	15.15 mm	1.00
K	15.0 mm	15.23 mm	1.53
L	10.0 mm	9.97 mm	-0.30
M	30.0 mm	29.95 mm	-0.17
N	8.0 mm	8.05 mm	0.63
O	6.0 mm	6.07 mm	1.17
P	5.0 mm	4.98 mm	-0.40
Q	4.0 mm	4.05 mm	1.25
R	3.0 mm	3.11 mm	3.67
S	40.0 mm	40.13 mm	0.33
T	60.0 mm	60.23 mm	0.38
U	0.99 mm	1.03 mm	4.04
V	50.00 º	49.30 º	-1.40
W	12.00 mm	10.60 mm	-11.67
X	7.83 mm	6.94 mm	-11.37
Y	7.83 mm	7.07 mm	-9.71
Z	2.00 mm	1.97 mm	-1.50
AA	5.00 mm	4.92 mm	-1.60
AB	20.00 mm	20.36 mm	1.80
AC	60.00 º	59.50 º	-0.83
AD	12.00 mm	10.92 mm	-9.00
AE	6.93 mm	6.86 mm	-1.01
AF	6.93 mm	6.40 mm	-7.65
AG	3.00 mm	2.96 mm	-1.33
AH	1.00 mm	Failed to Print	-

Total print time: 1 hour 11 minutes

THIS PAGE INTENTIONALLY LEFT BLANK

APPENDIX B. DESIGN DRAWINGS

The following drawings are the property of Naval Postgraduate School. These drawings were made for the purpose of this thesis and are provided for the potential to replicate this research's results. Included in this APPEDNIX B are Figures 58 through 66. Drawings are of Configurations 1 through 3, Payload v1, and Payload v2.

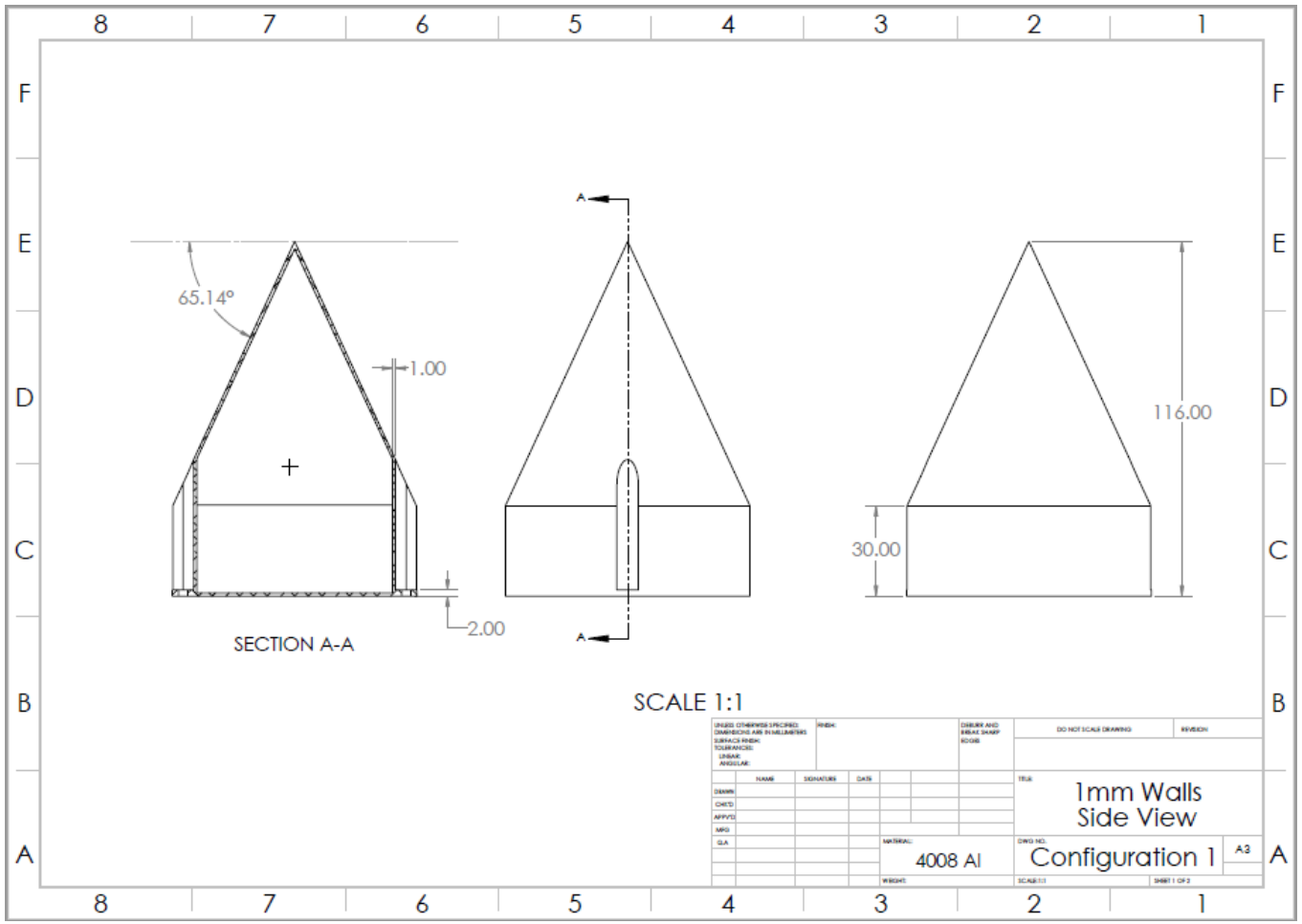

Figure 58. Configuration 1 Side View

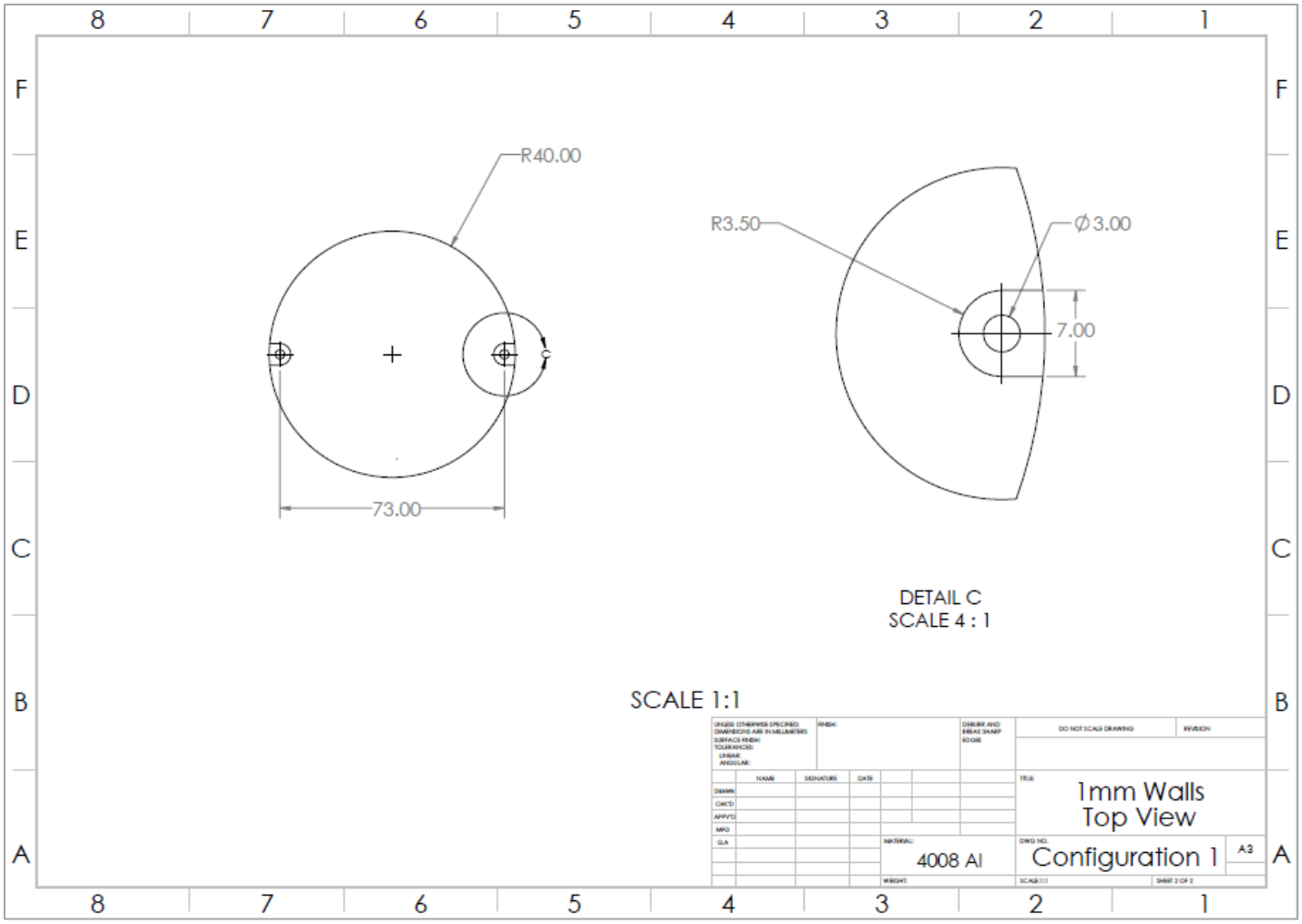

Figure 59. Configuration 1 Top View

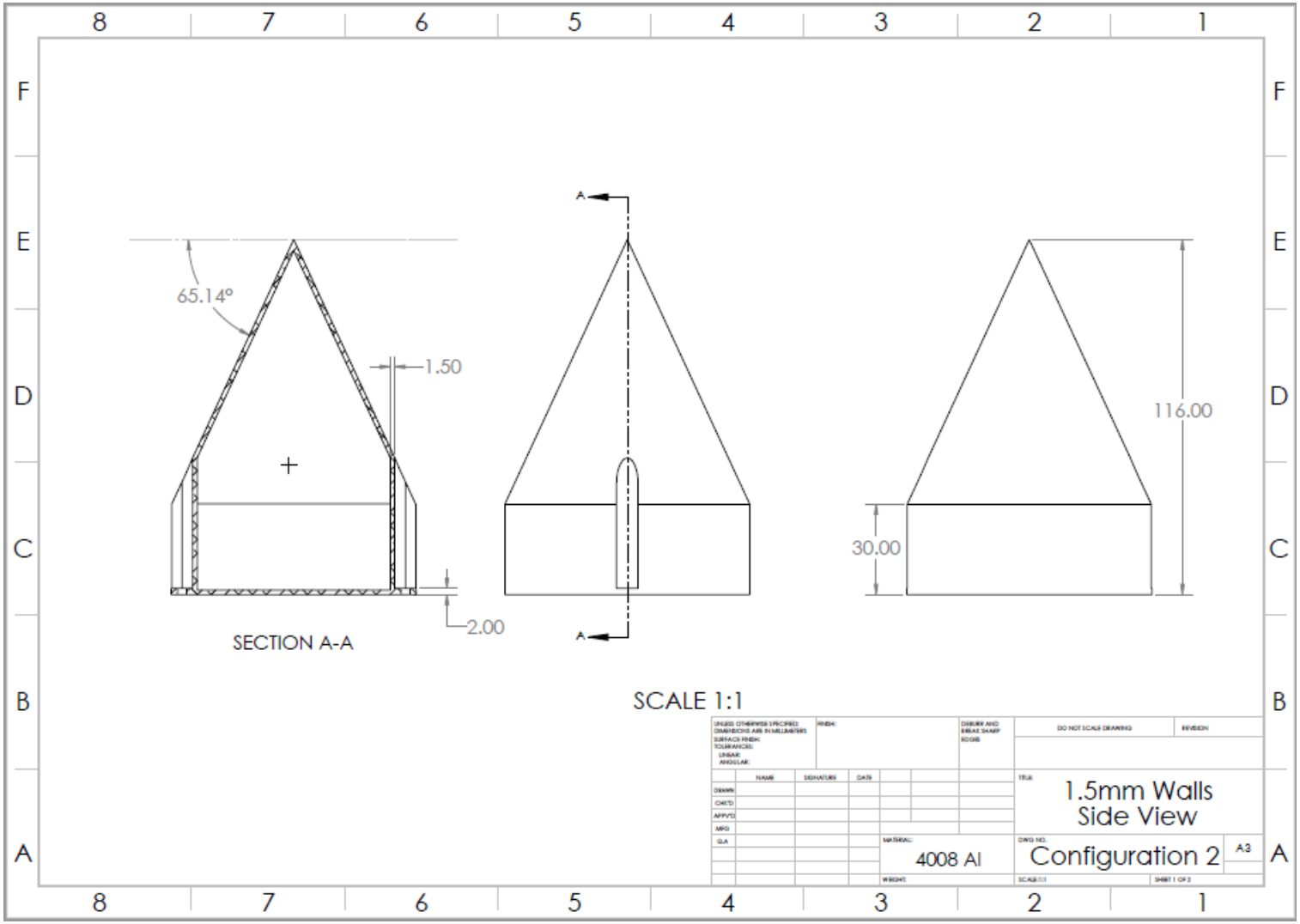

Figure 60. Configuration 2 Side View

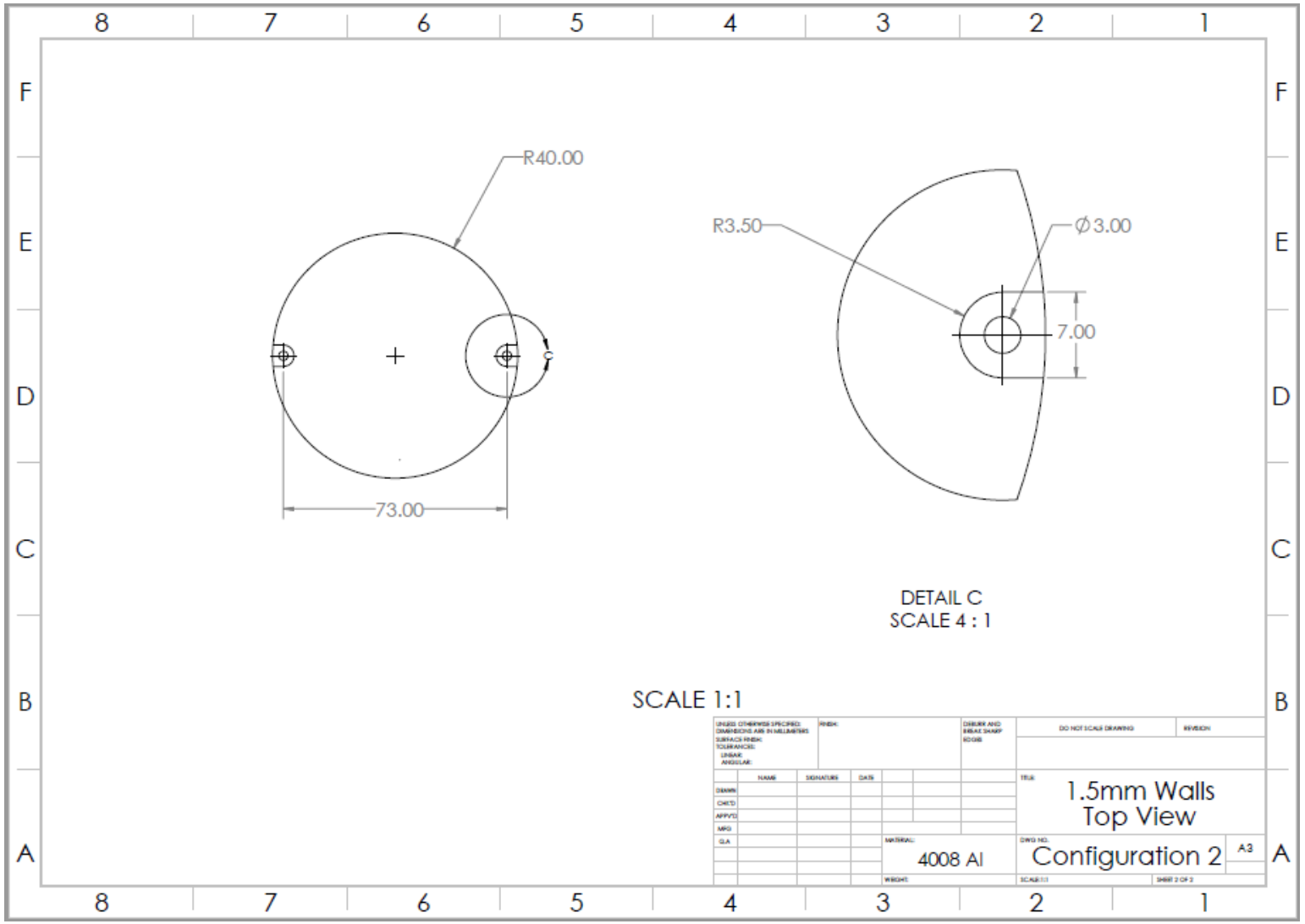

Figure 61. Configuration 2 Top View

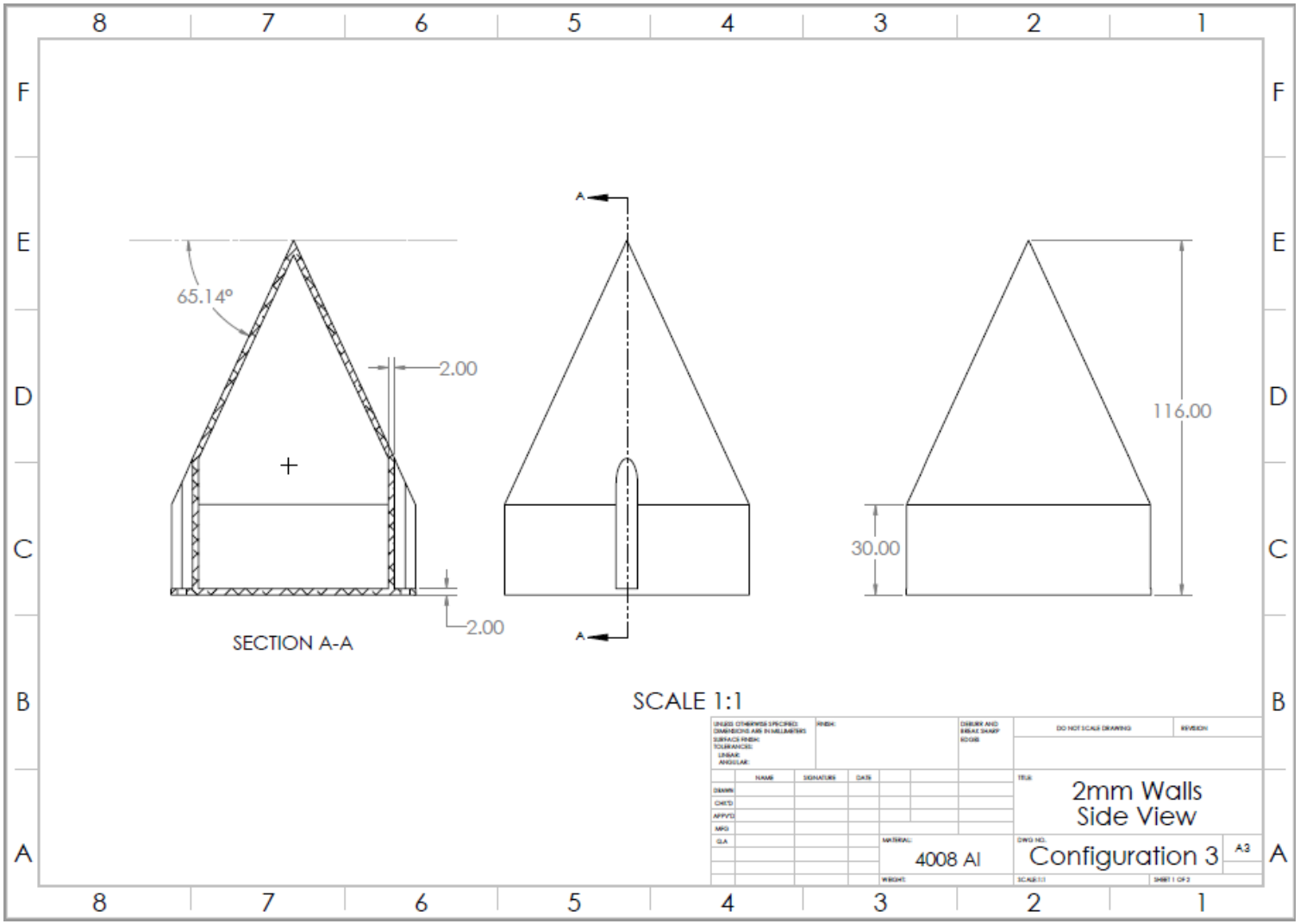

Figure 62. Configuration 3 Side View

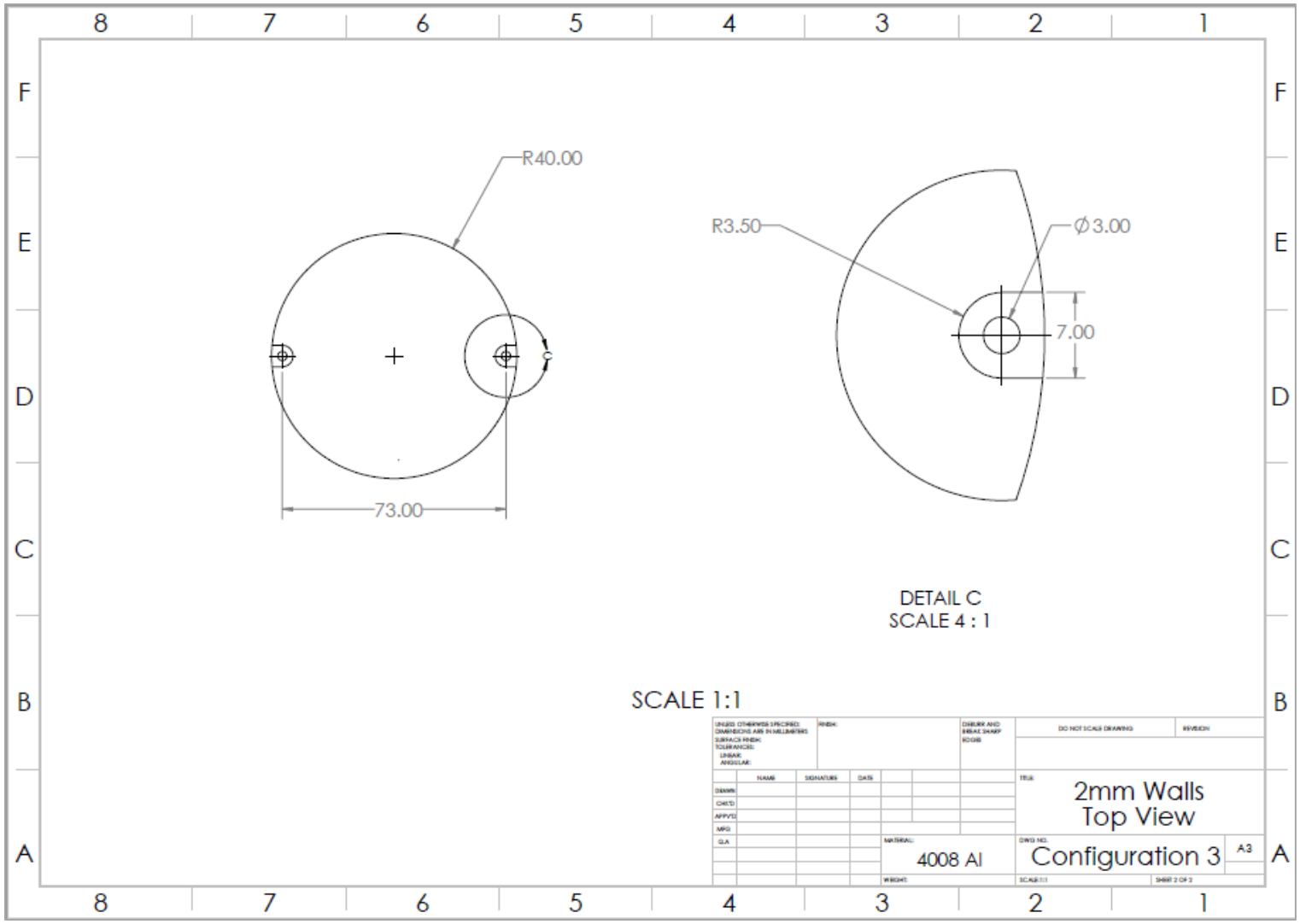

Figure 63. Configuration 3 Top View

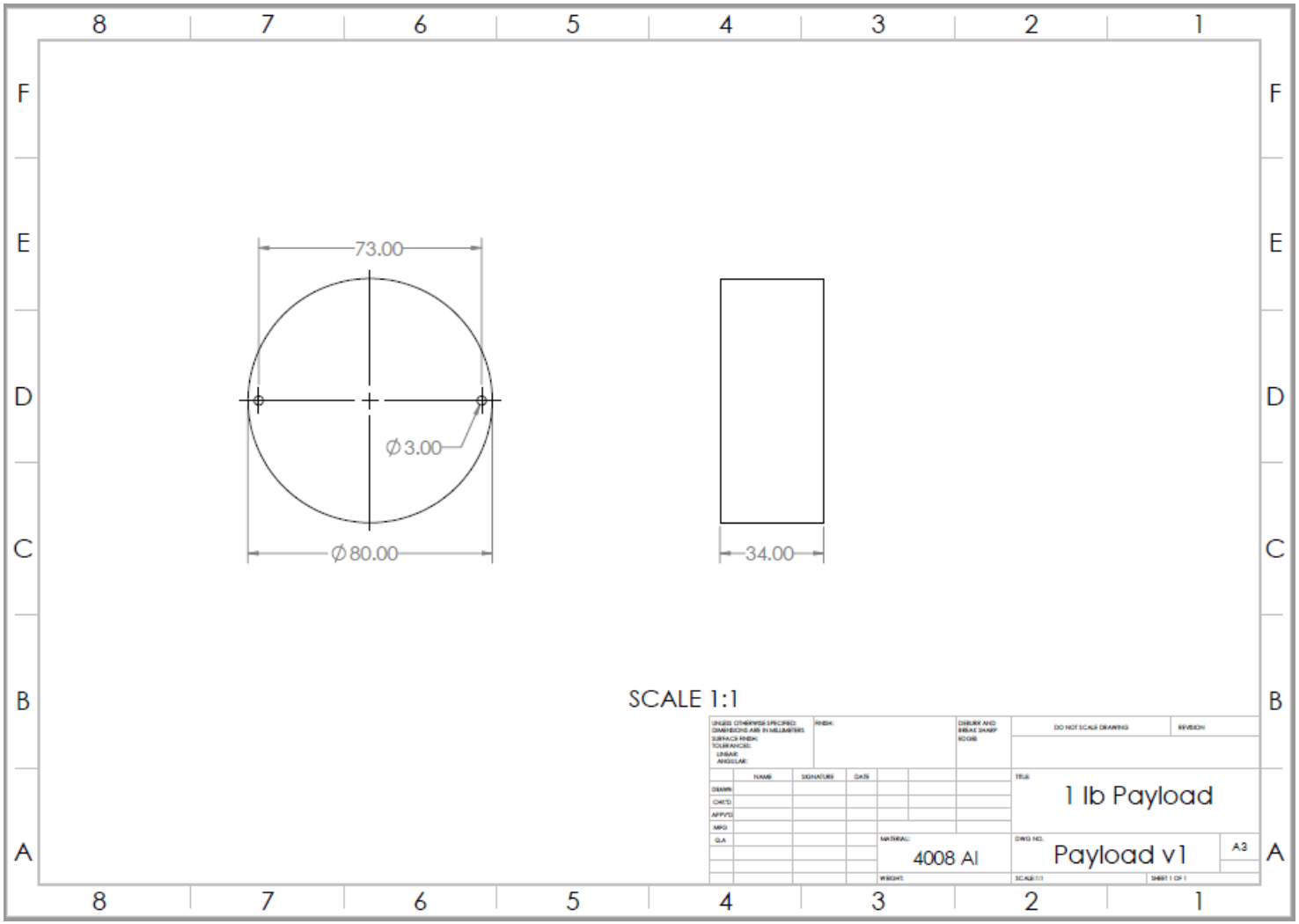

Figure 64. Payload v1 Drawing

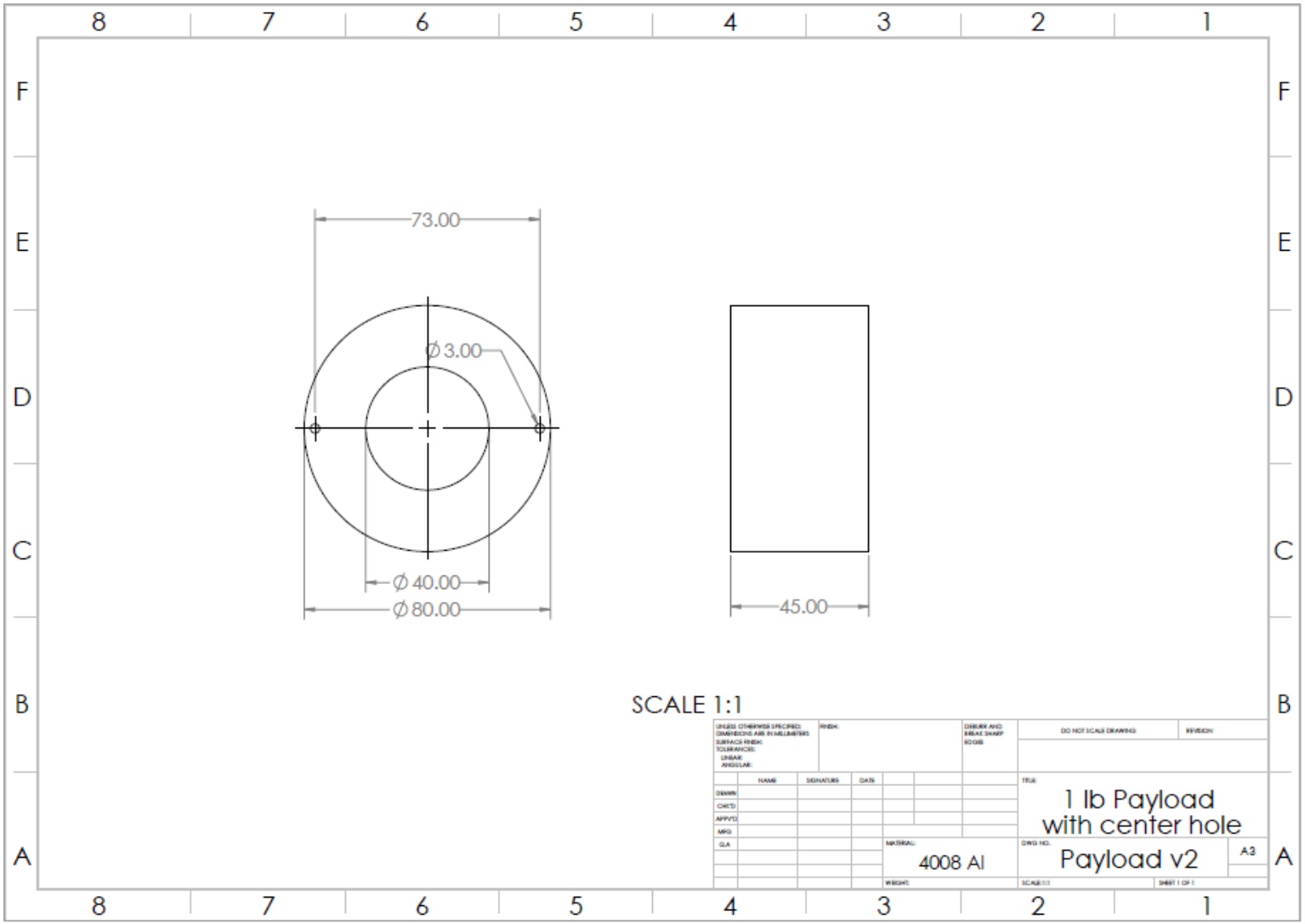

Figure 65. Payload v2 Drawing

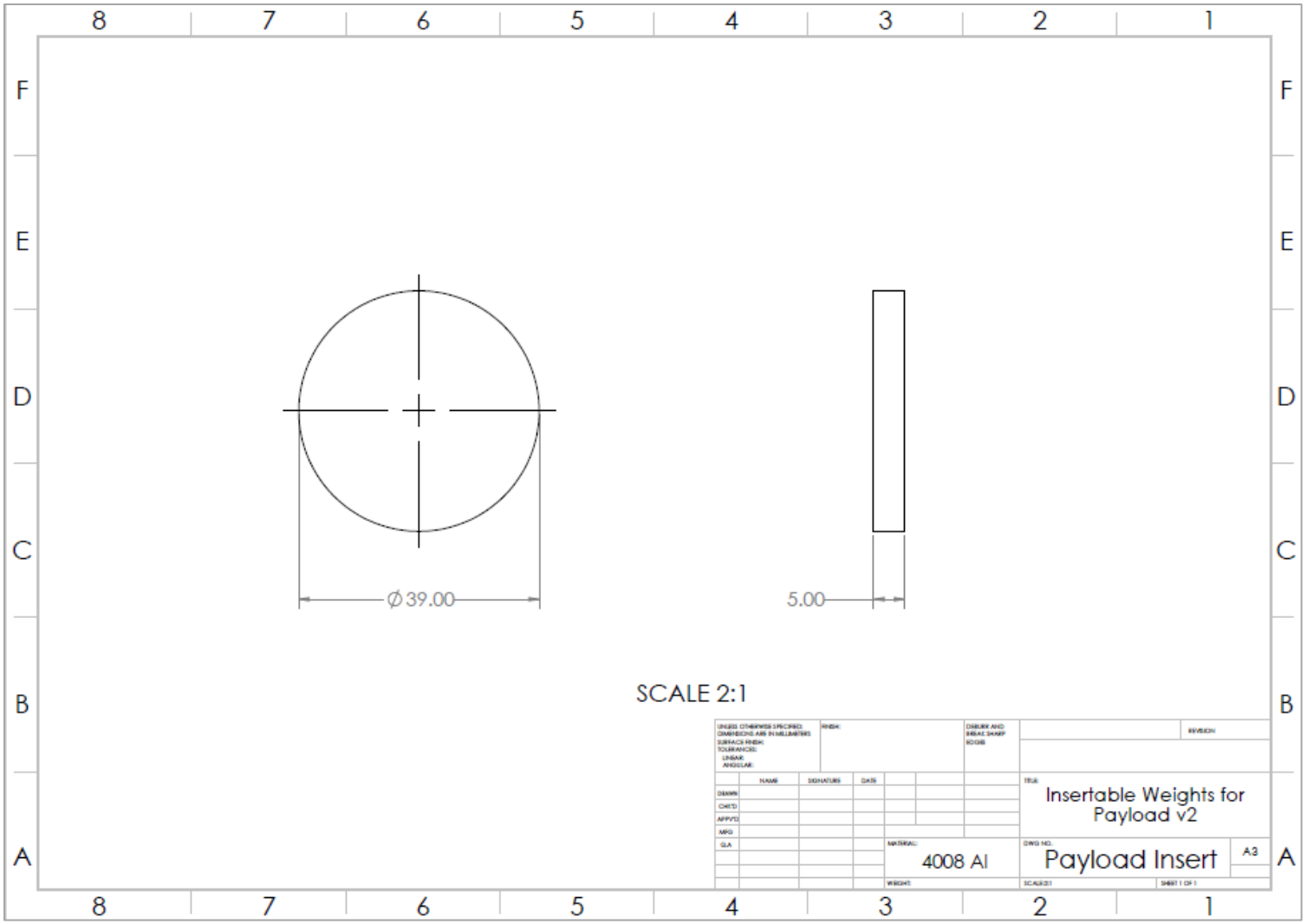

Figure 66. Payload Inserts Drawing

APPENDIX C. BUCKLING MATLAB SCRIPTS

```
function [outputstress outputcase] = SAM_bucklingF(L,r,t)

mu = 0.33; %poisson's ratio
mu_e = mu ; % Elastic Poissons ratio (pg. 33)
E=  71705475800; %Pasclas
E_t = E; % tangent Modulus (pg. 32)
E_s = E ; % Secant Modulus (pg. 32)

KYDATA = xlsread('Figure_8_24.xlsx','A2:B25');
kyx = KYDATA(:,1);
kyy = KYDATA(:,2);


x = (L.^2).*(1-(mu)^2)^(1/2)./(r*t);
        ky = interp1(kyx,kyy,x,'pchip');

eta = (E_s/E).*(1-mu_e.^2)./(1-mu.^2).*(1/4 + 3/4*E_t/E_s);

if L^2/(r*t) < 100,
    Fcr = ((ky.*(pi^2).*E)./(12.*(1-mu_e.^2))).*(t/L).^2;
    casetype = 1;
elseif (L/r).^2 > 100*t/r & (L/r).^2 < 5*r/t, % is this an error??? r/t, t/r
    Fcr = 0.93.*E.*((t/r).^1.5).*(r/L);
    casetype = 2;
else Fcr = eta*((0.25*E)./(1-mu_e.^2)).*(t/r).^2;
    casetype = 3;
end

P = Fcr*t/r;

outputstress = P;
outputcase = casetype;
```

Figure 67. SAM_buckingF.m script

```
clear all;close all;clc;

L = 1.811*0.0254:0.0005:23.622*.0254; % 1.811in = 30mm , 23.633in = 600mm
r = 1.5748*0.0254; %1.5748in = 30mm
t = 0.0394*0.0254:0.0001:0.138*0.0254; % 0.0394in = 1mm , 0.138in = 3.5mm

[LLL,ttt] = meshgrid(L,t);

for iii = 1:length(L),
    for jjj = 1:length(t),
        [outputpressure(iii,jjj) outputcase(iii,jjj)] = SAM_buckling_new(L(iii),r,t(jjj));
    end
    disp([num2str(100*iii/length(L)) '% done...']);
end
disp('...done done...');
%%

figure(1);
% hc = contourf(ttt,rrr,outputcase',3,'linestyle','none')
hc = contour(ttt,LLL.*1000,outputcase',3)
xlabel('Thickness [mm]');
ylabel('Length [mm]');
txt = {'Radius = 30 mm'};
hcb = colorbar;
hcb.Label.String = 'Analysis Type (1=SC,2=LC,3=VLC)';

depthtoCrush = (outputpressure')/(1026*9.81);
depthtoCrush(depthtoCrush>10^4) = NaN;

figure(2);
contourf(ttt,LLL.*1000,depthtoCrush, [0 50 100 200 300 ...
    400 500 600 700 800 900 1000 2000 3000 4000 ...
    5000 6000 7000 8000 9000])
xlabel('Thickness [mm]');
ylabel('Length [mm]');
txt = {'Radius = 30 mm'};
hcb = colorbar;
hcb.Label.String = 'Depth To crush [m]';
```

Figure 68. Run_SAM_bucklingF.m script

```
%Critical Load Estimation - Single Calculation
clear all
close all
clc

%SC

E=71000000000;     % Pasclas
mu=0.33;           % Poison's ratio
r = 40;            % Radius of cylinder
L = 30;            % Length of cylinder
t=1                % thickness of Cylinder. 1.5,2,3.5 also used

Check_less_Than_100=(L^2)/(r*t)

x = ((L^2)*(1-(mu)^2)^(1/2))/(r*t)
Ky=1.853+0.141714*x.^(0.83666)
Fcr=((Ky.*(pi^2)*E)/(12*(1-mu^2)))*(t/L)^2

%LC

E=71000000000;     % Pascals
mu=0.33;           % Poison's ratio

r = 40;            % Radius of cylinder
L = 200;           % Length of cylinder
t= 1               % thickness of Cylinder. 1.5,2,3.5 also used

Check_100tr=100*t/r
Check_Lr2=(L/r)^2
Check_5rt=5*(r/t)

Fcr=(0.93*E*((t/r)^(3/2))*(r/L))

%VLC

E=71000000000;     % Pascals, Mod of Elast
mu=0.33;           % Poison's ratio
N=1

r = 40;            % Radius of cylinder
L = 600;           % Length of cylinder
t=1                % thickness of Cylinder. 1.5,2,3.5 also used

Check_Lr2=(L/r)^2
Check_5rt=5*(r/t)

Fcr=((0.25*E)/(1-mu^2))*(t/r)^2
```

Figure 69. Critical Load Estimation Script

THIS PAGE INTENTIONALLY LEFT BLANK

APPENDIX D. SUMMARY OF ANSYS TO GALLETLY RESULTS

Table 22. Summary of ANSYS Buckling Analysis to Galletly Buckling

Galletly Model No.	Ansys Mode	Ansys Buckling (Pa)	Galletly BOSOR (lbf/in^2)	Galletly BOSOR (Pa)	Galletly Experimental (lbf/in^2)	Galletly Experimental (Pa)	%Diff Ansys to BOSOR	%Diff Ansys to Exp
1	1	4541400	598	4123210	559	3854305	10.14	17.83
	2	4817100	598	4123210	559	3854305	16.83	24.98
	3	5194400	598	4123210	559	3854305	25.98	34.77
	4	6055900	598	4123210	559	3854305	46.87	57.12
	5	6456300	598	4123210	559	3854305	56.58	67.51
	6	8392300	598	4123210	559	3854305	103.54	117.74
2	1	4174300	472	3254440	410	2826950	28.26	47.66
	2	4672700	472	3254440	410	2826950	43.58	65.29
	3	4879400	472	3254440	410	2826950	49.93	72.60
	4	5514600	472	3254440	410	2826950	69.45	95.07
	5	6459300	472	3254440	410	2826950	98.48	128.49
	6	8006500	472	3254440	410	2826950	146.02	183.22
3	1	2587700	210	1447950	185	1275575	78.71	102.87
	2	2635900	210	1447950	185	1275575	82.04	106.64
	3	4338100	210	1447950	185	1275575	199.60	240.09
	4	4872400	210	1447950	185	1275575	236.50	281.98
	5	4956800	210	1447950	185	1275575	242.33	288.59
	6	6172500	210	1447950	185	1275575	326.29	383.90
4	1	2288800	287	1978865	279	1923705	15.66	18.98
	2	2398800	287	1978865	279	1923705	21.22	24.70
	3	3687200	287	1978865	279	1923705	86.33	91.67
	4	5260700	287	1978865	279	1923705	165.84	173.47
	5	5622700	287	1978865	279	1923705	184.14	192.28
	6	6064900	287	1978865	279	1923705	206.48	215.27
5	1	2301600	287	1978865	274	1889230	16.31	21.83
	2	2510200	287	1978865	274	1889230	26.85	32.87
	3	3686900	287	1978865	274	1889230	86.31	95.15
	4	4184500	287	1978865	274	1889230	111.46	121.49
	5	5501900	287	1978865	274	1889230	178.03	191.22
	6	5609300	287	1978865	274	1889230	183.46	196.91
6	1	2314000	210	1447950	186	1282470	59.81	80.43
	2	2558700	210	1447950	186	1282470	76.71	99.51
	3	2585400	210	1447950	186	1282470	78.56	101.60
	4	2668100	210	1447950	186	1282470	84.27	108.04
	5	3686500	210	1447950	186	1282470	154.60	187.45
	6	4362800	210	1447950	186	1282470	201.31	240.19

THIS PAGE INTENTIONALLY LEFT BLANK

APPENDIX E. SUMMARY OF PRINTED PARTS

Table 23. Summary of Printed Parts and Mass Comparison

Part Name	Calculated Weight SW (g)	Calculated Weight Slicer (g)	Actual Weight (g)	% Difference SW	% Difference Slicer
Tolerance Part Test a	108.25	106.63	106.48	1.66	0.14
Tolerance Part Test b	108.25	106.63	105.39	2.71	1.18
Configuration Test a	45.98	44.54	43.22	6.39	3.05
Configuration Test b	127.12	124.13	126.89	0.18	2.18
Configuration Test c	127.12	124.13	129.17	1.59	3.90
TPRC 60% (1)	107.43	105.88	104.88	2.43	0.95
TPRC 60% (2)	107.43	105.88	104.38	2.92	1.44
TPSC 60% (1)	107.84	106.25	107.09	0.70	0.78
TPSC 60% (2)	107.84	106.25	104.41	3.29	1.76
TPRC 100% (1)	107.43	105.88	107.97	0.50	1.94
TPRC 100% (2)	107.43	105.88	105.44	1.89	0.42
TPSC 100% (1)	107.84	106.25	109.1	1.15	2.61
TPSC 100% (2)	107.84	106.25	105.41	2.31	0.80
Payload v1	456.73	454.46	448.87	1.75	1.25
Payload v2	452.95	447.99	447.49	1.22	0.11
Payload Insert 1	16.01	15.69	15.65	2.30	0.23
Payload Insert 2	16.01	15.69	15.31	4.57	2.46
Payload Insert 3	16.01	15.69	15.24	5.05	2.93
Payload Insert 4	16.01	15.69	15.67	2.17	0.11
Payload Insert 5	16.01	15.69	14.40	11.18	8.94
Payload Insert 6	16.01	15.69	14.49	10.49	8.26
Payload Insert 7	16.01	15.69	14.81	8.10	5.92
Payload Insert 8	16.01	15.69	14.77	8.40	6.21
Configuration 1a	60.92	61.71	58.21	4.66	6.01
Configuration 1b	60.92	61.71	54.78	11.21	12.65
Configuration 1c	60.92	61.71	54.00	12.81	14.28
Configuration 1d	60.92	61.71	50.93	19.62	21.17
Configuration 2a	92.15	90.93	98.80	6.73	7.97
Configuration 2b	92.15	90.93	99.18	7.09	8.32
Configuration 2c	92.15	79.09	99.37	7.27	20.41
Configuration 2d	92.15	79.09	98.77	6.70	19.93
Configuration 3a	122.44	119.32	129.27	5.28	7.70
Configuration 3b	122.44	119.32	130.23	5.98	8.38
Configuration 3c	122.44	119.32	132.11	7.32	9.68
Configuration 3d	122.44	119.32	128.87	4.99	7.41

THIS PAGE INTENTIONALLY LEFT BLANK

LIST OF REFERENCES

[1] R. Burcher and L. J. Rydill, *Concepts in Submarine Design*, 2nd ed. Cambridge, UK: Cambridge University Press, 1998.

[2] San Francisco Maritime National Park Association, "Sonar gear" October 23, 2013 [Online]. Available: https://maritime.org/doc/fleetsub/sonar/chap1.htm

[3] University of Rhode Island, "Sound speed minimum," January 28, 2019 [Online]. Available: https://dosits.org/science/movement/sofar-channel/sound-speed-minimum/

[4] University Corporation for Atmospheric Research, "Introduction to Ocean Acoustics," Accessed January 17, 2022 [Online]. Available: http://stream1.cmatc.cn/pub/comet/MarineMeteorologyOceans/IntroductiontoOceanAcoustics/comet/oceans/acoustics/print.htm

[5] D. Miller, "Liquid Metal 3D printing makes its debut," Automation World, February 18, 2021 [Online]. Available: https://www.automationworld.com/factory/3d-printing-additive-manufacturing/article/21283987/liquid-metal-3d-printing-makes-its-debut

[6] G. Potter, "Vader Systems may have created a quantum leap in manufacturing," University of Buffalo, January 12, 2017 [Online]. Available: http://www.buffalo.edu/news/releases/2017/01/020.html

[7] T. Wohlers and T. Gornet, *Wohlers Report 2014*, 1st ed. Fort Collins, CO, USA: Wohlers Associations, 2014.

[8] B. Gibson, D. Rosen, and B. Stucker, *Additive Manufacturing Technologies: 3D Printing, Rapid Prototyping, and direct digitial manufacturing*, New York, NY, USA: Springer Science+Business Media, 2016.

[9] Aerospace Industries Association, "Recommended guidance for certification of AM components," AIA, Arlington, VA, USA, 2020 [Online]. Available: https://www.aia-aerospace.org/report/certification-of-am-component/

[10] A. Staffanson and P. Ragnartz, "Improving the product development process with additive manufacturing," M.S. thesis, Mech Eng., Mälardalens Univ., Västerås, Sweden, 2018.

[11] D. MCCarthy, "Creating complex hollow metal geometries using additive manufacturing and metal plating," M.S. thesis, Dept. of Mech Eng., Virgina Tech. Univ., Blacksburg, VA, USA 2012.

[12] O. Ifayefunmia and M.S. Ismai, “An overview of buckling and imperfection of cone- cylinder transition under various loading condition,” *Latin Am. J. of Solids and Struct.,* vol. 17, no. 8, pp. 1–21, Oct 22, 2020.

[13] G. D. Galletly, “An experimental and theoretical investigation of elastic and elastic-plastic buckling of cylinder-cone combinations subjected to uniform external pressure,” Ph.D. dissertation, Dept. of Mech. Eng., Univ. of LVP., Liverpool, Eng, 1974.

[14] E. Wenk Jr. and C.E. Taylor, “Analysis of stresses at the reinforced intersection of conical and cylindrical shells,” USN, Washington, D.C., USA, R-826 NS 731-038, 1953 [Online]. Available: https://apps.dtic.mil/sti/pdfs/AD0008694.pdf

[15] R. W. Aylward, G. D. Galletly, and D. G. Moffat, “Buckling under external pressure of cylinders with toriconical or pierced torispherical ends: a comparison of experiment with theory,” *Inst. of Mech. Eng*., vol. 17, no. 1, pp. 11–18, Feb 1, 1975.

[16] “Linear vs. nonlinear buckling,” class notes for Pressure Vessel Analysis for Safety, CAE Eng., NFX Int. Support., San Fransisco, CA, 2020.

[17] Predictive Engineering, “Linear and nonlinear buckling analysis and flange crippling,” Livermore Software Tech. Corp., Portland, OR, USA, 2012 [Online]. Available: https://www.predictiveengineering.com/sites/default/files/whitepapers/Predictive%20Engineering%20Buckling%20White%20Paper%20Rev.pdf

[18] B. Dave, “Linear vs. nonlinear buckling analyses,” Hitech, September 11th, 2013 [Online]. Available: https://www.hitechfea.com/fea-knowledgebase/linear-nonlinear-buckling-analyses.html

[19] Xerox ElemX 3D Printer Design Guide V1.0, Xerox, Norwalk, CT, USA, 2021, pp. 1–10.

[20] S. Kitten, “Exploring orientation based design limitations of the Xerox ElemX,” KDS LLC, Cypress, TX, USA, RR-22-01, 2022.

[21] M. Walsh, “Buoyancy,” Cornell Center for Materials Research, Ithica, NY, USA, 2014 [Online]. Available: https://www.ccmr.cornell.edu/wp-content/uploads/sites/2/2015/11/Buoyancy.pdf

[22] S. Ling, J. Sanny, W. Moebs, *University Physics Volume 1,* Houston, TX, USA, Rice University, 2021.

[23] G. Maddux, “Stress analysis manual,” AF. Flight Dyn. Lab., Dayton, OH, USA, AFFDL-TR-69-42, 1969.

[24] *Ansys User Manual* Release 5.6, ANSYS, Canonsburg, PA, USA, 1999, pp. 1–1286.

THIS PAGE INTENTIONALLY LEFT BLANK

INITIAL DISTRIBUTION LIST

1. Defense Technical Information Center
   Ft. Belvoir, Virginia

2. Dudley Knox Library
   Naval Postgraduate School
   Monterey, California